

Mitigation of Earthquake-Induced Soil Liquefaction via Microbial  
Denitrification: A Two-Stage Process

by

Sean O'Donnell

A Dissertation Presented in Partial Fulfillment  
of the Requirements for the Degree  
Doctor of Philosophy

Approved March 2016 by the  
Graduate Supervisory Committee:

Edward Kavazanjian, Chair  
Bruce Rittmann  
Sandra Houston

ARIZONA STATE UNIVERSITY

May 2016

## ABSTRACT

The dissimilatory reduction of nitrate, or denitrification, offers the potential of a sustainable, cost effective method for the non-disruptive mitigation of earthquake-induced soil liquefaction. Worldwide, trillions of dollars of infrastructure are at risk for liquefaction damage in earthquake prone regions. However, most techniques for remediating liquefiable soils are either not applicable to sites near existing infrastructure, or are prohibitively expensive. Recently, laboratory studies have shown the potential for biogeotechnical soil improvement techniques such as microbially induced carbonate precipitation (MICP) to mitigate liquefaction potential in a non-disruptive manner. Multiple microbial processes have been identified for MICP, but only two have been extensively studied. Ureolysis, the most commonly studied process for MICP, has been shown to quickly and efficiently induce carbonate precipitation on particle surfaces and at particle contacts to improve the stiffness, strength, and dilatant behavior of liquefiable soils. However, ureolysis also produces copious amounts of ammonium, a potentially toxic byproduct. The second process studied for MICP, denitrification, has been shown to precipitate carbonate, and hence improve soil properties, much more slowly than ureolysis. However, the byproducts of denitrification, nitrogen and carbon dioxide gas, are non-toxic, and present the added benefit of rapidly desaturating the treated soil. Small amounts of desaturation have been shown to increase the cyclic resistance, and hence the liquefaction resistance, of liquefiable soils. So, denitrification offers the potential to mitigate liquefaction as a two-stage process, with desaturation providing short term mitigation, and MICP providing long term liquefaction resistance. This study presents the results of soil testing, stoichiometric modeling, and microbial ecology characterization to better

characterize the potential use of denitrification as a two-stage process for liquefaction mitigation.

## DEDICATION

This dissertation is dedicated to my family. To my parents, Patti and Tom O'Donnell who have always supported me and encouraged me to pursue my dreams. Also, to my grandmother, Betsy Skillman, who has kept me optimistic and focused throughout my graduate career.

## ACKNOWLEDGMENTS

I would like to express my gratitude to my advisor, Dr. Edward Kavazanjian, for his guidance and mentorship throughout my graduate studies at Arizona State University. I am especially grateful for his availability and willingness to help me with anything from classwork to research to career advice. His constant support has been instrumental to my graduate career and I am very appreciative of all that he has done for me.

I would also like to thank the members of my committee, Dr. Bruce Rittmann and Dr. Sandra Houston. In addition to providing me with guidance and insight on my research, Dr. Rittmann allowed me to work and train in his laboratory, for which I am extremely grateful. I am also very grateful to Dr. Houston for her constant willingness to help and her optimistic support of my class and research endeavors.

I would like to offer a special thanks to Nasser Hamdan, Peter Goguen, and Aura Ontiveros-Valencia for training and mentoring me in the laboratory. Their help is very much appreciated. Angel Gutierrez, Amelia Ochsenbein, Jake Andreson, and Abdullah Almajed have also assisted me on various projects, for which I am very thankful.

Finally, I would like to acknowledge the support for this work that was funded by the Geomechanics and Geotechnical Systems, GeoEnvironmental Engineering and GeoHazards Mitigation program of the National Science Foundation (NSF) Division of Civil, Mechanical, and Manufacturing Innovation under grants numbered CMMI-07030000 and CMMI-1233658. I am very thankful for this support.

## TABLE OF CONTENTS

	Page
LIST OF TABLES .....	x
LIST OF FIGURES .....	xi
CHAPTER	
1 INTRODUCTION .....	1
Background.....	1
Scope and Organization.....	2
2 LITERATURE REVIEW .....	4
MICP for Ground Improvement .....	4
Mechanisms.....	4
Microbial Processes for MICP.....	5
Potential Applications of MICP.....	8
Earthquake-Induced Soil Liquefaction .....	10
Conventional Liquefaction Mitigation Techniques .....	11
Desaturation for Liquefaction Mitigation .....	15
MICP for Liquefaction Mitigation .....	19
Conclusions.....	21
3 CHARACTERIZATION OF TEST SOILS .....	22
Introduction.....	22
Means and Methods.....	22
Soil Index Properties .....	22
Soil-Water Characteristic Curve.....	23

CHAPTER	Page
Triaxial Testing .....	24
Cyclic Simple Shear Testing.....	24
Simple Shear Tests for Correlating P-Wave Velocity and Degree of Saturation .....	26
Results.....	27
Soil Index Properties .....	27
Soil-Water Characteristic Curve.....	29
Triaxial Testing .....	30
Cyclic Simple Shear Testing and Correlation of P-Wave Velocity with Saturation .....	32
Conclusions.....	37
 4 LIQUEFACTION MITIGATION VIA MICROBIAL DENITRIFICATION: A LABORATORY STUDY USING SEMI-STAGNANT SOIL COLUMNS .....	 39
Introduction.....	39
Means and Methods.....	39
Initial Testing .....	39
Testing of Reconstituted Specimens .....	45
Results.....	46
Initial Testing .....	46
Desaturation .....	46
Carbonate Precipitation .....	50
Mechanical Testing.....	65

CHAPTER	Page
Testing of Reconstituted Specimens .....	79
Conclusions.....	83
5 LIQUEFACTION MITIGATION VIA MICROBIAL DENITRIFICATION: A LABORATORY STUDY USING SOIL COLUMNS SUBJECTED TO CONTINUOUS FLOW .....	85
Introduction.....	85
Means and Methods.....	86
Initial Tests .....	86
Second Generation Tests .....	88
Third Generation Tests .....	89
Results.....	91
Initial Tests .....	91
Second Generation Tests .....	93
Third Generation Tests .....	99
Conclusions.....	110
6 CHARACTERIZATION AND ANALYSIS OF MICROBIAL COMMUNITIES FOR SOIL IMPROVEMENT VIA DENITRIFICATION .....	111
Introduction.....	111
Means and Methods.....	112
Initial Column Tests .....	112
Analysis of Microbial Community in Semi-Stagnant and Continuous Flow Columns.....	113



CHAPTER	Page
Results.....	114
Initial Column Tests.....	114
Semi-Stagnant Columns .....	117
Continuous Flow Columns .....	124
Conclusions.....	132
 7 A STOICHIOMETRIC MODEL FOR BIOGEOTECHNICAL SOIL IMPROVEMENT VIA MICROBIAL DENITRIFICATION .....	   135
Introduction.....	135
Stoichiometric Model .....	135
Balanced Chemical Equations .....	135
Kinetics Expressions .....	138
Carbonate Equilibrium and Precipitation .....	139
Experiments .....	140
Model Calibration and Validation.....	143
Sensitivity Analysis .....	146
Varying Calcium Concentration.....	146
Varying Acetate Concentration .....	148
Varying Carbon Source.....	150
Conclusions.....	153
 8 CONCLUSIONS AND RECOMMENDATIONS FOR FUTURE WORK .....	 154
Overview.....	154

CHAPTER	Page
Conclusions.....	155
Recommendations for Further Study .....	161
REFERENCES.....	164

## LIST OF TABLES

Table	Page
1. Soil Index Properties for Ottawa and Bolsa Chica sands .....	28
2. Pore Fluid Properties for the Duration of Semi-Stagnant Testing .....	42
3. Changes in Relative Density, Shear Wave Velocity, and Carboante Content during Semi-Stagnant Testing .....	65
4. Results of Initial Continuous Flow Column Tests.....	91
5. Concentrations of Major Nutrients, pH, and Ionic Conductivity at Sampling Ports in Semi-Stagnant Columns for Microbial Ecology Analysis .....	118
6. Concentrations of Nitrate and Nitrite, as well as pH and Ionic Strength of Pore Fluid with Time at Each Sampling Location in Column OS-CF-4.....	125
7. Alpha Diversity Measurements (Chao1, Faith) with Time at Each Sampling Location in Column OS-CF-4.....	128
8. Taxonomy to Genus Level for DNA Extracted from Each Sampling Location in Column OS-CF-4 with Time.....	130
9. Microbial Metabolisms Considered in Stoichiometric Modeling.....	137
10. Kinetics Coefficients Used to Fit Model Output to Experimental Data .....	143

## LIST OF FIGURES

Figure	Page
1. Experimental Setup for Cyclic Simple Shear Testing .....	26
2. Grain Size Distributions for Ottawa sand and Bolsa Chica sand .....	28
3. Soil-Water Characteristic Curves for Ottawa Sand ( $D_r = 50\%$ ) and Bolsa Chica Sand ( $D_r = 60\%$ ) .....	29
4. Triaxial Data for Ottawa and Bolsa Chica sands.....	31
5. Cyclic Strength Curves for Ottawa sand at relative densities of 45% and 75% and degrees of saturation of 100%, 99%, 97%, and 93% .....	33
6. P-Wave Velocity Versus Degree of Saturation for Ottawa Sand ( $D_r = 45\%$ ) and confining stresses of 3, 20, 50, and 100 kPa (A). Compared to Literature Values at Low Confining Stress (B) .....	34
7. Normalized Cyclic Resistance for Partially Saturated Ottawa Sand Versus P- Wave Velocity as Compared to Tsukamoto et al. (2002) .....	36
8. Shear Wave Velocity versus Confining Stress for dry Ottawa Sand ( $D_r = 40\%$ ) and dry Bolsa Chica Sand ( $D_r = 65\%$ ) .....	37
9. Typical Semi-Stagnant Column Setup.....	41
10. Equilibrium Degree of Saturation in Semi-Stagnant Columns with Time from Dialysis Bag Method.....	46
11. Total Gas Volume per mol of Nitrate Reduced to Nitrogen Gas versus pH (A) and Degree of Saturation versus Total Gas Volume (B) for Semi-Stagnant Columns .....	48

Figure	Page
12. P-Wave Velocity (A) and Corresponding Degree of Saturation (B) for a Typical Treatment Cycle in Columns OS-SS-1 and OS-SS-2 .....	49
13. Mass Percentage Calcium Carbonate Versus Treatment Time for Semi-Stagnant Soil Columns.....	51
14. Equilibrium pH versus time for Semi-Stagnant Soil Columns .....	53
15. Calcium Carbonate Precipitation Versus mols of Nitrate Reduced to Nitrogen Gas for Semi-Stagnant Soil Columns.....	55
16. Comparison in Carbonate Content as Measured by Acid Digestion and IC Analysis for Semi-Stagnant Columns .....	56
17. Carbonate Content (Acid Digestion and IC Analysis) and SEM Images with Depth in Column OS-ACR-1 .....	58
18. Carbonate Content (Acid Digestion and IC Analysis) and SEM Images with Depth in Column OS-ACR-2 .....	59
19. Carbonate Content (Acid Digestion and IC Analysis) and SEM Images with Depth in Column BC-ACR-1 .....	61
20. Carbonate Content (Acid Digestion and IC Analysis) and SEM Images with Depth in Column BC-ACR-2.....	62
21. Biofilm Bridging Soil Particles near the Top of Column OS-ACR-2 .....	64
22. Change in Shear Wave Velocity for OS soil Columns Versus Carboante Content Compared with DeJong et al. (2014) .....	67
23. Carbonate Crystals Precipitated via Ureolysis (A) from Cheng et al. (2014) and via Denitrification (B) from this study.....	68

Figure	Page
24. SEM Images Showing Interaction Between Gas Bubbles and Carbonate Precipitation in Column OS-ACR-1 and Column BC-ACR-1 .....	69
25. Deviator Stress (A) and Excess Pore Pressure (B) from Undrained Testing of OS- TRX Columns at Initial $D_r = 40\%$ and Confining Stress of 100 kPa.....	71
26. Deviator Stress (A) and Excess Pore Pressure (B) from Undrained Testing of OS- TRX Columns at Initial $D_r = 30\%$ and Confining Stress of 100 kPa.....	73
27. Interpreted Unconfined Compressive Strength of Ottawa Sand Treated via Denitrification (this study) at Initial $D_r = 30\%$ and $40\%$ compared with data on soil treated via Ureolytic MICP and EICP from Zhao et al. (2014) .....	74
28. Deviator Stress (A) and Excess Pore Pressure (B) from Undrained Testing of Column BC-TRX-1 at Confining Stress of 100 kPa .....	76
29. Deviator Stress Versus Axial Strain for Drained Testing of Ottawa Sand Samples (A) and Bolsa Chica Sand Samples (B) at a Confining Stress of 75 kPa .....	77
30. Cyclic Direct Simple Shear Testing of Untreated Ottawa Sand, Column OS-SS-1, and Column OS-SS-2 .....	78
31. Deviator Stress (A) and Excess Pore Pressure (B) with Axial Strain for Untreated, Treated, and Reconstituted Specimens .....	79
32. Shear Wave Velocity with Confining Stress for Untreated Soil and Soil from Column OS-TRX-3 after One and Three Reconstitutions ( $D_r = 40\%$ ).....	81
33. SEM Images of Sand Taken from Column OS-TRX-3 after Zero (A), One (B) and Three (C) Reconstitutions.....	82

Figure	Page
34. Cyclic Resistance of Untreated Soil Compared to Column OS-SS-2 after Treatment and Two Reconstitutions .....	83
35. Experimental Setup for First Generation Continuous Flow Column.....	87
36. Observed Desaturation with Time in Column OS-CF-3 .....	94
37. Cemented Sand at Base of Column OS-CF-3 .....	95
38. SEM Images Showing Interparticle Cementation (A) and Particle Roughening (B) of Treated Soil from Column OS-CF-3.....	95
39. Nitrate (A), Acetate (B), Calcium (C), Nitrite (D), pH (E) and Carboante Alkalinity (F) with Time for Column OS-CF-3 .....	97
40. Mass of Carboante Precipitated Versus mols of Nitrate Consumed for Column OS-CF-3.....	98
41. Mass Percentage of Carbonate Precipitated from IC Analysis for Column OS-CF-3.....	99
42. Nitrate (A), Acetate (B), Calcium (C), Nitrite (D), pH (E) and Carboante Alkalinity (F) with Time for Column OS-CF-4 .....	100
43. Mass of Carboante Precipitated Versus mols of Nitrate Consumed for Column OS-CF-4.....	102
44. Organic Nitrogen Concentrations in Column OS-CF-4 with time .....	103
45. Mass Percentage of Carboante Precipitated from IC Analysis for Column OS-CF-4.....	104
46. SEM Images of Treated Soil from Column OS-CF-4 showing Interparticle Cementation (A) and Particle Roughening (B) .....	105

Figure	Page
47. Carboante Content in Column OS-CF-4 from IC and Acid Digestion.....	105
48. P-Wave Velocity and Corresponding Degree of Saturation with time for Column OS-CF-5 .....	107
49 Shear Wave Velocity with time for Column OS-CF-5 .....	108
50. Change in Shear Wave Velocity Versus Carbonate Content for Column OS-CF-5, Semi-Stagnant Denitrification Columns, and Soil Treated via Ureolysis by DeJong et al. (2014).....	109
51. Nitrate and Nitrite Concentrations in Uninoculated Column, Column Inoculated with Mixed Culture, and Column Inoculated with Pure Culture .....	115
52. Calcium Carboante Precipitation in Uninoculated, Mixed Culture, and Pure Culture Soil Columns with Time from IC Analysis and Mass Balance .....	116
53. Estimated Number of Species (Chao1 Index) in Column OS-ACR-1 (A), OS-ACR-2 (B), BC-ACR-1 (C), and BC-ACR-2 (D) .....	119
54. Phylogenetic Diversity (from Faith 1992) in Column OS-ACR-1 (A), OS-ACR-2 (B), BC-ACR-1 (C), and BC-ACR-2 (D) .....	121
55. Taxonomy of Microbial Ecology in Each Sample from Semi-Stagnant Columns Showing Major Phyla (A) and Major Genera (B) .....	122
56. Stoichiometric Model Output and Experimental Results for Nitrate (A), Acetate (B), Carboante Alkalinity (C), pH (D), Calcium (E), Total Gas Volume (F), Nitrite (G), and Biomass (H) .....	145



Figure	Page
57. Results of Sensitivity Analysis. Total Calcium Carbonate Mass and Calcium Removal from Pore Water (A) and Total Gas Generated and Final pH (B) Versus Initial Ratio of Calcium to Nitrate Concentration .....	147
58. Results of Sensitivity Analysis. Total Calcium Carbonate Mass and Calcium Removal from Pore Water (A) and Total Gas Generated and Acetate Removal (B) Versus Initial Ratio of Acetate to Nitrate Concentration .....	149
59. Results of Sensitivity Analysis. Total Carboante Precipitation (A) and Total Gas Volume Generated (B) with Varying Carbon Source .....	152

# CHAPTER 1

## INTRODUCTION

### BACKGROUND

Earthquake-induced liquefaction is a natural phenomenon that threatens trillions of dollars of infrastructure worldwide built on and in liquefiable soil deposits in earthquake prone regions. Liquefaction damage alone led to the abandonment of over 15,000 modern single family residences in Christchurch, New Zealand following the Moment Magnitude 6.3 earthquake of February, 2011 (Rogers et al. 2015). While liquefaction is a serious issue, few sustainable, cost effective methods can remediate the potential for liquefaction in a non-disruptive manner beneath or around existing infrastructure. Furthermore, besides being economically prohibitive, many of the existing methods for non-disruptive liquefaction mitigation, such as compaction grouting and permeation grouting, rely on the use of Portland cement grouts, which contribute to a sizeable amount of greenhouse gas emissions worldwide.

Recent innovations in geotechnical engineering have highlighted the potential use of bio-mediated systems to improve soil properties (DeJong et al. 2010). Specifically, microbially induced carbonate precipitation (MICP) has gained interest as a potential method to improve the mechanical properties of the soil via interparticle cementation (Whiffin et al. 2007, Karatas et al. 2008, DeJong et al. 2010, van Paassen et al. 2010, Montoya and DeJong 2015). MICP has also shown the ability to mitigate liquefaction potential in susceptible soils (Montoya et al. 2013, Burbank et al. 2013). MICP acts as a carbon sink, whereby potentially harmful CO<sub>2</sub> is actually sequestered in the carbonate minerals used to cement soil together. So, not only does it show promise as a liquefaction

mitigation technique, but MICP also presents a much more sustainable alternative to traditional ground improvement methods.

Multiple microbial mechanisms have been identified for MICP (Karatas et al., 2008). This study focuses on the use of microbially mediated dissimilatory reduction of nitrogen (denitrification) for soil improvement. Denitrification has been shown to induce carbonate precipitation without the production of potentially harmful byproducts, as opposed to other MICP processes (van Paassen et al. 2010, Hamdan et al. 2011). Additionally, microbial denitrification has shown the potential to mitigate liquefaction potential through the production of biogas and its subsequent desaturation of the soil (He et al. 2013). This study will focus on the potential of microbial denitrification to mitigate liquefaction potential as a two-stage process, with desaturation providing short term liquefaction resistance and MICP providing long term liquefaction mitigation.

## **SCOPE AND ORGANIZATION**

The purpose of this study is to determine the effectiveness of microbial denitrification as a two-stage technique for the non-disruptive mitigation of earthquake-induced soil liquefaction. Specifically, the goals of this work are to:

- 1) Demonstrate the ability of denitrification to mitigate earthquake-induced liquefaction as a two-phase process.
- 2) Identify and analyze the microbial communities responsible for providing liquefaction mitigation via denitrification.
- 3) Develop a stoichiometric model for soil improvement via denitrification for the calculation of the necessary material (i.e. chemical) resources.

In order to meet these goals, this work is organized in the following way. A review of the relevant literature is provided in Chapter 2 to give context to the use of denitrification for liquefaction mitigation via desaturation and MICP. Chapter 3 presents the results of abiotic testing of the soils used in this work to provide a baseline from which to assess the ability of denitrification to mitigate liquefaction potential of the soil. Semi-stagnant biotic column experiments to assess the ability of denitrification to improve soil properties via desaturation and MICP are described in chapter 4. As these semi-stagnant tests do not accurately represent potential field conditions, the results of continuous-flow soil column tests are presented in Chapter 5. These continuous flow columns show the ability of denitrification to mitigate liquefaction potential in a system with flowing groundwater. An analysis of the microbial communities present in the semi-stagnant and continuous flow soil columns is presented in Chapter 6. Chapter 7 presents a stoichiometric model for the prediction of soil improvement via desaturation and MICP via denitrification. This work closes with conclusions and recommendation for future study in Chapter 8.

## CHAPTER 2

### LITERATURE REVIEW

#### **MICP FOR GROUND IMPROVEMENT**

Microbially induced carbonate precipitation (MICP) has been shown to significantly improve the mechanical properties of sands. Specifically, precipitation of carbonate minerals at soil particle contacts and on particle surfaces can lead to improved strength, stiffness, and dilatant behavior of a soil through interparticle cementation and particle roughening (van Paassen et al. 2010, Montoya and DeJong 2015, O'Donnell and Kavazanjian 2015).

#### **Mechanisms**

MICP occurs when microbes (bacteria, archaea, or single celled eukaryotes) alter the geochemistry of their aqueous environment to favor the precipitation of carbonate minerals (DeJong et al. 2010). Carbonate precipitation is favored when the activity of carbonate and a suitable cation (e.g., calcium, magnesium, manganese, iron, cobalt) are high enough to surpass the solubility product of the resulting carbonate mineral (Ehrlich and Newman 2009). The solubility product for a given mineral is governed by intermolecular forces between water and that mineral, the entropy change associated with dissolution of the mineral, temperature, and pressure (Anderson 2009). Some of the more common carbonate minerals include calcite ( $\text{CaCO}_3$ ), aragonite ( $\text{CaCO}_3$ ), magnesite ( $\text{MgCO}_3$ ), dolomite ( $\text{CaMg}(\text{CO}_3)_2$ ), and siderite ( $\text{FeCO}_3$ ) (Ehrlich and Newman 2009). In general, geotechnical engineers are most interested in the microbially induced precipitation of calcite due to its low solubility, thermodynamic stability, and high strength.

Microorganisms can create geochemical conditions favoring carbonate precipitation by increasing either the pH, the total carbonate content of their environment, or both. Increasing the pH of a solution will favor the speciation of inorganic carbon toward carbonate, increasing carbonate concentration and hence causing precipitation of carbonate minerals in the presence of a high enough concentration of a suitable cation. Increasing the total carbonate content of a well buffered solution will also increase the carbonate concentration, causing precipitation of carbonate minerals (Karatas et al. 2008). A wide variety of microbial processes have been identified with the capability to induce carbonate precipitation (Karatas 2008).

### **Microbial Processes for MICP**

Cyanobacteria and other photosynthetic microbes have been shown to induce carbonate precipitation through photosynthesis (Bundeleva et al. 2014, Kazmierczak et al. 2015). When exposed to sunlight, photosynthetic microorganisms consume dissolved carbon dioxide (carbonic acid). While this lowers the total carbonate content of the environment, it also increases the pH, driving the speciation of the remaining inorganic carbon toward carbonate and inducing precipitation of carbonate minerals (Kamennaya et al. 2012). Through the precipitation of carbonate minerals, photosynthetic microbes have been implicated in the formation of stromatolites, layered natural deposits of limestone, as well as calcium carbonate-cemented sandstone deposits found in the tidal zones of beaches worldwide often referred to as beachrock (Kazmierczak et al. 2015, Neumeier 1999). While photosynthesis has been shown to induce carbonate precipitation in nature and laboratory experiments, its application to geotechnical engineering is limited. Sunlight, the source of energy for photosynthetic organisms, only penetrates a few millimeters below

the ground surface, so photosynthesis would only be applicable for the formation of carbonate-cemented soil crusts (Karatas et al. 2008).

Sulfate reducing bacteria have also been shown to induce carbonate precipitation. These bacteria use sulfate as a terminal electron acceptor in their anaerobic metabolism and, in the process, consume sulfuric acid. The consumption of sulfuric acid raises the pH of the environment, favoring the precipitation of carbonate minerals. When sulfate reducing bacteria use organics as their electron source, they also generate aqueous carbon dioxide, raising the total carbonate content of their environment, further favoring the precipitation of carbonates (DeJong et al. 2010). Warthmann et al. (2000) showed, through pure-strain culture experiments, that sulfate reducing bacteria are capable of inducing the precipitation of dolomite ( $\text{CaMg}(\text{CO}_3)_2$ ) from hypersaline environments. However, while sulfate reducing bacteria are capable of inducing carbonate precipitation, they also generate large quantities of hydrogen sulfide, a potentially toxic gas. This makes sulfate reduction a rather undesirable method for soil improvement through MICP.

Urea hydrolysis, or ureolysis, is another microbial process capable of inducing carbonate precipitation. Ureolysis is a common process through which certain plants and microorganisms scavenge nitrogen, an essential nutrient, through the hydrolysis of urea, an animal waste product. This process results in both a pH increase through the production of ammonia, and an increase in the total carbonate content through the production of carbon dioxide. Both of these favor the precipitation of carbonate species (Whiffin et al. 2007). Whiffin et al. (2007) showed that soil treated via ureolytic MICP demonstrated significant improvement in peak strength at carbonate contents greater than 4% by weight. Through a large box experiment with fine to medium poorly graded sand, van Paassen et al. (2010)

showed that ureolysis can be used to induce the precipitation of calcium carbonate very quickly (within 16 days), and in large amounts (0.8 – 24% CaCO<sub>3</sub> by weight). While these results suggest that ureolysis is an extremely efficient process for MICP, ureolysis also produces ammonium chloride, a potentially toxic byproduct. In a large scale field test in which MICP via ureolysis was induced for seven days to stabilize a natural gravel deposit, van der Star et al. (2011) reported that three additional days of groundwater extraction at “higher flow rates” were needed to remove ammonium chloride to meet regulatory groundwater requirements. This fluid needed to be treated in a wastewater facility, raising the cost of the operation considerably. So, while ureolysis induces the precipitation of large amounts of carbonates in a very short period of time, it also has the potential to lead to environmental contamination and associated cleanup costs.

Another microbial process capable of inducing the precipitation of carbonate minerals is microbial denitrification. Denitrifying microbes consume nitric acid and organics to produce nitrogen gas and carbon dioxide. The consumption of nitric acid raises the pH, while the production of carbon dioxide increases the total carbonate content of the surrounding solution. In the presence of cations, such as calcium, this leads to the precipitation of carbonate minerals (Karatas 2008, Hamdan 2013). van Paassen et al. (2010) found, through a continuously flowing soil column experiment, that MICP via denitrification was capable of precipitating anywhere from 1% to 9.5% CaCO<sub>3</sub> by weight after 100 days of treatment. One reason for the relatively slow (compared to ureolysis) precipitation of carbonate during this experiment was the accumulation of toxic intermediates, such as nitrite and nitrous oxide. Nitrite, or more specifically nitrous acid, acts as an uncoupler (i.e. it degrades the pH gradient across the cell membrane necessary



for energy production in bacterial cells) in microbial metabolism, leading to inhibition of cell growth (Almeida et al. 1994, Sijbesma 1996). This means that denitrification works most efficiently as an MICP process at low initial nitrate concentrations (Hamdan 2013). So, while denitrification is capable of inducing significant amounts of carbonate precipitation, it is a considerably slower process than ureolysis. However, denitrification produces only nontoxic nitrogen and carbon dioxide gases as byproducts. So, unlike ureolysis, denitrification should not incur any environmental cleanup costs (van Paassen et al. 2010).

Martin et al. (2013) found that *Halomonas halodenitrificans* was able to induce MICP via denitrification at ambient pressure and under a pressure of 8 MPa with very little difference in the amount of calcium carbonate precipitated. The same bacteria was shown to grow without any significant inhibition at pressures up to 20 MPa. This result indicates that MICP via denitrification has the potential for deep applications, such as sealing of abandoned oil wells and remediation of hydraulic fracturing from shale gas extraction (Martin et al. 2013).

### **Potential Applications of MICP**

MICP has a variety of potential applications to geotechnical engineering. One application of MICP is for surficial stabilization of wind-blown soils. Meyer et al. (2011) found that surficial treatment of soils with ureolytic microbes and an MICP solution containing urea and calcium chloride led to a significant decrease in the amount of soil mass lost during wind tunnel testing. Meyer et al. (2011) also found that a variety of factors affect the extent of improvement via MICP, including treatment time, relative humidity, temperature, initial cell density, treatment volume, and soil type. Gomez et al. (2013) also

determined that MICP via ureolysis represented a viable method to reduce fugitive dust and surficial erosion from mine tailings, as verified at a test section at a mine site in Canada through direct cone penetrometer testing, measurement of carbonate content, and visual observation of a competent 2.5 cm thick soil crust in the treated zone. Hamdan and Kavazanjian (2016) also found that surficial treatment with a cementation solution containing urease enzyme was able to significantly raise the detachment velocity of native desert soil, mine tailings, and fine sand in wind tunnel testing.

MICP has also shown promise for stabilization of slopes against water erosion. Knorr (2014) showed that surficial treatment of mine tailings at an inclination of fifteen degrees from the horizontal with cementation solution and urease enzyme led to a significant reduction in soil mass loss after exposure to three minutes of surficial water flow when compared to untreated mine tailings. Similarly, Salifu et al. (2016) found that treatment of soil slopes (angles of 35° and 53° from the horizontal) with ureolytic microbes and MICP solution led to significant reductions in sediment detachment as well as improved slope stability when subjected to 30 tidal cycle simulations. These results indicate that treatment of soils via MICP may not only improve the resistance of slopes to surface water and tidal erosion, but also increase the overall global slope stability (Salifu et al. 2016).

Another potential application of MICP is for the improved performance of foundations systems. Lin et al. (2016) found that the ultimate compressive strength of pervious concrete piles in sand subjected to treatment via ureolytic MICP increased by a magnitude of 2.5, while the stiffness of the load-displacement curve increased by 2.8 times. It is theorized that cementation of sand around the pile significantly increased the effective area, skin friction, and load transfer rate of the pile, leading to such dramatic improvement.

Kavazanjian and Hamdan (2015) found that, through injection of urease enzyme and cementation solution into loose sands, fairly strong cemented bulbs of soil could be formed. These authors note that this development has applications to the formation of cemented soil columns for support of shallow foundations.

A very important potential application of MICP is as a mitigation measure for earthquake-induced soil liquefaction, as discussed in the next section of this chapter.

## **EARTHQUAKE-INDUCED SOIL LIQUEFACTION**

Earthquake-induced soil liquefaction is a process whereby cyclic loading induces the generation of excess pore pressures in loose, cohesionless soil deposits, leading to a loss of effective vertical stress and shear strength in the soil. It is well established that dry cohesionless deposits densify under cyclic loading. However, when the soil is saturated, cyclic loading induces an undrained response, leading to the generation of excess pore pressures. These excess pore pressures may rise to the extent that the vertical effective stress becomes very small, approaching zero, at which point the soil loses all shear strength and effectively behaves like a liquid. It is at this point that the soil is said to have liquefied (Kramer 1996).

Soil liquefaction can have a variety of undesirable side effects. For instance, loss of shear strength beneath buildings can lead to bearing failure of shallow foundations. Liquefaction of soil in or beneath dams or embankments can lead to flow slides. On level (or nearly level) ground, liquefaction of soils can induce severe seismic settlement, leading to damage to lifelines and above-ground structures. Also, if the cyclic stresses induced by earthquake loading exceed the liquefied strength of a soil in even gently sloping ground and in level ground adjacent to a free face, the soil can deform incrementally during

shaking, leading to large permanent displacements. This phenomenon, known as lateral spreading, can lead to serious damage on relatively flat land near rivers and ports (Kramer 1996).

Liquefaction related damage can be extremely severe during even moderate earthquake events. Following the moderate (magnitude 6.3) 2011 Christchurch earthquake, approximately 15,000 single family homes were damaged beyond economic repair and were abandoned (Rogers et al. 2015). Typical damage from liquefaction in residential areas included bearing failure, severe differential settlement, lateral stretching (from lateral spreading), and racking or twisting of the structures. In addition to residential damage, the central business district of Christchurch also experienced significant liquefaction damage, with differential settlements, foundation damage and bridge collapse from lateral spreading near the Avon River, and punching settlement of structures on liquefied ground (Cubrinovski et al. 2011). Lifelines, including wastewater and potable water lines, were also severely affected by liquefaction. Approximately 81% of damaged pipes in the Christchurch earthquake were in areas that experienced some degree of liquefaction. Overall, liquefaction contributed significantly to the roughly \$30 B (NZD) in damages during the Christchurch earthquake sequence of 2010 and 2011 (Cubrinovski et al. 2012).

### **Conventional Liquefaction Mitigation Techniques**

There are a variety of ground improvement techniques available for the mitigation of earthquake-induced liquefaction potential. Broadly, these techniques can be split into five groups: densification, reinforcement, drainage, solidification, and desaturation (Kramer 1996). Densification techniques work by densifying the existing soil, increasing the strength and stiffness, while also making the soil more dilatant (Orense 2015). Many

densification techniques, like vibrocompaction, deep dynamic compaction, and blast densification, can be fairly inexpensive but produce ground settlement and vibrations and/or shockwaves which can be very disruptive to nearby existing structures and utilities (Andrus and Chung 1995). Furthermore, the application of these techniques may be limited in finer grained liquefiable soils that are not particularly susceptible to densification by vibration, e.g., low plasticity silt.

Of the available densification techniques, only compaction grouting offers the opportunity to remediate liquefaction potential beneath or adjacent to existing structures. Compaction grouting works by injecting a high viscosity, low slump grout at high pressures to displace and densify the surrounding soil (Sharma 2010). The injected grout replaces the ground volume lost through densification, mitigating the potential for undesirable ground movement. Compaction grouting can be used to create a series of grout bulbs, to densify soil beneath and around existing facilities (Orense 2008). While compaction grouting can be deployed for liquefaction mitigation near existing facilities, it cannot be used for near surface treatment, as the grout pressures induce significant heave. It is also a fairly expensive technique to use, as a large amount of grout is necessary to treat a comparably small volume of soil (Andrus and Chung 1995).

Reinforcement techniques for liquefaction mitigation involve the installation of reinforcing elements to improve the strength and stiffness of a soil mass. These reinforcing elements may consist of steel, concrete, timber, densified gravel, or other competent materials. (Kramer 1996). One of the most commonly used methods of reinforcement for liquefaction mitigation is the installation of stone columns. Stone columns are columns of densified gravel which serve to mitigate liquefaction in four ways: reinforcing the soil

mass, providing a reduced drainage path to mitigate the accumulation of excess pore pressures, densifying the surrounding soil during installation (vibratory methods are often used), and increasing the lateral stress in the soil around the columns (Farrell et al. 2010). They can also be used in both coarse and fine grained soil deposits, meaning that they are applicable to both liquefiable sands and silts. This makes stone columns an especially popular method for liquefaction mitigation at new building sites. However, the fact that they use vibratory methods for installation means that they are not suitable for mitigating liquefaction potential beneath or near existing structures (Andrus and Chung 1995).

One potential reinforcement technique that has been used beneath existing structures is jet grouting. Jet grouting involves the lateral injection of high pressure grout in a circular pattern from bottom to top to generate a column of cemented soil. Jet grout columns have been found to mitigate liquefaction risk by stiffening the soil mass, thereby lowering the cyclic shear strains in the surrounding soil. However, numerical modeling has also found that the stiffening effect of jet grout columns may not be enough to considerably reduce the cyclic shear strains and excess pore pressure generation in the surrounding soil unless the columns are closely spaced (Ozener et al. 2015). This means that jet grout columns may not be a very efficient liquefaction countermeasure. Jet grouting is also a fairly inexact art since the size and strength of jet grout columns can be affected by a variety of factors, including the soil type, ground water conditions, grout mix, injection rate, jet pressure, withdrawal rates, etc. (Andrus and Chung 1995). This means that jet grouting may not be a very reliable method for ground improvement beneath existing structures, where verification of improvement might be difficult to obtain.

Drainage techniques for liquefaction mitigation involve the installation of free draining materials, usually stone columns, gravel drains, or prefabricated vertical drains (PVDs), in the liquefiable soil layer to mitigate the buildup of excess pore pressures during cyclic loading. Drainage techniques are not suitable for placement beneath existing structures as they generally involve vibratory installation techniques and, in the case of gravel drains and PVDs, they do nothing to mitigate seismic settlement (Kramer 1996).

Solidification techniques involve injecting or mixing cementitious materials, e.g. Portland cement, into the soil to solidify the soil mass. Solidification can be accomplished through permeation grouting or soil mixing, although soil mixing can usually not be applied beneath existing facilities (Andrus and Chung 1995). Permeation grouting involves the injection of a low viscosity chemical or particulate grout into the soil pores with little to no change in the soil structure. Chemical grouting techniques include the injection of silica gel (Gallagher et al. 2007), lignin gels, phenolic resins, or acrylic resins to solidify the soil mass. The applicability of chemical grouting is limited by the ability of grout to pass through pore spaces and relatively uniformly permeate the soil. Particulate grouts include dilute suspensions of cement, fly ash, bentonite (Rugg et al. 2011), or some combination of these. In general, chemical grouts are more applicable to finer grained soils than cementitious grouts due to their lower viscosities (Kramer 1996). However, even chemical grouting is of limited applicability in fine sand, silts, and stratified soils. While permeation grouting has been shown to be effective at reducing liquefaction risk beneath existing structures in soils where it is applicable, it is generally a very expensive method to implement and verification of successful treatment is difficult (Andrus and Chung 1995).

## **DESATURATION FOR LIQUEFACTION MITIGATION**

Desaturation as a ground improvement method for liquefaction mitigation has attracted increasing interest over the past 15 years. It is well established that slightly desaturated soils require much stronger shaking to induce liquefaction, as even small amounts of gas can add considerable compressibility to the pore fluid, mitigating the buildup of excess pore pressures. Tsukamoto et al. (2002) found that the cyclic resistance of Toyoura sand increased in a non-linear manner with decreasing values for Skempton's B parameter (a parameter related to the degree of saturation of the soil). These investigators also determined that the cyclic resistance of the sand increased non-linearly with decreasing P-wave velocity, suggesting that P-wave velocity could be an indicator of degree of saturation and also liquefaction resistance. Arab et al. (2011) found that the cyclic resistance of a natural sand from Drome, France increased considerably (roughly 100%) when the Skempton's B-value decreased from 0.90 to 0.25 (corresponding to degrees of saturation of 100% and 98% respectively). Furthermore, it was determined that the data from this analysis matched well with the equation relating B-value and normalized cyclic strength ratio proposed by Yang (2004). The Yang equation was established based on analysis of cyclic data from four different sands and two different test apparatus (torsional shear and cyclic triaxial). The results of these studies indicate that small amounts of desaturation (as determined by the B-value and P-wave velocity) can lead to significant increases in the cyclic resistance of a sand.

Okamura and Soga (2006) also found that the cyclic resistance of Toyoura sand increased dramatically with decreasing saturation, though at a decreasing rate (i.e. a roughly 100% increase in cyclic resistance upon lowering from 100% to 90% saturation,



with only a minimal increase in cyclic resistance upon lowering from 90% to 70% saturation). However, they also found that the change in cyclic resistance for unsaturated sand depended on both the initial pore pressure and the initial effective confining stress. Desaturation provided slightly greater increases in cyclic resistance at lower initial pore pressures. Desaturation of soil at higher initial effective confining stresses led to greater increases in cyclic resistance than those at lower initial effective confining stresses. The overall results of this study confirm that even small amounts of desaturation (<10%) can lead to very significant increases in the liquefaction resistance of a sand. This study also highlights some of the other factors affecting the potential use of desaturation for liquefaction mitigation, including initial pore pressure and initial effective confining stress.

The traditional approach to desaturation in geotechnical engineering practice is dewatering, or the lowering of the groundwater table through continuous pumping. While this technique may offer the potential for liquefaction mitigation beneath existing structures, the associated settlement, while smaller than the settlement due to vibratory densification, may be unacceptable in some cases and the costs associated with constant pumping are generally prohibitive to its use in practice (Nakai et al. 2015). In recent years, new desaturation techniques to induce desaturation of the soil have gained notice as potential cost effective liquefaction mitigation techniques.

Yegian et al. (2007) demonstrated the effectiveness of electrolysis as a means to induce desaturation for liquefaction mitigation (termed induced partial saturation by the authors). Electrolysis involves sending an electric current through the ground, causing water to split into hydrogen gas and oxygen gas at the cathode and anode respectively. Using electrolysis, degrees of saturation of roughly 96% were achieved in Ottawa sand samples

in laboratory testing. When these unsaturated samples and saturated samples of the same sand were subjected to the same cyclic loading regimen, pore pressure measurements showed that the unsaturated specimens did not liquefy, but the fully saturated specimens did liquefy. It was also found that unsaturated specimens did not re-saturate (in a stagnant column) even after 442 days of monitoring. These results showed that desaturation can lead to significant liquefaction resistance and that in cases with no groundwater flow desaturation may represent a viable intermediate to long term solution for liquefaction.

Esseler – Bayat et al (2013) also demonstrated the feasibility of desaturation for liquefaction mitigation. Sodium perborate, which reacts with water to form small oxygen gas bubbles, was mixed with Ottawa sand to generate slightly desaturated specimens. It was determined that, at different cyclic strain amplitudes and different relative densities, lowering the degree of saturation with sodium perborate to anywhere from 40% to 90% induced significant reductions in pore pressure generation during cyclic loading. It was also demonstrated that slightly desaturated sand remained unsaturated under hydrostatic conditions, when subjected to constant upward flow, and under horizontal base excitation with over 10,000 cycles at 0.7 – 0.99g. It should be noted that the soil was contained in a tall, thin rigid container when subjected to base excitation, so it remains unclear if the soil would remain unsaturated when subjected to cyclic shear. These results also suggest that induced desaturation of sands represents a viable solution for liquefaction mitigation.

Okamura and Teraoka (2006) found that sand compaction piles, constructed with the aid of pressurized air, unintentionally led to desaturation of the soil. Taking undisturbed frozen samples from soil adjacent to the sand compaction piles showed that the degree of saturation in these treated sand layers was lower than 91%. Subsequent sampling of older

sites revealed that this induced desaturation could last as long as 26 years. In subsequent shake table test, it was determined that desaturation not only reduced pore pressure generation but also considerably reduced the amount of seismic settlement following cyclic loading. These results suggest that sand compaction piles represent a viable method for liquefaction mitigation via desaturation.

He et al. (2013) demonstrated that slight desaturation of sand can be induced with gas-producing microorganisms, specifically denitrifying bacteria. Dry biomass of *Acidovorax* species isolated from anaerobic wastewater sludge was mixed with dry soil in a laminar soil box. The soil was then saturated with a bacterial medium containing potassium nitrate, ethanol, and trace nutrients to promote microbial growth. The initial nitrate concentration was used to control the amount of gas generation. After incubating the soil for several days to allow for microbial growth and gas generation, the laminar box was subjected to cyclic loading on a shake table. Testing revealed that denitrifying microbes were capable of desaturating the soil to degrees of saturation in the range of 80% - 95% depending on the initial nitrate concentration. It was also found that pore pressure generation, volumetric strain, and settlement were reduced following cyclic loading when biogas was used to desaturate the soil. These results indicate that desaturation induced via denitrifying microbes represents a viable method for liquefaction mitigation.

He and Chu (2014) demonstrated that desaturation to the level of 88% - 95% through biogas generation by denitrifying bacteria was capable of increasing the monotonic triaxial undrained strength of soil by up to two times in both compression and extension. They also demonstrated that higher levels of desaturation (degree of saturation < 95%) led to strain hardening of the soil rather than strain softening at large strains. These results

indicate that desaturation through biogas production can significantly reduce the risk of static liquefaction.

Rebata-Landa and Santamarina (2012) were able to induce unsaturated soil conditions in multiple soil types (sands, silts, clayey soils) by inoculating soils with *Paracoccus denitrificans* and a bacterial medium containing nutrients, including nitrate. Desaturation was confirmed through the measurement of P-wave velocity and Skempton's B-value. It was also demonstrated that sands with little to no fines were unable to effectively trap bubbles, leading to a partial recovery in P-wave velocity (and hence, degree of saturation). Soils with higher fines content demonstrated higher retention of gas bubbles. These results indicate that the biogenic generation of gas using denitrifying organisms is applicable in multiple soil types, but may not lead to long term desaturation in clean sands or gravel.

## **MICP FOR LIQUEFACTION MITIGATION**

MICP shows significant potential as a liquefaction mitigation mechanism as a solidification technique. As discussed earlier, soil treated via MICP can experience significant static strength increases (Whiffin et al. 2007, van Paassen et al. 2010). Montoya and DeJong (2015) showed that treatment via MICP (ureolysis) significantly increases the shear wave velocity of the soil, indicating a corresponding improvement to the small strain stiffness. Through undrained triaxial testing of treated sand, these authors also show that the strength, stiffness, and dilatant behavior of the soil also increase significantly with increasing carbonate content. These improvements in strength, stiffness (both small and medium strain) and dilatant behavior of MICP-treated soil under monotonic compressive loading indicate that soils treated via MICP will also be more resistant to liquefaction under earthquake loading.

Burbank et al. (2011) showed, through field testing, that biostimulation of ureolytic microbes could result in moderate amounts of carbonate precipitation (1% - 2.5%). Subsequent testing demonstrated that CPT tip resistance was increased significantly with carbonate levels as low as 1.8%. As CPT tip resistance is correlated to liquefaction resistance (Roberston and Wride 1998) the results of Burbank et al. (2011) indicate that not only can ureolytic microbes be stimulated in the natural environment but also that MICP via these stimulated organisms can improve the soil to the point that it may no longer be susceptible to liquefaction.

Burbank et al. (2013) showed, through cyclic triaxial testing of natural sands, that moderate treatment via ureolytic MICP (2.2 – 2.6%  $\text{CaCO}_3$ ) could increase the cyclic resistance of the sand (i.e., the cyclic stress ratio inducing liquefaction) by an order of two, while major treatment via MICP (3.8 – 7.4%  $\text{CaCO}_3$ ) could increase the cyclic resistance by as much as four times. These results indicate that moderate amounts of carbonate precipitation via MICP may be enough to significantly improve the liquefaction resistance of the soil.

Montoya et al. (2013) showed through centrifuge model testing of Monterey sand that soil treated via ureolytic MICP (2.6% - 8.0%  $\text{CaCO}_3$ ) displayed significantly lower pore pressure generation, much less settlement, and higher surface accelerations when compared to untreated sand. All of these results indicate mitigation of liquefaction via MICP. Similarly, much greater shear wave velocities were measured in the MICP treated soil, indicating improved small strain stiffness. However, during shaking, the shear wave velocity of treated soil degraded toward that of untreated soil. Direct cyclic simple shear testing of the treated soil showed an improvement in the cyclic resistance of the soil by at

least four times. These results strongly indicate the ability of MICP to mitigate the liquefaction potential of a soil.

## **CONCLUSIONS**

Microbial denitrification shows promise as a ground improvement technique for liquefaction mitigation through solidification via MICP and desaturation via biogas generation. A two-stage approach to liquefaction mitigation is presented herein, with desaturation via biogas generation providing short term mitigation and interparticle cementation via MICP providing long term mitigation of liquefaction.

## **CHAPTER 3**

### **CHARACTERIZATION OF TEST SOILS**

#### **INTRODUCTION**

The geotechnical characterization of two test soils is presented in this chapter. Characterization of these soils included grain size distribution, minimum and maximum densities, triaxial compression test results, and cyclic simple shear test results. This characterization information is important for understanding how the microbial process of denitrification may influence the behavior of these soils.

#### **MEANS AND METHODS**

##### **Soil Index Properties**

Two different soils were used in this work: Ottawa 20-30 crystal silica sand and a natural beach sand collected from Bolsa Chica State Beach in Huntington Beach, CA. The grain size distribution of both soils was evaluated using sieves of various sizes per ASTM D6913-04. Soil classification in accordance with the Unified Soil Classification System (USCS) was established for each soil from the sieve analysis results.

In addition to grain size distribution, characterization data for granular soils typically includes the minimum and maximum density. The maximum and minimum density for the Ottawa sand were taken from Santamarina and Cho (2001). The minimum density of the Bolsa Chica soil was found by placing a funnel full of dry soil into a cylindrical mold of predetermined volume. The funnel was then raised slowly, allowing soil to fill the mold in a very loose configuration. The mass of sand that filled the mold was then used to calculate the minimum density. Following determination of the minimum density, the

mold was placed on a vibratory table and shaken for five minutes with an overburden pressure of roughly 10 kPa. The volume of soil was calculated following vibratory densification by measuring the decrease in height of the soil surface to determine the maximum density.

Finally, the carbonate content of the Bolsa Chica sand was determined through acid digestion. Clean, dry Bolsa Chica soil was washed with 4M Hydrochloric acid for roughly 10 minutes to dissolve all carbonate minerals in the sand. Following treatment, the soil was rinsed with tap water, followed by deionized water to remove residual acid and dissolved salts before drying in the oven for 24 hours at 200 °F. The difference in mass before and after digestion was taken to be the mass of carbonate minerals in the soil. The Ottawa sand is referred to as Crystal Silica sand and its mineralogical composition is reported to be greater than 99.7% silica by the provider of the sand (US Silica, Co. 2014) and was found to be 99.8% silica in an independent study (Ojuri and Fijabi 2012). Therefore, testing for carbonate content was not performed on this soil.

### **Soil-Water Characteristic Curve**

The laboratory procedure used to determine the soil-water characteristic curve for the test soils followed ASTM D6836 with some minor adjustments. Each soil was placed into a brass ring (61.5 mm diameter, 23.8 mm height) at a relative density of 50 – 60% and then saturated with deionized water. In place of a Fredlund SWC-150 device for measuring matric suction, a Tempe cell was used to determine suction values greater than 2.5 kPa. For values of matric suction lower than 2.5 kPa, a hanging manometer device was used. Five data points were obtained for the Ottawa sand (two from Tempe cell, three from hanging manometer) and four data points were obtained for the Bolsa Chica sand (two from



Tempe cell, two from hanging manometer). The Fredlund and Xing sigmoidal function was then used to fit a curve through the data points for each soil (Fredlund and Rahardjo 1993).

### **Triaxial Testing**

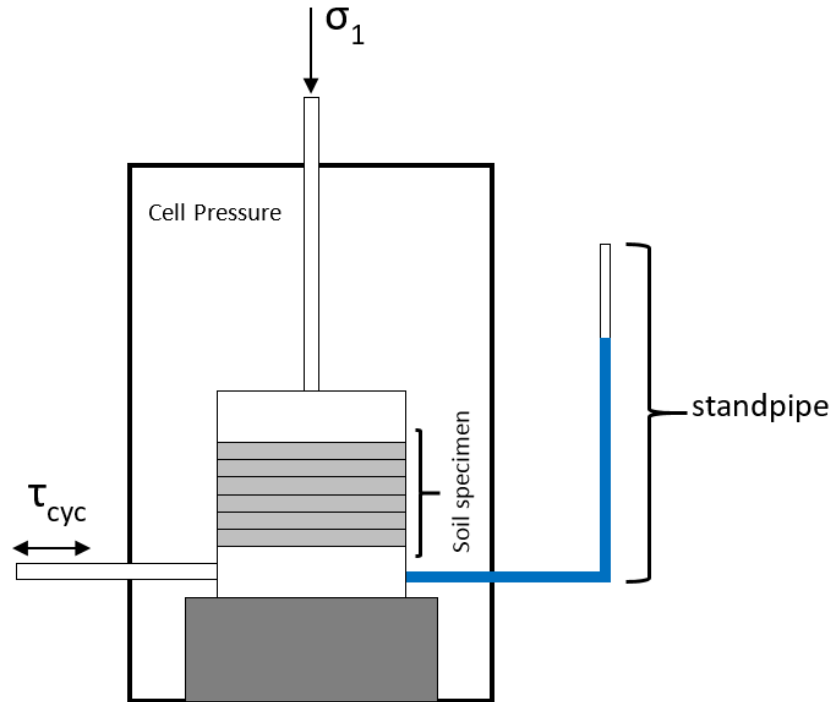
Drained triaxial tests were performed on each soil at a confining stress of 75 kPa to determine the drained strength and drained friction angle (assuming zero cohesion) for each sand. The Ottawa sand was tested at a relative density of 50%, while the Bolsa Chica sand was tested at relative densities of 45% and 90%. Each test was performed at a constant axial strain rate of 0.5% per minute to a final strain of 15%.

Undrained triaxial tests were also performed to determine the undrained strength, the undrained friction angle, and the volume change behavior of each soil (inferred based upon excess pore pressure generation). Ottawa sand samples were prepared at relative densities of 40% and 70%, while Bolsa Chica sand was tested at a relative density of 65%. Each sample was backpressure saturated at an effective confining stress of 100 kPa until the value of Skempton's B parameter was found to be greater than 0.95 (indicative of a degree of saturation greater than 99%) before loading the specimen at a rate of 0.5% axial strain per minute to a final strain of 15%.

### **Cyclic Simple Shear Testing**

To demonstrate the impact of desaturation on liquefaction potential, Ottawa 20-30 crystal silica sand was tested in cyclic simple shear at relative densities ( $D_R$ ) of 45% and 75% and degrees of saturation (S) of 100%, 99%, and 97%. Specimens 40 mm-tall were air pluviated into a latex membrane-lined stack of 100 mm-diameter stainless steel rings and purged with CO<sub>2</sub> for ten minutes. The specimens were then permeated with roughly

two pore volumes of de-aired water. An effective cell pressure of 50 kPa was applied and the specimens were backpressure saturated ( $S > 99\%$ ,  $B > 0.95$ ). Once saturated, an effective vertical pressure of 100 kPa was applied and the specimens were allowed to consolidate for 30 minutes. For the tests at  $S < 100\%$ , the saturated specimens were allowed to equilibrate for 30 minutes with a standpipe containing a predetermined volume of air to bring the soil-standpipe system to the desired degree of saturation (Lade and Pradel 1990). Cyclic stress controlled tests at a frequency of one Hertz were then performed at varying cyclic stress ratios (CSRs) in order to develop cyclic strength curves for each of the target  $S$  values. Liquefaction was defined in these tests as the point where the pore pressure ratio ( $r_u$ ) was equal to 1.0 (based on the at rest confining condition of the sand) and cyclic strains rapidly increased. The at rest earth pressure coefficient of the sand was determined to be approximately 0.56 based on changes in pore pressure during the application of vertical stress. A schematic diagram showing the experimental setup for these tests is presented in Figure 1.



**Fig. 1.** Experimental setup for cyclic simple shear testing at varying degrees of saturation

### Simple Shear Tests for Correlating P-Wave Velocity and Degree of Saturation

Another set of simple shear specimens were generated to correlate the degree of saturation to the velocity of compression waves (P-waves) in soil. Simple shear specimens were prepared at a relative density ( $D_r$ ) of 45% using specialized pedestal and top caps containing bender elements capable of measuring both P-wave velocity and shear wave (S-wave) velocity. Specimens were prepared at five different degrees of saturation: 100%, 97.5%, 90%, 60% and 0%. The  $S=100\%$  specimen was backpressure saturated to  $B > 0.95$ . The specimen at  $S = 97.5\%$  was generated by permeating the soil from the bottom without applying any backpressure and measuring the volume of water added to the soil. The 90% saturation specimen was made by premixing the appropriate amounts of soil and water in a bowl and then tamping them into the simple shear ring stack to a relative density of 45%.

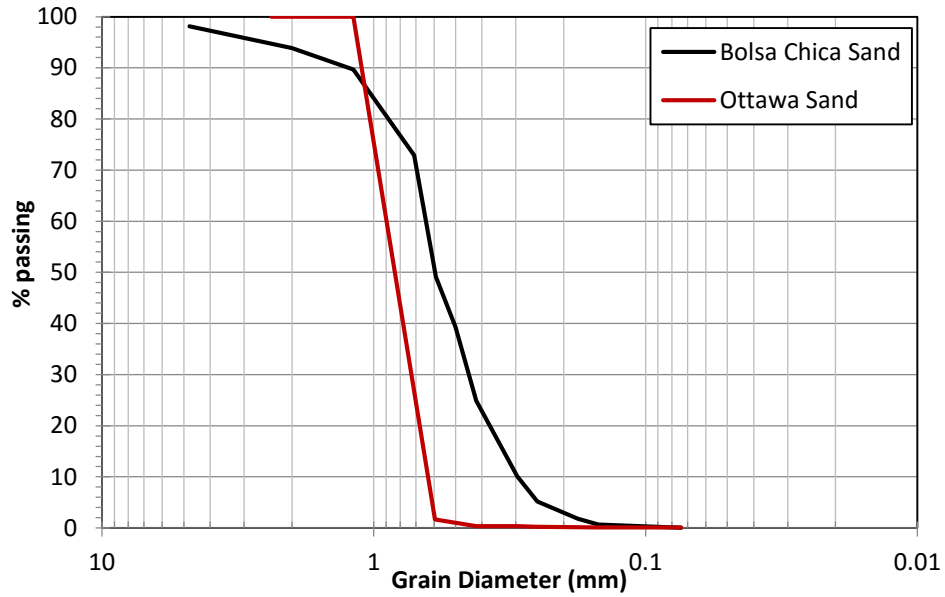
The specimen at 60% saturation was prepared by allowing a saturated specimen to drain under gravity for fifteen minutes. The P-wave velocity of each of these specimens was then measured at four different confining stresses (3 kPa, 20 kPa, 50 kPa, 100 kPa) to produce a relationship between degree of saturation, P-wave velocity, and confining stress. The shear wave velocity of the dry Ottawa sand ( $D_r = 45\%$ ) was also determined with varying confining stress. A similar specimen was generated using dry Bolsa Chica sand ( $D_r = 65\%$ ) to determine the relationship between S-wave velocity and confining stress in this soil.

## **RESULTS**

### **Soil Index Properties**

As noted previously, Ottawa 20-30 Crystal Silica sand (Ottawa sand) consists of 99.8% silica. Ottawa sand has a specific gravity of 2.65 (Ojuri and Fijabi 2012). The natural beach sand from Bolsa Chica State Beach in Huntington Beach, California (Bolsa Chica sand) was found to contain 1.85% carbonates. The specific gravity of the Bolsa Chica sand was assumed also to be 2.65.

The grain size distributions for both soils (Ottawa sand and Bolsa Chica sand) are shown below in Figure 2. As shown in Figure 2, The Ottawa sand is both slightly coarser, and slightly less well graded than the Bolsa Chica sand. Neither sand contains any measurable amount of fine grained particles ( $D < 0.074$  mm). The minimum and maximum void ratios for each sand as well as the coefficient of uniformity ( $C_u$ ), coefficient of curvature ( $C_c$ ), and the Unified Soil Classification System (USCS) classification are presented in Table 1 below.



**Fig. 2.** Grain size distribution for Ottawa sand and Bolsa Chica sand

**Table 1.** Minimum and maximum void ratios as well as the coefficient of uniformity, coefficient of curvature, and USCS soil classification for the Ottawa and Bolsa Chica sands.

Soil	$e_{min}$	$e_{max}$	Cu	Cc	USCS classification
<b>Ottawa 20-30</b>	0.502*	0.742*	1.45	0.903	SP
<b>Bolsa Chica</b>	0.670	0.887	2.17	1.01	SP

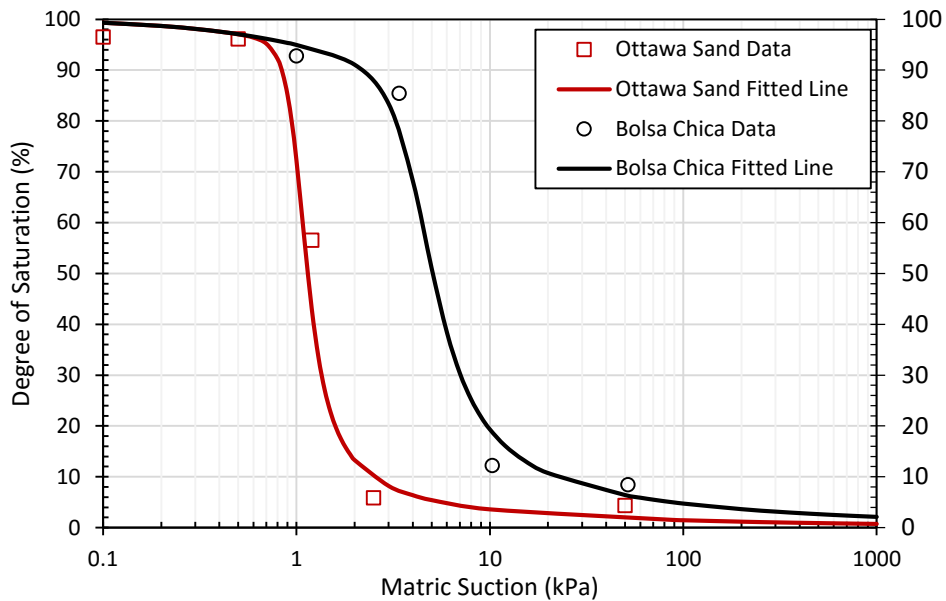
\*From Santamarina and Cho (2001)

As shown in Table 1, the Bolsa Chica sand has a higher minimum and maximum void ratios than the Ottawa sand. This indicates that the Bolsa Chica sand particles are more angular than the Ottawa sand particles, as more angular soils generally display less dense particle packing behavior (Cho et al. 2006). Visual inspection of both soils as well as

inspection under a scanning electron microscope confirmed that the Bolsa Chica sand is more angular than the Ottawa sand. Both soils are classified as poorly graded sands (SP).

### Soil-Water Characteristic Curve

Figure 3 below shows the soil water characteristic curves for both the Ottawa sand ( $D_r = 50\%$ ) and Bolsa Chica sand ( $D_r = 60\%$ ).



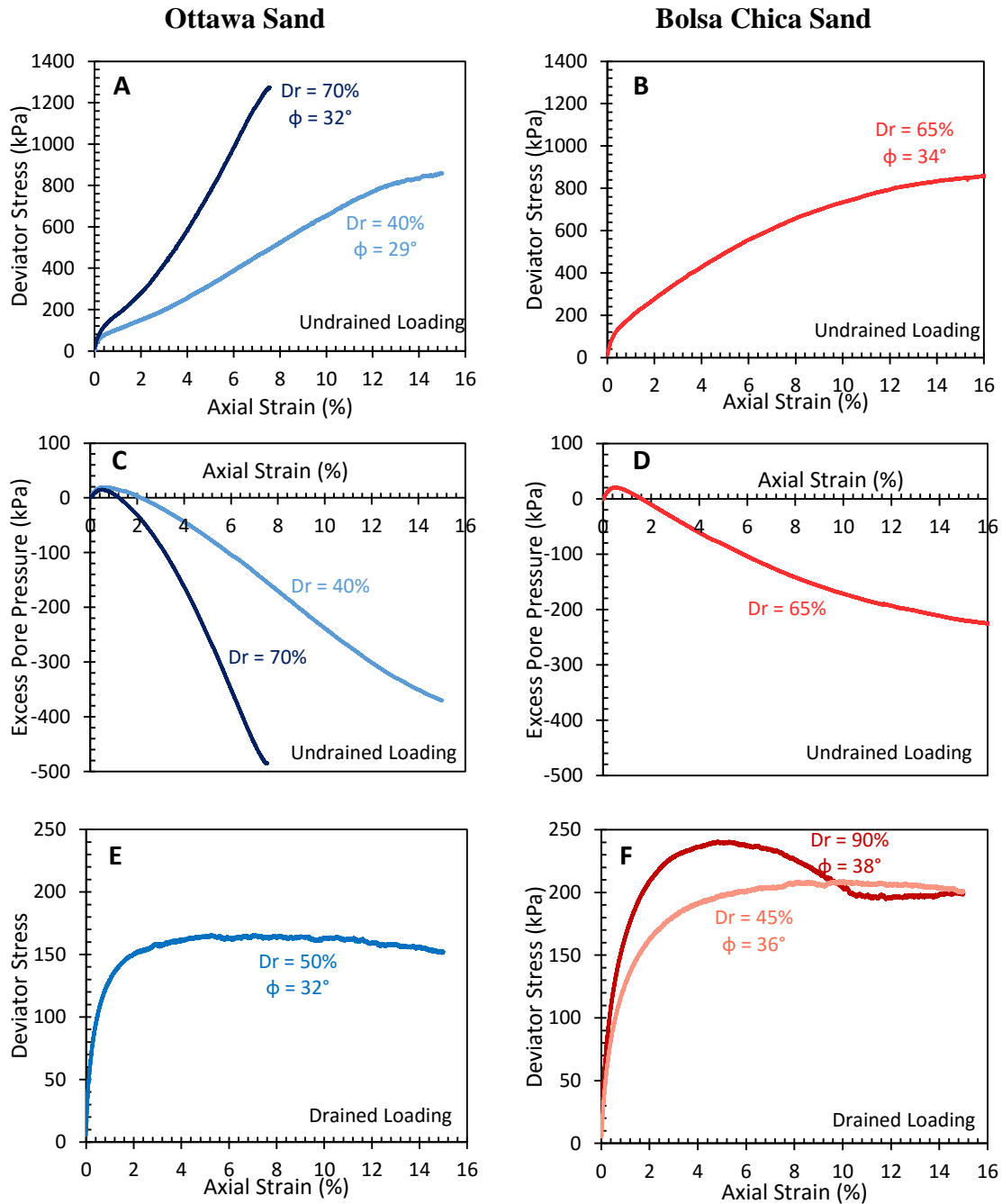
**Fig. 3.** Soil water characteristic curves for Ottawa sand ( $D_r = 50\%$ ) and Bolsa Chica sand ( $D_r = 60\%$ ).

As shown in Figure 3, the Ottawa sand exhibits lower suction values at the same degree of saturation when compared to the Bolsa Chica sand. This makes sense as the Bolsa Chica sand is finer grained than the Ottawa sand, and thus more likely to retain moisture. The air entry value for the Ottawa sand was found to be 0.85 kPa, at a degree of saturation of 95%, while the air entry value for the Bolsa Chica sand was found to be 2.8 kPa at a degree of saturation of 91%. The residual degree of saturation for the Ottawa sand is roughly 0.5%,

while the residual degree of saturation for the Bolsa Chica sand was found to be closer to 3%. The residual degree of saturation was taken as the degree of saturation at 1000 kPa suction. It should be noted that, while the SWCC's are useful for characterizing the properties of the test soils subjected to desaturation due to drying, these properties may not be applicable to conditions in which the soil is desaturated via biogas production from denitrification. It is expected that the pressure difference between the gas phase and liquid phase in soil desaturated with biogas will be a function of the size of bubbles produced in the soil. According to the Young-Laplace equation, the pressure difference between the gas inside of a spherical bubble and the surrounding liquid should be a function of the bubble radius and the surface tension of the interface between the gas and the liquid. The pressure differential will be greater for smaller bubble sizes (Wang and Fredlund 2003). As an example, for a bubble of air in pure water at a temperature of 25°C, the pressure differential between the inside and outside of the bubble would be 0.3 kPa for a bubble 1 mm in diameter, 3 kPa for a bubble 0.1 mm in diameter, and 30 kPa for a bubble 0.01 mm in diameter. However, this pressure differential between pore gas and pore fluid may not result in any matric suction, as bubbles produced via denitrification would most likely be occluded, meaning that the pressure differential between the gas and liquid phase would not act on the soil skeleton.

### **Triaxial Testing**

The triaxial data for both the Ottawa sand and the Bolsa Chica sand under drained and undrained conditions are presented in Figure 4.



**Fig. 4.** Triaxial Data for both soils. Deviator stress and excess pore pressure vs. axial strain for Ottawa sand (A, C) and Bolsa Chica sand (B, D) from undrained triaxial testing at an effective confining stress of 100 kPa. Deviator stress versus axial strain for Ottawa sand (E) and Bolsa Chica sand (F) from drained testing at an effective confining stress of 75 kPa. Friction angles shown are apparent friction angles assuming zero cohesion.

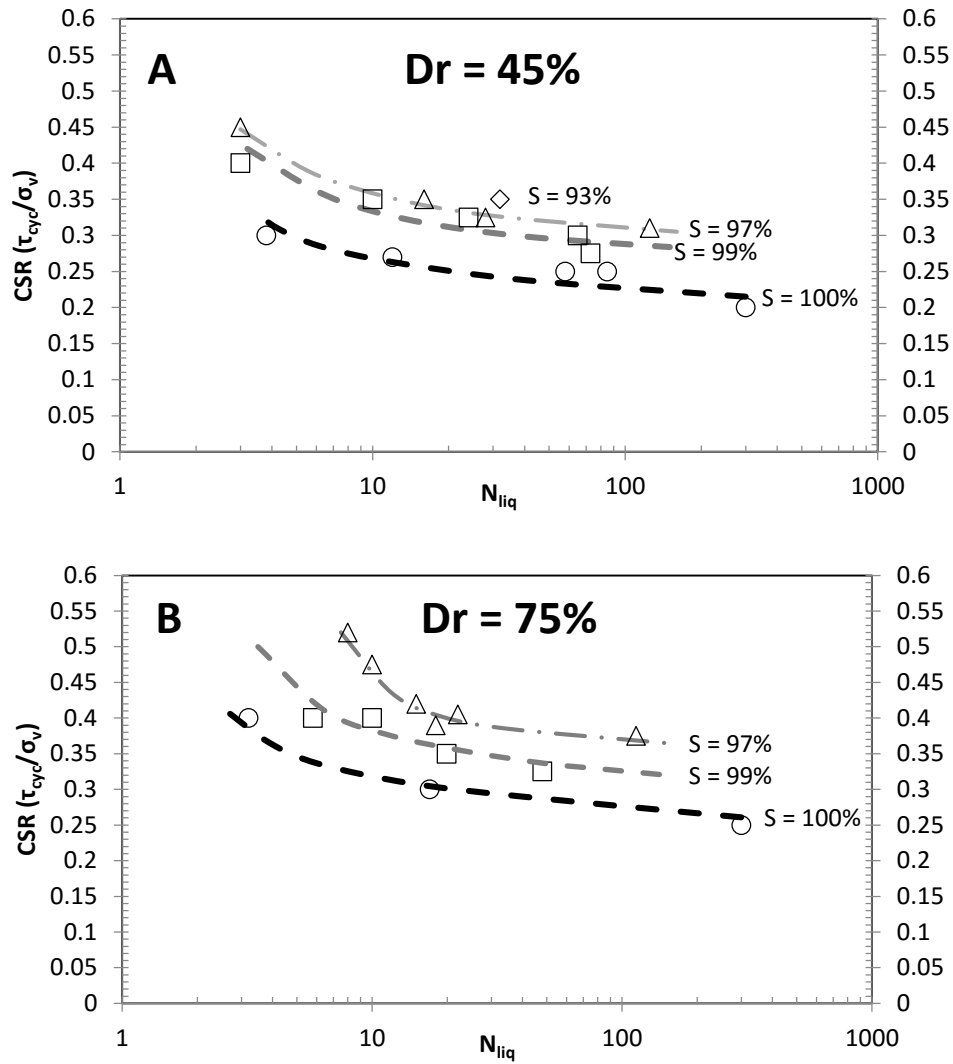


As shown in Figure 4A and 4B, the Bolsa Chica sand displays a higher undrained friction angle than the Ottawa sand at similar relative densities. However, the Bolsa Chica soil displays a lower undrained strength than the Ottawa sand at a similar relative density. Figures 4C and 4D show that the Ottawa sand is considerably more dilatant than the Bolsa Chica sand at similar relative densities. These results (lower undrained strength, less dilatant) indicate that the Bolsa Chica sand is more likely to liquefy in an earthquake event than the Ottawa sand. This is most likely due to the fact that the Bolsa Chica sand is more angular and displays a wider range in density than the Ottawa sand (Table 1). Figures 4E and 4F show that the Bolsa Chica sand is slightly stronger under drained conditions than the Ottawa sand. This result supports the assumption that the Bolsa Chica sand is more angular than the Ottawa sand, as more angular soils display higher friction angles (Cho et al. 2006).

### **Cyclic Simple Shear Testing and Correlation of P-Wave Velocity with Saturation**

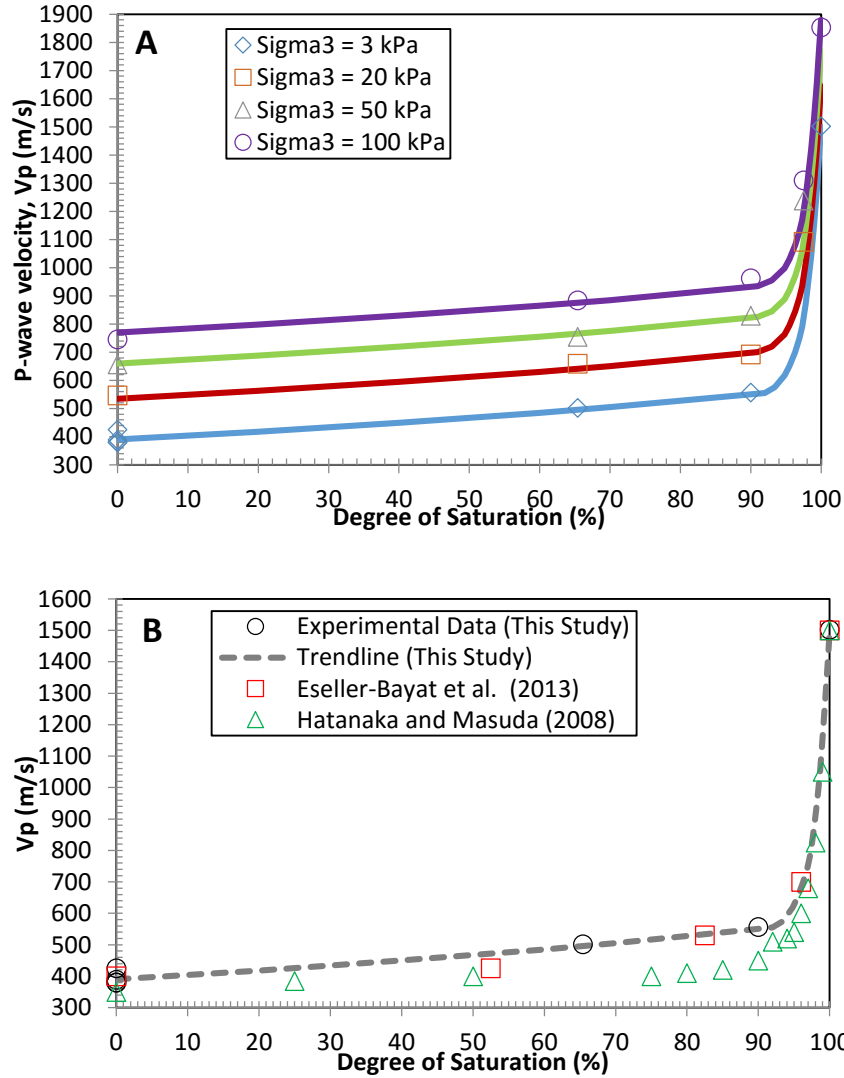
Figure 5 shows the cyclic strength of Ottawa 20-30 sand at relative densities of 45% and 75% and varying degrees of saturation. As shown in Figure 5, the cyclic resistance of the Ottawa sand improves significantly with decreasing degree of saturation at relative densities of 45% and 75%. In both cases, decreasing the degree of saturation from 100% to 97% leads to a corresponding increase in the cyclic resistance of roughly 40%. However, further desaturation does not lead to a significantly larger increase in cyclic resistance, as shown by the only slight increase in cyclic resistance obtained by dropping the degree of saturation from 97% to 93% (Figure UA). These results indicate that even small amounts of desaturation can lead to significant improvement in the liquefaction resistance of a soil,

but that there may be a limit to the degree of improvement due to relatively small amounts of desaturation.



**Fig. 5.** Cyclic strength curves for Ottawa 20-30 sand at relative densities of 45% (A) and 75% (B) and degrees of saturation of 100%, 99%, 97%, and 93%.

Figure 6 shows the P-wave velocity ( $V_p$ ) versus the degree of saturation for samples of Ottawa 20-30 sand at a relative density of 45%.



**Fig. 6.** P-wave velocity versus degree of saturation for Ottawa 20-30 sand at a relative density of 45% and confining stresses of 3, 20, 50, and 100 kPa (A). Data from this study compared to literature values at low confining stresses (B).

As shown in Figure 6A, the P-wave velocity increases slightly between a degree of saturation of 0% and 95%, but then increases much more rapidly between a degree of saturation of 95% and 100%. Also, the P-wave velocity generally increases with increasing confining stress. In general, at low confining stress, the P-wave velocity approaches that

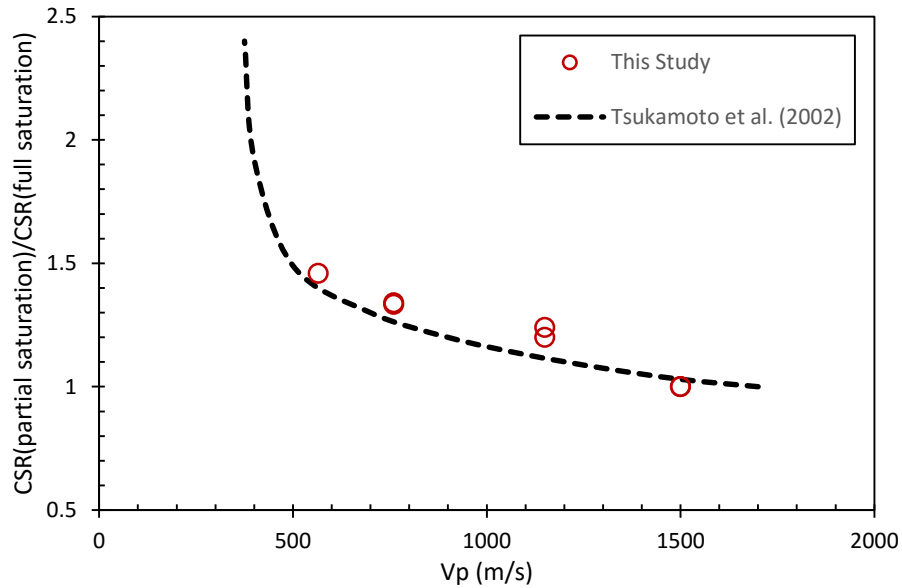
of water at a degree of saturation of 100%. This data indicates that P-wave velocity could be a useful way of measuring the degree of saturation between 95% and 100% saturation.

As shown in Figure 6B, the data from this study matches data presented in Esseler-Bayat et al. (2013) and in Hatanaka and Masuda (2008) fairly well. The slight discrepancy between the data from this study and that presented in Hatanaka and Masuda (2008) can most likely be attributed to the type of sand used. Hatanaka and Masuda (2008) used Toyoura sand, Futsu sand, and Keisa sand, while Ottawa sand was used in this study. This also explains the generally good agreement between data from this study and Esseler-Bayat et al. (2013), as Ottawa 20-30 sand was used in both studies.

It should be noted, however, that the data presented in this study does not match that presented by Valle-Molina and Stokoe (2012), which suggests that P-wave velocity should not increase until degrees of saturation of 99.7% or higher are reached. However, Valle-Molina and Stokoe (2012) did not directly measure the degree of saturation in their soil specimens and instead relied upon correlations with Skempton's B-value. The tests performed in this study, as well as those performed by Esseler-Bayat (2013) and Hatanaka and Masuda (2008) were performed on specimens in which degree of saturation was measured directly, either by measuring the amount of water expelled through the introduction of gas bubbles, or the amount of water added due to the application of pore pressure. As such, the data from Esseler-Bayat (2013) and Hatanaka and Masuda (2008) was found to be more comparable to the data obtained in this study.

Using Figures 5 and 6, a plot of cyclic stress ratio inducing liquefaction normalized by the cyclic shear strength of a saturated specimen versus P-wave velocity was created and plotted against data from Tsukamoto et al. (2002). This plot is presented in Figure 7. The

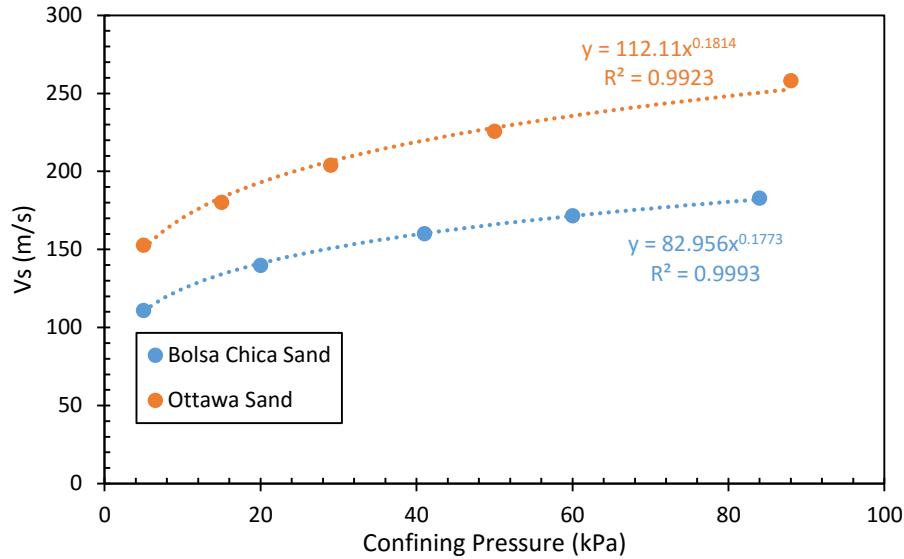
cyclic stress was taken at  $N_{liq} = 20$  as this value was taken by Tsukamoto et al. (2002) as a representative cyclic strength for characterizing the soil liquefaction resistance



**Fig. 7.** Normalized cyclic resistance at  $N_{liq} = 20$  for partially saturated Ottawa sand ( $D_r = 45\%$  and  $75\%$ ) versus P-wave velocity as compared to literature values for Toyoura sand ( $D_r = 40 - 70\%$ ) from Tsukamoto et al. (2002).

As shown in Figure 7, the data from this study matches the data from Tsukamoto et al. (2002) very closely, although it does show slightly greater improvement with decreasing P-wave velocity. The slight discrepancy between the two data sets may have to do with the type of sand used (Ottawa 20-30 vs. Toyoura sand). As shown in Figure 6B, Toyoura sand tends to have lower P-wave velocities at similar degrees of saturation when compared to Ottawa sand. This would effectively cause the Ottawa sand data to plot slightly to the right of the Toyoura sand data points in Figure 7.

Figure 8 below shows the relationship between shear wave velocity and confining stress for both soils.



**Fig. 8.** Shear wave velocity ( $V_s$ ) versus confining stress for dry Ottawa sand at a relative density of 40% and dry Bolsa Chica sand at a relative density of 65%.

As shown in Figure 8, the Ottawa sand exhibits higher shear wave velocities at all confining stresses. Additionally, the Ottawa sand displays a greater increase in shear wave velocity with confining pressure than the Bolsa Chica sand. This makes sense as the Ottawa sand displays denser packing than the Bolsa Chica sand (Table 1).

## CONCLUSION

The baseline properties of the Ottawa 20-30 sand and Bolsa Chica sand used in the denitrification experiments were quantified. While both sands are classified as poorly graded sands (USCS classification SP), the Bolsa Chica sand is slightly finer and slightly better graded. These characteristics give the Bolsa Chica soil slightly higher capillarity when compared to the Ottawa sand. The Bolsa Chica sand also displayed looser packing densities than the Ottawa sand, indicating that it is composed of more angular soil particles (as confirmed through visual inspection of the sand). The Bolsa Chica soil showed a

slightly higher undrained and drained friction angle than the Ottawa sand, further indicating the more angular nature of the Bolsa Chica soil. However, while the Ottawa sands exhibited dilative behavior at a relative density as low as 45% in undrained conditions under 100 kPa effective confining pressure, the Bolsa Chica soil was found to be less dilatant than the Ottawa sand, an observation attributed to looser packing density.

Cyclic direct simple shear testing of Ottawa sand at various degrees of saturation indicate that the cyclic resistance of the sand increases significantly with very small decreases in the degree of saturation. This indicates that small amounts of desaturation can lead to significant liquefaction mitigation. Finally, the P-wave velocity was found to be strongly correlated to the degree of saturation of Ottawa sand above a degree of saturation of 95%, indicating that it could be a useful way to quantify the degree of saturation in this range.

## CHAPTER 4

### LIQUEFACTION MITIGATION VIA MICROBIAL DENITRIFICATION: A LABORATORY STUDY USING SEMI-STAGNANT SOIL COLUMNS

#### INTRODUCTION

The characterization and abiotic testing of test soils presented in the previous chapter provides a baseline from which to demonstrate soil improvement via denitrification. This chapter presents the results of testing using semi-stagnant soil columns (i.e. columns subjected to periodic drainage and refilling with fresh media) to assess the ability of denitrifying microbes to improve the mechanical properties of the soil. More specifically, this chapter presents the results of biotic testing (i.e. with microbes) that demonstrates the ability of microbial denitrification to provide liquefaction resistance via desaturation and MICP.

#### MEANS AND METHODS

##### Initial Testing

In total, seventeen soil columns were employed in the semi-stagnant column testing. Twelve of these columns were prepared using dry Ottawa 20-30 sand air-pluviated to  $D_R = 30\%$  or  $40\%$ , while five of the columns were prepared using the natural beach sand from Bolsa Chica State Beach in Huntington Beach California, wet pluviated to  $D_R = 65\%$ . Eight of the Ottawa sand columns (OS-TRX-1, OS-TRX-2, OS-TRX-3, OS-TRX-4, OS-TRX-5, OS-TRX-6, OS-TRX-7, OS-TRX-8) and three of the Bolsa Chica columns (BC-TRX-1, BC-TRX-2, BC-TRX-3) were prepared using 70 mm-diameter triaxial base and top caps with imbedded bender elements for S-wave velocity measurements. Two of the

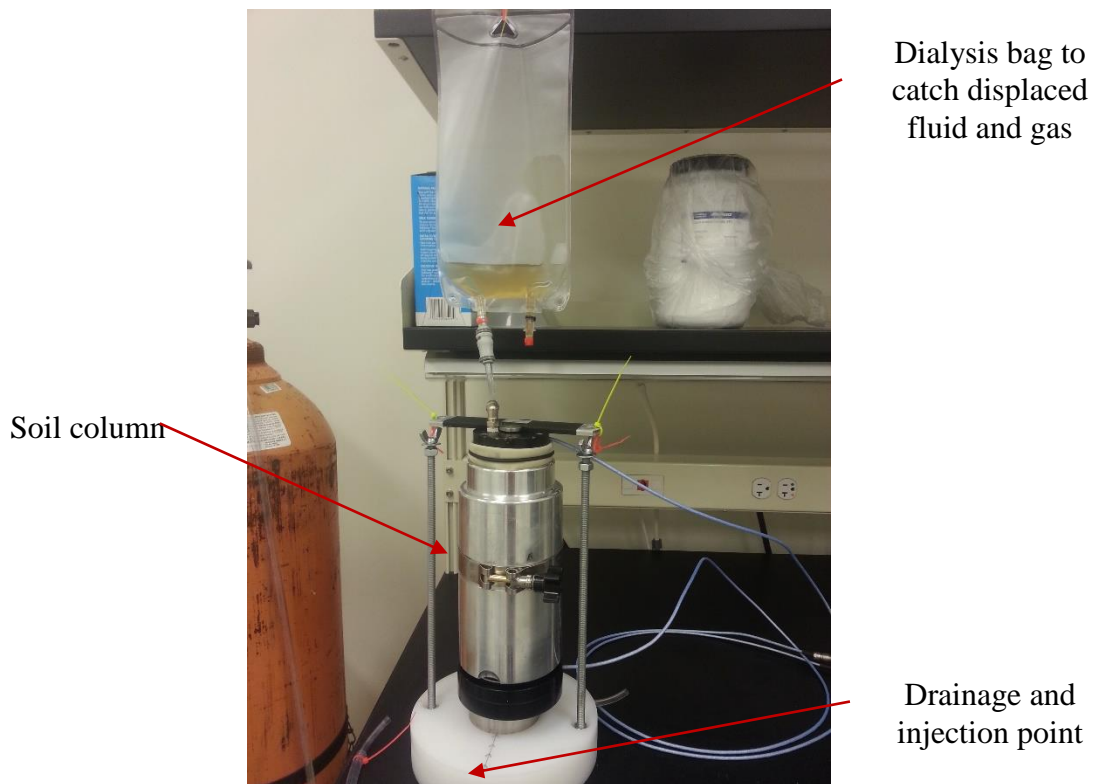


Ottawa sand columns (OS-SS-1 and OS-SS-2) were prepared using 100 mm-diameter simple shear base and top caps with embedded bender elements for measurement of both P- and S-wave velocities. Each of the triaxial and simple shear columns was encased in a latex membrane lined rigid jacket under very low overburden stress (weight of top cap) for the duration of treatment so that they could be subsequently moved into soil testing equipment. Two Ottawa sand columns (OS-ACR-1, OS-ACR-2) and two Bolsa Chica columns (BC-ACR-1, BC-ACR-2) were prepared in 150 mm-tall, 73 mm-diameter acrylic columns equipped with a drainage port at the base, a gas collection port at the top, and sampling ports located 5 cm from the base and 2.5 cm from the top. Prior to setting up the columns, the pedestals, top caps, membranes, and all acrylic column surfaces were alcohol sterilized (70% v/v ethanol) and the sand was autoclaved. After pluviation, the columns were flushed from the top with nitrogen gas ( $N_{2(g)}$ ) to minimize oxygen ( $O_{2(g)}$ ) in the soil pores and facilitate denitrification.

Thirteen of the columns (OS-TRX-1, OS-TRX-2, OS-TRX-3, OS-TRX-4, OS-TRX-5, OS-TRX-6, OS-TRX-7, OS-TRX-8, OS-SS-1, OS-SS-2, OS-ACR-1, BC-TRX-2, BC-ACR-1) were inoculated with a mixed culture of bacteria grown from natural sand and water collected from Bolsa Chica State Beach in Huntington Beach, CA. The inoculum was grown by mixing 2 g of Bolsa Chica sand, 5 mL of Bolsa Chica water, and 95 mL of a solution containing 20 g/L nutrient broth (Difco, BD Brand), 12.5 mM  $Ca(NO_3)_2$ , and 12.5 mM  $Ca(CH_3COO)_2$  in deionized (DI) water and then incubating the mixture for five days at 30°C. A separate solution consisting of 25 mM  $Ca(NO_3)_2$ , 50 mM  $Ca(CH_3COO)_2$ , 2 mM  $MgSO_4$ , and 125 mM anhydrous  $CaCl_2$  was prepared to serve as the pore fluid in each column. The pore fluid solution also received 0.5 mL/L of a trace metals solution

consisting of 0.5% (w/v)  $\text{CuSO}_4$ ,  $\text{FeCl}_3$ ,  $\text{MnCl}_2$ ,  $\text{Na}_2\text{MoO}_4 \cdot 2\text{H}_2\text{O}$  to promote microbial growth in the columns. The solution was adjusted to a pH of approximately 8 using 1 M NaOH. The thirteen inoculated columns were injected with 30 mL of the bacterial culture prior to saturation with the pore fluid solution. The remaining columns were simply filled with pore fluid solution. Pore fluid solution was slowly added to each column via the bottom port until fluid began to exit the top cap (roughly 230 mL for TRX and ACR columns, 120 mL for SS columns).

After filling the columns, dialysis bags were connected to the top caps to collect gas and displaced fluid produced during denitrification. Figure 9 shows a typical column set up.



**Fig. 9.** Typical column setup

The pore fluid in all columns was drained at approximately two week intervals and refilled with fresh pore fluid up to 30 times. While draining, the pore fluid in the columns was replaced with N<sub>2(g)</sub> so that the columns remained anaerobic. For each refilling interval, the concentration of NO<sub>3</sub><sup>-</sup> and acetate in the pore fluid was slowly raised while keeping the ionic strength and calcium (Ca<sup>2+</sup>) concentration of the added solution constant. Tryptic Soy Broth (Fluka Analytical) and K<sub>2</sub>HPO<sub>4</sub> were also added in very minimal amounts after twelve weeks of treatment to further promote microbial growth in the soil columns. Table 2 contains a detailed account of pore fluid characteristics for the duration of testing (67 weeks).

**Table 2.** Pore fluid properties for the duration of testing.

Treatment number	Date	[CaCl <sub>2</sub> ] (mM)	[Ca(NO <sub>3</sub> ) <sub>2</sub> ] (mM)	[Ca(CH <sub>3</sub> COO) <sub>2</sub> ] (mM)	[MgSO <sub>4</sub> ] (mM)	[K <sub>2</sub> HPO <sub>4</sub> ] (mM)	[TSB] (g/L)	pH
1	6/12/2014	125	25	50	2	0	0	8.33
2	6/28/2014	112.5	37.5	50	2	0	0	7.97
3	7/17/2014	100	50	50	2	0	0	7.69
4	8/3/2014	100	50	50	2	0	0	7.93
5	8/25/2014	125	25	50	2	0	0	8.21
6	9/7/2014	125	25	50	2	0	3	6.21
7	9/20/2014	115	30	60	2	0	1.5	7.96
8	10/3/2014	87.5	37.5	75	2	0	0.75	7.94
9	10/16/2014	87.5	37.5	75	2	0.4	0	8.18
10	10/30/2014	87.5	37.5	75	2	0.4	0	8.13
11	11/13/2014	137.5	37.5	75	2	0	1.5	8.02
12	11/25/2014	137.5	37.5	75	2	0	1.5	8.08
13	12/11/2014	130	40	80	2	0	1.5	8.11
14	1/7/2015	122.5	42.5	85	2	0	1.5	8.12
15	1/22/2015	115	45	90	2	0	1.5	8.25
16	2/5/2015	107.5	47.5	95	2	0	0.75	8.11
17	2/20/2015	100	50	100	2	0	0.75	8.17
18	3/6/2015	100	50	100	2	0	0.75	7.94
19	3/24/2015	100	50	100	2	0	0.75	7.76
20	4/7/2015	100	50	100	2	0	0.75	8.01
21	4/21/2015	100	50	100	2	0	0.75	8.06
22	5/5/2015	100	50	100	2	0	0.75	8.07
23	5/19/2015	100	50	100	2	0	0.75	8.04
24	6/2/2015	100	50	100	2	0	0.75	8.08
25	6/16/2015	100	50	100	2	0	0.75	8.11
26	7/1/2015	100	50	100	2	0	0.75	8.09
27	7/21/2015	100	50	100	2	0	0.75	8.47
28	8/4/2015	100	50	100	2	0	0.75	8.04
29	8/18/2015	100	50	100	2	0	0.75	8.26
30	9/1/15	100	50	100	2	0	0.75	8.53

The Ottawa sand triaxial columns were treated according to Table 2 for various lengths of time, ranging from 10 to 67 weeks in order to achieve various carbonate contents in each column. The simple shear columns were treated according to Table 2 for 12 and 23 weeks to achieve different levels of carbonate precipitation. The Bolsa Chica triaxial columns as well as all of the acrylic columns were treated for 67 weeks according to Table 2.

The degree of saturation in each column was evaluated in two ways: 1) in the SS columns, saturation was evaluated based upon the measured P-wave velocity and the curves in Figure 7 (Chapter 3); 2) in all columns, saturation was evaluated based upon the assumption that the volume of fluid displaced into the dialysis bag was equal to the volume of gas retained in the pores. This was considered a reasonable assumption, as the other products of treatment, calcium carbonate and biomass, are produced in fairly small volumes compared with the volume of fluid expelled from the columns (i.e. 1 g of calcium carbonate, a typical amount precipitated in a two week treatment interval, occupies just 0.37 mL of space, while anywhere from 20 – 40 mL of fluid may be expelled from the column in the same time period). Total gas production in each column was taken as the total change in volume (including gas and fluid) of the dialysis bag over each treatment interval.  $\text{CaCO}_3$  precipitation in each column was monitored in three ways. First, a sample of the pore fluid was taken at each draining interval, filtered through a 0.2  $\mu\text{m}$  screen, and tested using ion chromatography (Dionex ICS-2000) to obtain an ionic profile for the pore fluid ( $\text{Ca}^{2+}$ ,  $\text{Mg}^{2+}$ ,  $\text{Na}^+$ ,  $\text{K}^+$ ,  $\text{NH}_4^+$ ,  $\text{NO}_3^-$ ,  $\text{NO}_2^-$ ,  $\text{CH}_3\text{COO}^-$ ,  $\text{SO}_4^{2-}$ ,  $\text{Cl}^-$ ,  $\text{CO}_3^{2-}$ ). Mass balance based upon the monitored  $\text{Ca}^{2+}$  levels in the pore fluid before and after treatment and the total volumes of fluid removed and added during each refilling event was used to estimate the amount of  $\text{CaCO}_3$  precipitated in each column.  $\text{CaCO}_3$  content was also quantified in

many of the columns by taking as much of the sand as possible from the column at the end of testing, washing it with four pore volumes of DI water, drying it, weighing it, exposing it to strong acid (2 M HCl), rinsing it with DI water, and then drying and weighing the sample again. Effervescence of the samples upon addition of HCl was taken as evidence of the presence of carbonate. The difference in mass before and after acid treatment was taken as the mass of CaCO<sub>3</sub> in the sand sample. Finally, samples of treated sand from the ACR columns were imaged under a JEOL JSM-6701F field emission high-voltage scanning electron microscope (SEM) to look for visual evidence of the presence of calcium carbonate and the phase of calcium carbonate as well as the precipitation pattern of the carbonate in the soil.

S-wave velocity measurements taken in each column before and after treatment (and during treatment for SS columns) were used to monitor the evolution of the small strain stiffness of the soil with time and carbonate content. Following treatment, all of the columns were flushed with roughly four pore volumes of DI water to remove any residual salts. Consolidated undrained triaxial compression tests with pore pressure measurement were conducted on most of the triaxial columns (OS-TRX-1, OS-TRX-2, OS-TRX-3, OS-TRX-4, OS-TRX-5, OS-TRX-6, OS-TRX-7, OS-TRX-8, BC-TRX-1) and consolidated undrained cyclic simple shear tests were conducted on the simple shear columns. The triaxial columns were back pressure saturated ( $B > 0.95$ ) at a confining stress of 100 kPa and the simple shear columns were backpressure saturated ( $B > 0.95$ ) at an effective cell pressure of 50 kPa prior to testing. After saturation, the simple shear columns were subjected to a vertical effective stress of 100 kPa for 30 minutes before cyclic testing commenced. Stress controlled cyclic simple shear tests were performed at a frequency of

1 Hz, while triaxial compression testing was conducted at a strain rate of 0.5% per minute to a maximum strain of 15%. The results of the triaxial and simple shear tests were compared to similar tests performed on untreated soil. Four of the triaxial soil columns (OS-TRX-7, OS-TRX-8, BC-TRX-2, BC-TRX-3) were subjected to drained triaxial compression testing at a cell pressure of 75 kPa and a strain rate of 0.5% per minute to a maximum strain of 15%. The two triaxial columns that were subjected to both undrained and drained testing were first tested undrained until roughly 5% strain, when leaks developed in both of the columns, forcing testing to halt. Then, these columns were sheared under drained conditions to a maximum strain of 15%.

### **Testing of Reconstituted Specimens**

Following mechanical (triaxial and simple shear) testing of the specimens from the stagnant columns, the soil from columns OS-TRX-2, OS-TRX-3, and OS-SS-2 was bathed in acetone for ten minutes to dissolve microbial biomass and then heated (300°C) to remove any residual biomass on the soil particles. The treated sand was then reconstituted twice (OS-TRX-2, OS-SS-2), or three times (OS-TRX-3) to a relative density of 45% and subjected to the same undrained triaxial compression testing (TRX columns) or simple shear testing (SS columns) regimes described above. The S-wave velocity of column OS-TRX-3 was also evaluated at several confining stresses for each reconstitution to investigate the effects of multiple reconstitutions on the small strain stiffness of the soil.

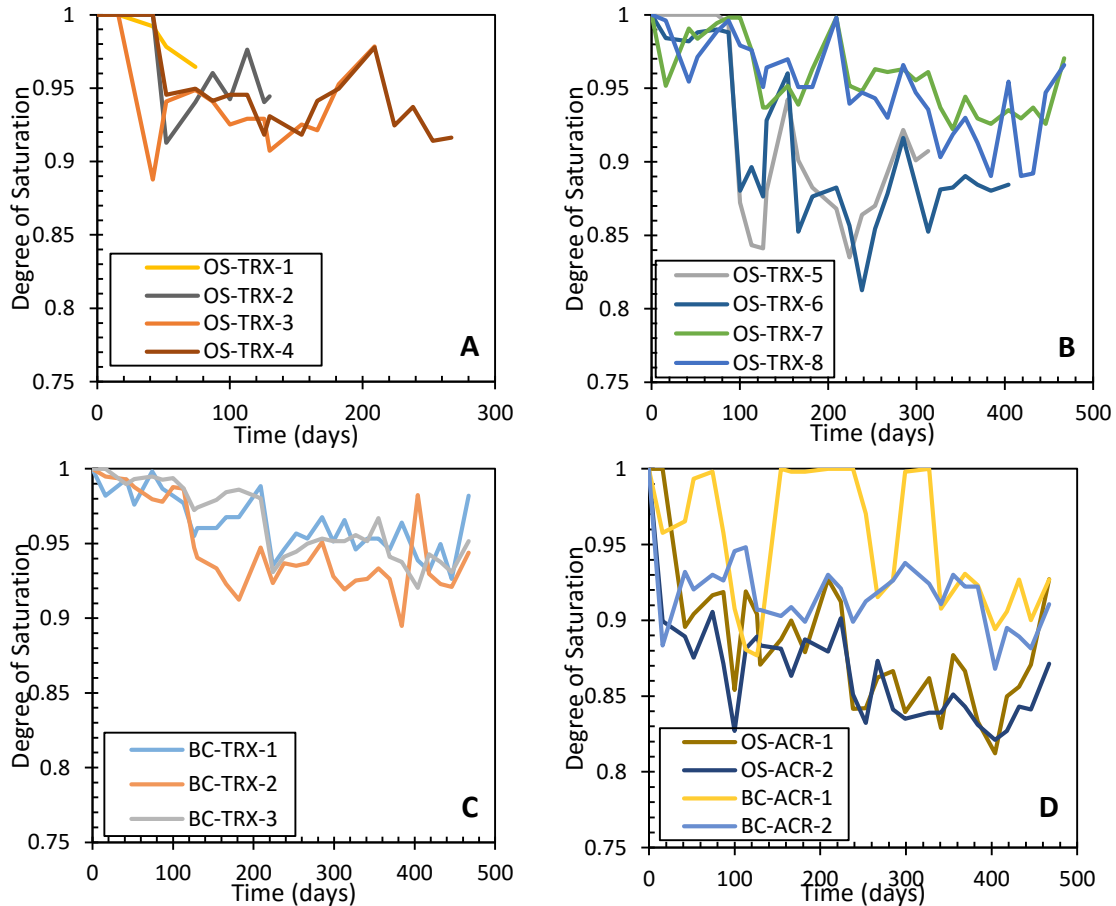
Following each reconstitution, a small sample of soil was taken and imaged under the SEM in order to look for visual evidence of changes in carbonate precipitate structure due to multiple reconstitutions. Following the reconstitution schedule, the sand from each column was digested with acid to quantify the carbonate content.

## RESULTS

### Initial Tests

#### *Desaturation*

The desaturation level evaluated from the dialysis bag measurements for the triaxial and acrylic columns are shown in Figure 10 below. The results from the simple shear columns are not presented, as slow leakage in both columns rendered the dialysis bag measurements inaccurate.



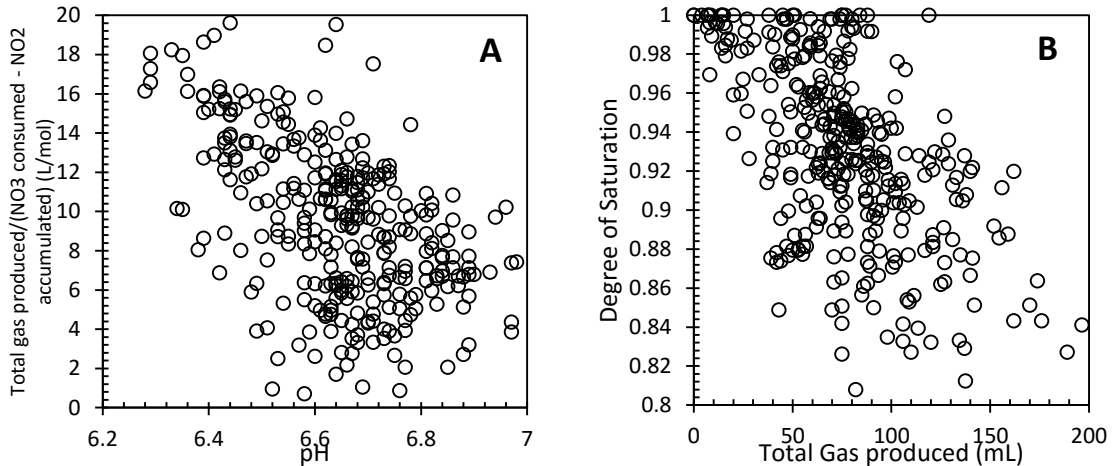
**Fig. 10.** Equilibrium degree of saturation in OS-TRX columns at initial relative densities of 40% (A) and 30% (B), BC-TRX columns (C) and ACR columns (D) with time as measured with the dialysis bag method.

As shown in Figure 10A, the degree of saturation in the OS-TRX columns at an initial relative density of 40% generally reached an equilibrium value of between 90% and 95% during each treatment cycle. In contrast, the degree of saturation in the OS-TRX columns at an initial relative density of 30% generally reached lower equilibrium degrees of saturation (85%- 95%) during each treatment cycle. This discrepancy may be due to the amount of fluid that was added to each column. The less dense columns (30% Dr) have more pore space. So, during each treatment cycle, more fluid could be added to these columns. This means that there was more substrate added to these columns from which the bacteria could generate gas.

The BC-TRX columns generally reached equilibrium degrees of saturation between 90% - 97% over the course of treatment (Figure 10C). Figure 10D shows that the OS-ACR columns generally reached much lower degrees of saturation (83% - 92%) during treatment, while the BC-ACR columns reached degrees of saturation of between 87% and 95%. It should be noted that Column BC-ACR-1 experienced slow leaks at various points in the treatment cycle, leading to what appears to be full saturation (due to lack of fluid in the dialysis bags, caused by leakage) at various points during treatment. In general, it appears that the Ottawa sand columns (OS) reached lower equilibrium degrees of saturation than the Bolsa Chica sand columns (BC). One reason for this may be that the BC sand has a higher residual degree of saturation than the Ottawa sand (Figure 3, Chapter 3). This means that during each draining cycle, less fluid was removed from the BC columns than the OS columns. Correspondingly, less fresh fluid was added at each treatment interval, meaning that there was less substrate for the microbes to generate gas in the BC columns.



The ACR columns also generally exhibited lower degrees of saturation than the TRX columns. One reason for this could be that the ACR columns consistently reached lower equilibrium pH values than the TRX columns (shown in Figure 14). Lower pH values mean that more dissolved inorganic carbon was present as  $\text{CO}_{2(\text{aq})}$ . This means that more  $\text{CO}_{2(\text{g})}$  was likely generated in these columns, contributing to the lower degrees of saturation. This trend is shown in Figure 11 below.

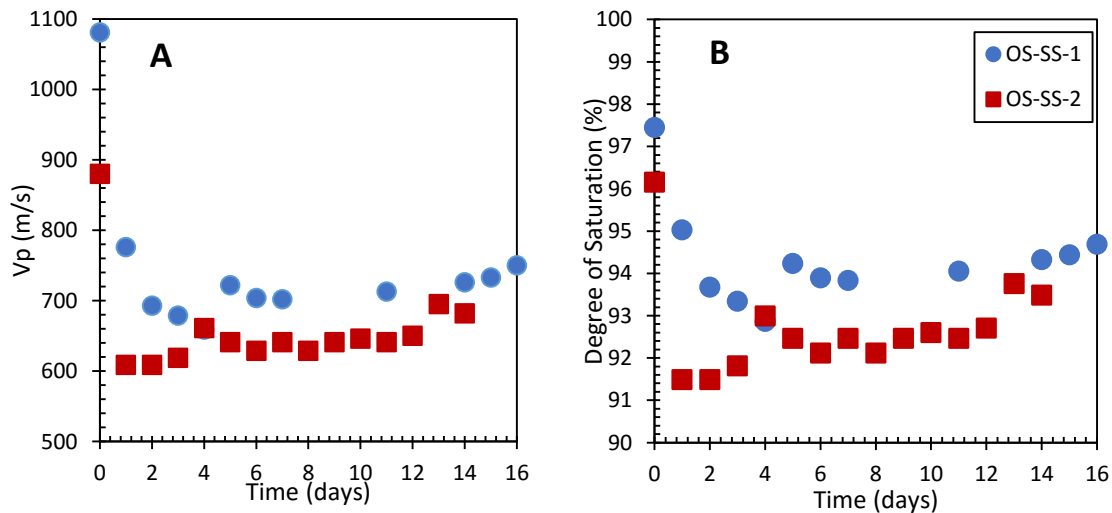


**Fig. 11.** Total gas volume per mol of nitrate reduced to nitrogen gas versus pH (A) and degree of saturation versus total gas volume (B) for all columns and all treatment cycles.

As shown in Figure 11A, the total gas produced per mol of nitrate reduced to nitrogen gas, which represents the amount of gas production normalized for the amount of biological activity in the column, generally decreases with increasing pH for all columns and all treatment cycles. Figure 11B shows that the equilibrium degree of saturation in each column and each treatment cycle generally decreases with increasing gas production. Together, these plots show that the degree of saturation decreases with increasing gas production, but also with decreasing pH.

Figure 10 suggests there is generally a downward trend in the degree of saturation with time. It is possible that this is due to the fact that  $\text{CaCO}_3$  is precipitating on particle surfaces, at particle contacts and in the void space of the columns. The carbonate essentially acts to trap gas bubbles in the soil and keep them from escaping (Li 2014). Another reason for the decrease in degree of saturation with time could be the accumulation of extracellular polymeric substances (EPS) generated by biomass in the columns. When EPS is produced in large quantities, it is known to trap and stabilize gas bubbles produced by microbes (Bengtson et al. 2009). As many of these soil columns were allowed to incubate for over a year, there was ample time for the microbes in the columns to generate significant amounts of EPS.

P-wave velocity and the correlated degree of saturation (based upon Chapter 3, Figure V) for typical treatment cycles from Column OS-SS-1 and Column OS-SS-2 are shown in Figure 12 below.

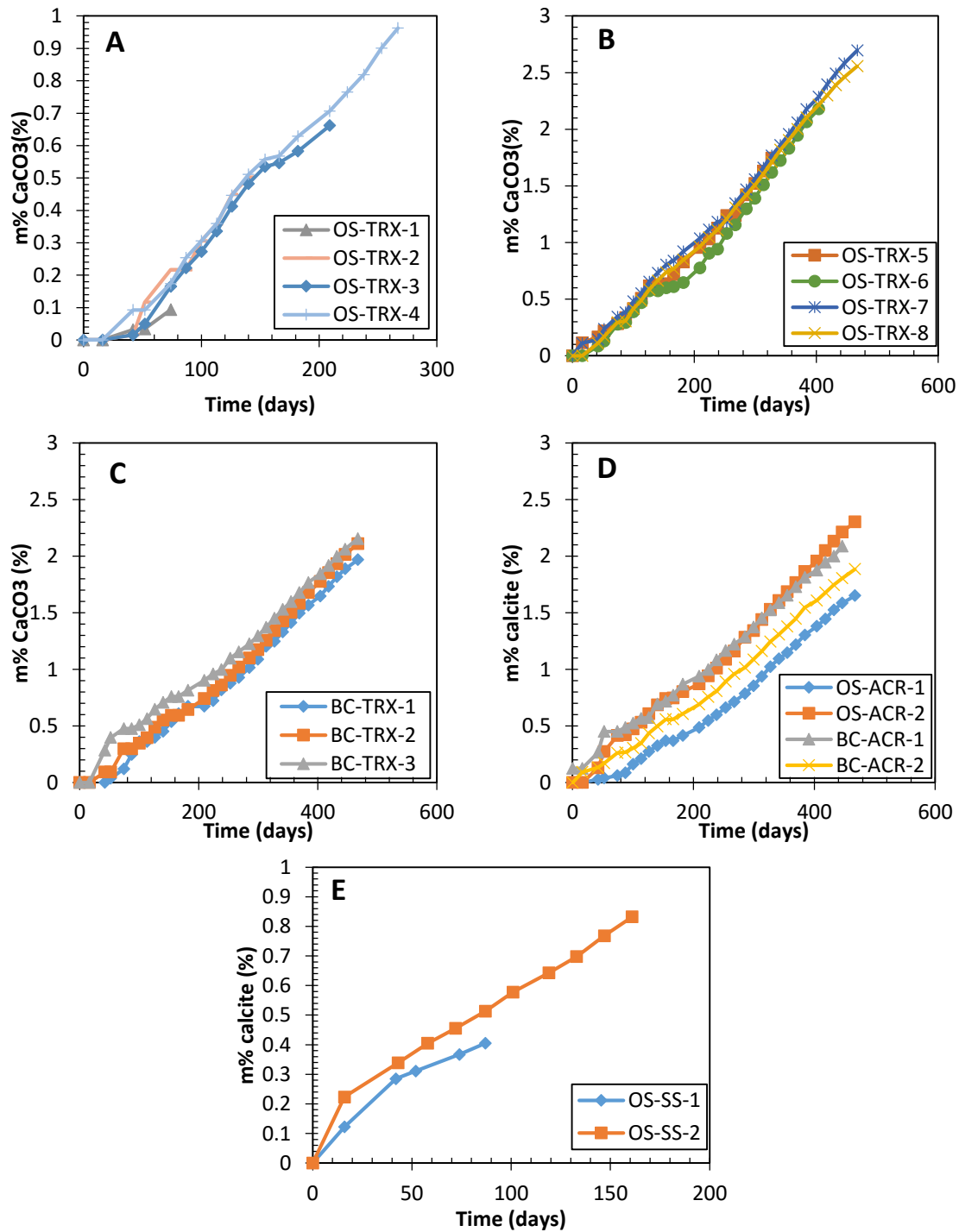


**Fig. 12.** P-wave velocity (A) and corresponding degree of saturation (B) for a typical treatment cycle in columns OS-SS-1 and OS-SS-2.

As shown in Figure 12A, in both column OS-SS-1 and OS-SS-2 the P-wave velocity quickly decreases within one to three days following the onset of a treatment cycle. Then, the P-wave velocities stabilize for the following eight to ten days, with a slight uptick after roughly twelve days of treatment. The degree of saturation in each column shows the same trend, with the equilibrium degree of saturation in both columns between 92% and 95%. These values are extremely consistent with the data for the other OS columns shown in Figure 10, indicating that P-wave velocity is a reasonably accurate way to monitor degree of saturation when the soil is between 90 – 100% saturated. The data in Figure 12 is also consistent with visual observations of the fluid level in the dialysis bags above the treated columns. The fluid level in each column rose quickly following treatment, followed by a period of relative stability, followed by a slow decrease in fluid level toward the end of each treatment cycle. These data together show that the soil columns desaturate rapidly after the onset of denitrification, stabilize while denitrification is ongoing, and then begin to slowly resaturate after biological activity slows down.

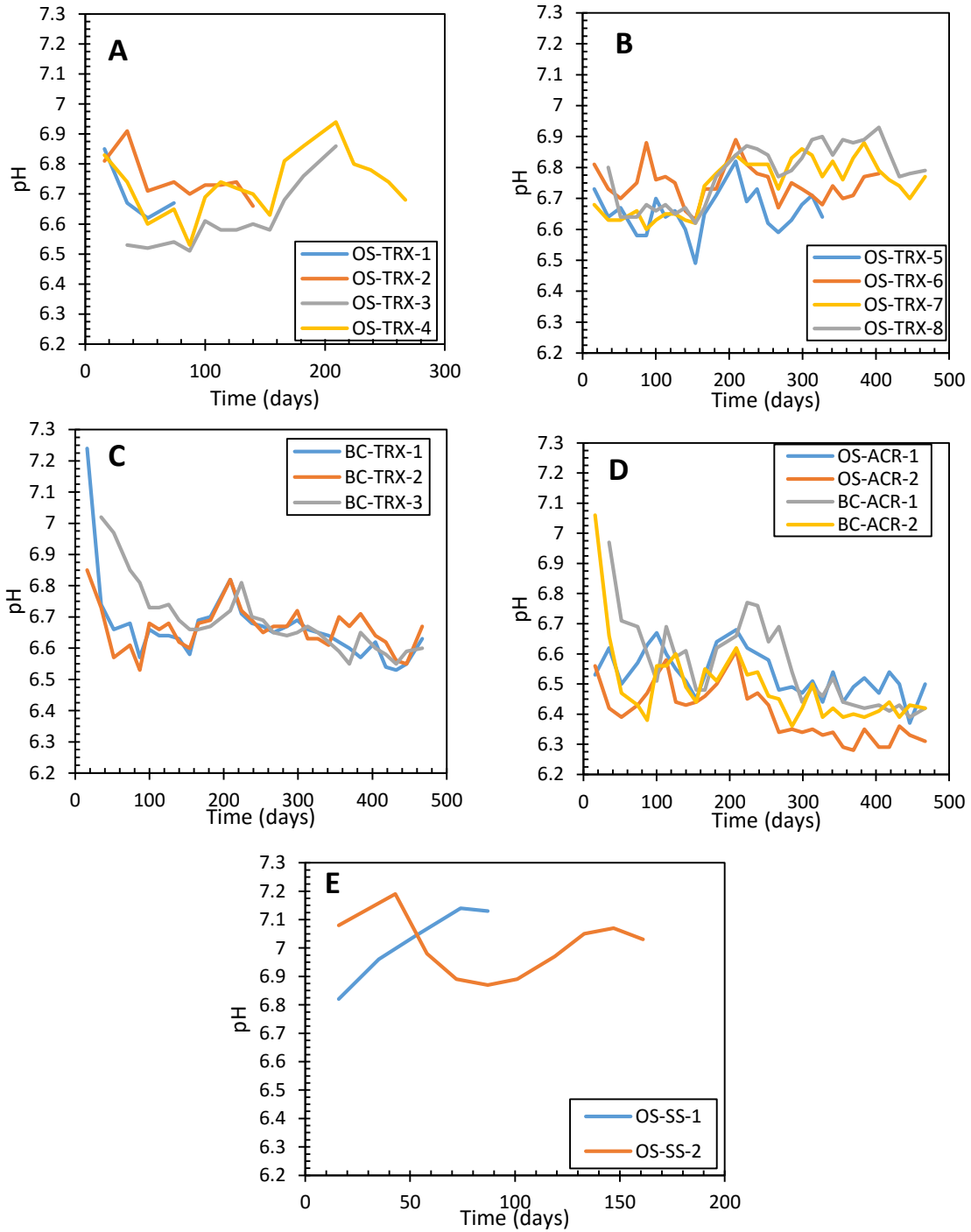
### *Carbonate Precipitation*

The calcium content evaluated from IC analysis and mass balance measurements on the pore fluid were used to determine the amount of  $\text{CaCO}_3$  precipitated in each column with time. These results are shown in Figure 13 below.



**Fig. 13.** Mass percentage calcium carbonate (m% CaCO<sub>3</sub>) versus treatment time for OS-TRX columns at Dr = 40% (A) and 30% (B), BC-TRX columns (C), ACR columns (D), and SS columns (E).

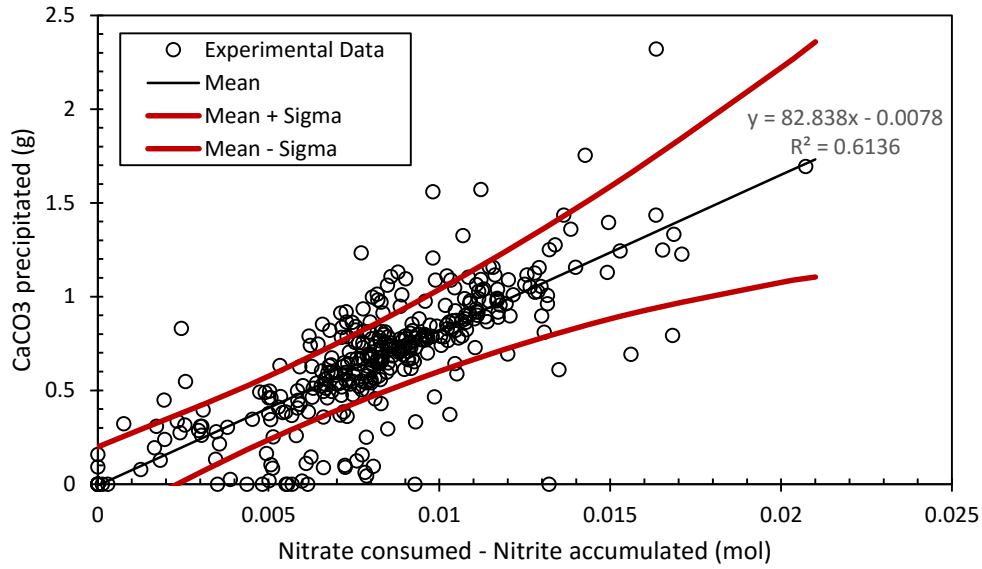
As shown in Figure 13, evaluation based upon the IC analysis and mass balance measurements indicate that the carbonate content in all of the columns increased relatively linearly with treatment time. However, as shown in Figure 13B and Figure 13C, it appears that, after the same amount of treatment time (467 days), less carbonate was precipitated in the BC-TRX columns than in the OS-TRX columns (2.1% versus 2.6% respectively). This is most likely due to the fact that the Bolsa Chica soil has a higher residual degree of saturation than the Ottawa sand (Chapter 3, Figure 3). This means that, every time the columns were drained, less fluid was removed from the BC columns than from the OS columns. Hence, less fresh fluid could be added to these columns, and less fresh fluid means less nutrients for the bacteria and less calcium to precipitate as  $\text{CaCO}_3$ . It is also interesting to note that, in general, less carbonate was precipitated in the ACR columns than in the TRX columns over the same treatment time. This is most likely due to the lower equilibrium pH values in the ACR columns when compared to the TRX columns (Figure 14). In general, the rate of precipitation in the SS columns was slightly higher than the TRX columns. This is most likely the result of higher equilibrium pH values in the SS columns (Figure 14). It should also be noted that, in general, the rate of precipitation in all of the columns is fairly slow (only 1.5 – 2% per year). However, it is possible that the rate of precipitation in these experiments was controlled to some extent by the frequency of pore fluid replenishment (i.e. fresh fluid every two weeks) rather than the rate of biological activity in the columns, which was limited by the availability of nutrients.



**Fig. 14.** Equilibrium pH versus time for OS-TRX columns at  $D_r = 40\%$  (A),  $D_r = 30\%$  (B), BC-TRX columns (C), ACR columns (D), and SS columns (E).

As shown in Figure 14, the OS-TRX columns maintained a relatively steady pH of between 6.5 and 6.9 for the duration of testing. Similarly, the BC-TRX columns maintained a steady equilibrium pH of between 6.5 and 6.8 for the duration of testing. The ACR columns generally reached an equilibrium pH of between 6.2 and 6.6, while the SS columns generally reached a pH of anywhere from 6.8 to 7.2. It is unclear why the ACR columns generally equilibrated at lower pH values after each treatment cycle, or why the SS columns generally equilibrated at higher pH values after each cycle than the TRX columns. However, the implications are clearly shown in Figure 11, Figure 12, and Figure 13 above. The ACR columns displayed slower rates of precipitation but lower degrees of saturation (Fig. 13, 10) due to lower equilibrium pH values, inhibiting carbonate precipitation and favoring the off-gassing of  $\text{CO}_{2(g)}$ . The SS columns generally showed higher rates of carbonate precipitation but slightly higher degrees of saturation (Fig. 13, 12) due to higher equilibrium pH values which favor carbonate precipitation and lower the amount of  $\text{CO}_{2(g)}$  production.

Figure 15 shows the relationship between carbonate production (based on IC measurements and mass balance) and the amount of denitrification in all of the columns for each treatment cycle (also determined through IC analysis). As shown in Figure 15, on average 83 grams of carbonate (or 0.83 mol of  $\text{CaCO}_3$ ) are precipitated for every mol of nitrate reduced to nitrogen gas. In contrast, ureolysis has an efficiency of roughly one mol of carbonate precipitate per mol of urea consumed (Hamdan 2015). This means that denitrification with acetate as the primary electron donor is a slightly less efficient process than ureolysis for MICP.

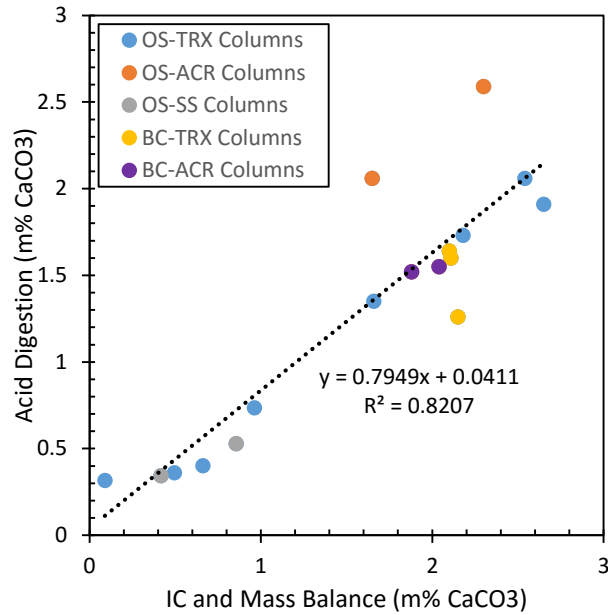


**Fig. 15.** CaCO<sub>3</sub> precipitation versus mols of nitrate reduced to nitrogen gas for every column and every treatment cycle.

Figure 16 shows a comparison between the amount of carbonate precipitation as measured via IC analysis and mass balance of pore fluid recovered during treatment and the carbonate content measured by acid digestion following treatment in both tabular and graphical formats.



Column	CaCO <sub>3</sub> (m% IC)	CaCO <sub>3</sub> (m% Acid)
OS-TRX-1	0.090	0.316
OS-TRX-2	0.495	0.360
OS-TRX-3	0.662	0.402
OS-TRX-4	0.963	0.736
OS-TRX-5	1.66	1.35
OS-TRX-6	2.18	1.73
OS-TRX-7	2.65	1.91
OS-TRX-8	2.54	2.06
BC-TRX-1	2.10	1.64
BC-TRX-2	2.09	1.60
BC-TRX-3	2.11	1.26
OS-SS-1	0.418	0.343
OS-SS-2	0.856	0.529
OS-ACR-1	1.65	2.06
OS-ACR-2	2.30	2.59
BC-ACR-1	2.04	1.55
BC-ACR-2	1.85	1.52

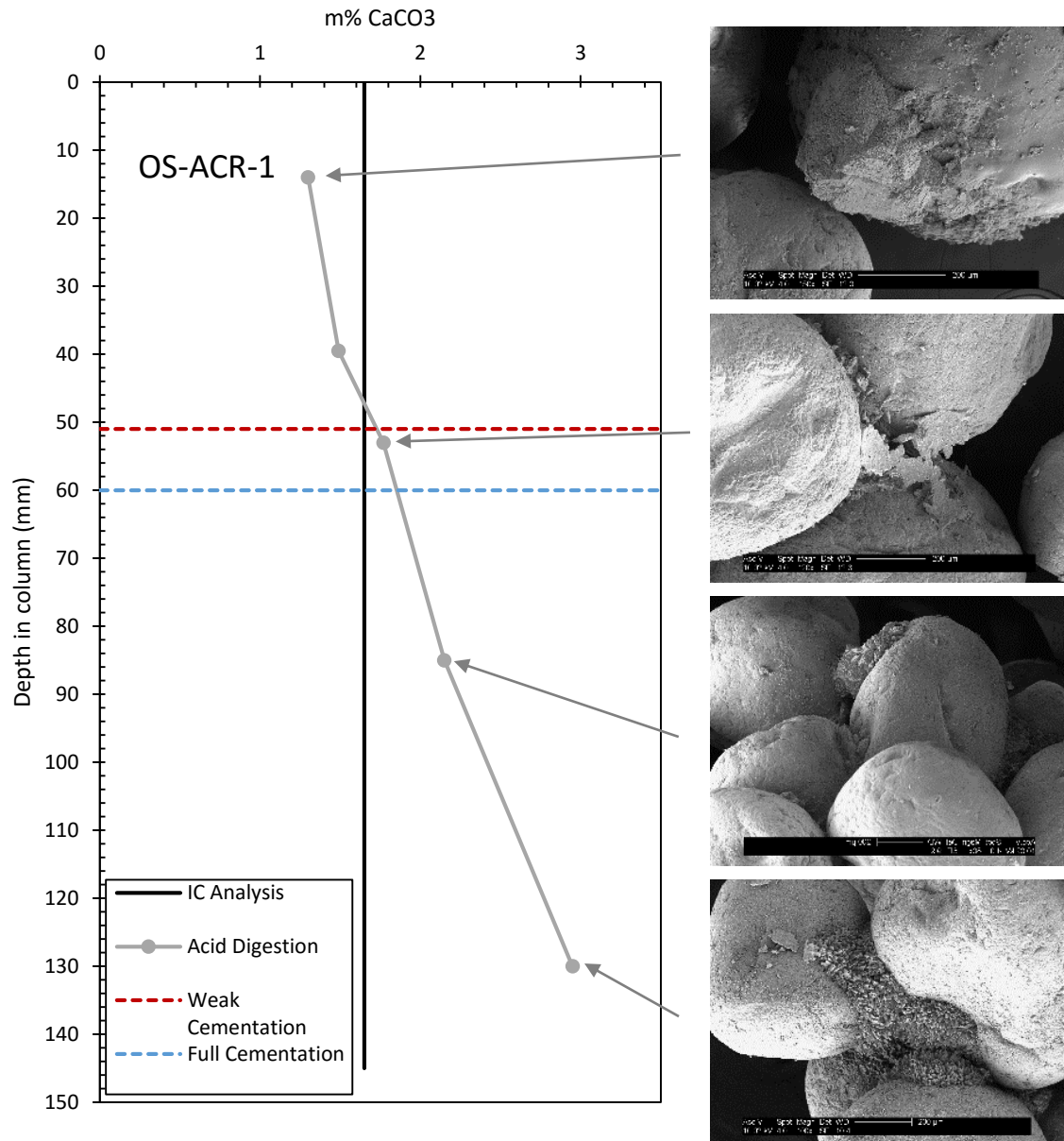


**Fig. 16.** Comparison in carbonate content as measured by acid digestion and IC analysis.

As shown in Figure 16, the carbonate content as measured by acid digestion was generally lower than that measured by IC analysis and mass balance, except at low percentages of carbonate and for the OS-ACR columns. The fact that acid digestion gives higher carbonate contents at low carbonate percentages is most likely due to the fact that some sand is almost always lost during the acid digestion process. This sand loss translates to an apparently higher amount of carbonate in the sample. This is represented by the positive intercept on the plot shown in Figure 16. However, at higher carbonate percentages, IC analysis and mass balance gives higher carbonate contents than acid digestion. This is most likely due to the fact that IC analysis and mass balance captures all of the carbonate precipitated in the entire system, including in the column bases, top caps, dialysis bags, membranes, etc., while acid digestion only captures the carbonate content of the sand. Additionally, some carbonate may be washed out of the columns through rinsing of the sand with DI water following treatment. In any case, this trend is reflected by the

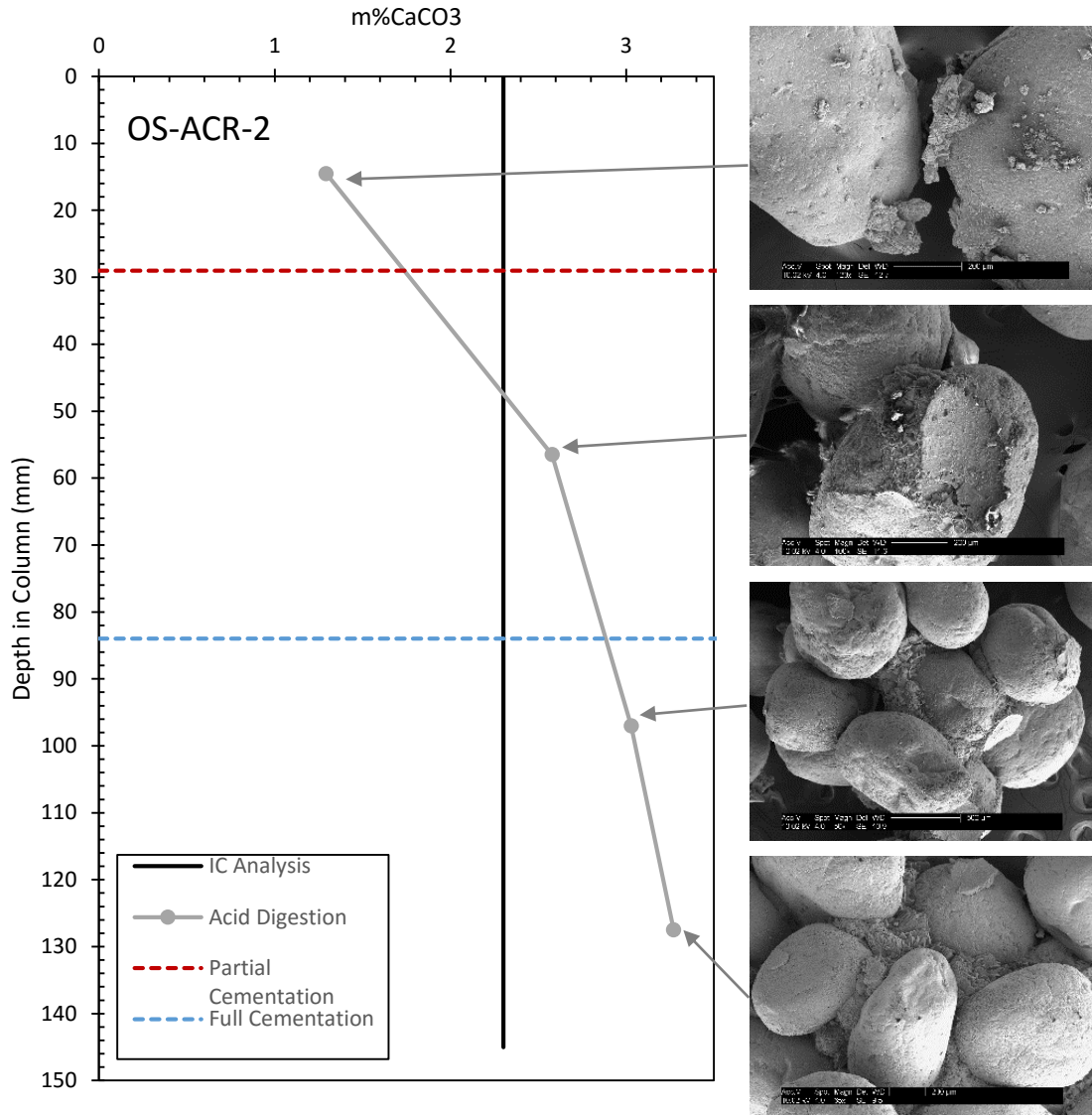
slope of the trend line in Figure 16, which is slightly less than one. The OS-ACR columns do not seem to follow this trend, however. This is most likely due to a few reasons. First, the OS-ACR columns were acid digested in multiple layers, meaning that there was more chance for sand loss than in the other columns. Also, there was little to no precipitation on the bases or top caps in these columns, meaning that almost all of the carbonate was accounted for in acid digestion. The other column which defies the general trend is column BC-TRX-2 (carbonate content approximately 2.3% by IC and mass balance), which plots considerably below the trend line in Figure 16. For this column, the acid used to digest the sand was later found to be quite a bit weaker than previously thought, suggesting that all of the carbonate was most likely not digested.

Figures 17 and 18 below show the carbonate content (from acid digestion and IC analysis) and SEM images of sand taken from Columns OS-ACR-1 and OS-ACR-2 respectively. As shown in Figure 17, the carbonate content (acid digestion) generally increased with depth in Column OS-ACR-1, with weak cementation (fell apart easily when excavated with plastic spatula) observed at around 50 mm depth in the column and full cementation (had to be chipped out of the column with a screwdriver and hammer) observed around 60 mm depth. As shown in the corresponding SEM images, more carbonate was observed on and between soil particles with depth. In general, carbonate crystals were observed on the surface of soil particles in the uncemented zone, carbonate was predominantly visible at particle contacts in the weakly cemented zone and the top of the cemented zone, and carbonate was observed generally filling void space in the base of the column (fully cemented zone). It is interesting to note that full cementation was observed in sand with anywhere from 2%-3% carbonate by weight.



**Fig. 17.** Carbonate content (acid digestion and IC analysis) and SEM images with depth in Column OS-ACR-1.

Figure 18 shows similar data for column on carbonate content versus depth for column OS-ACR-2.

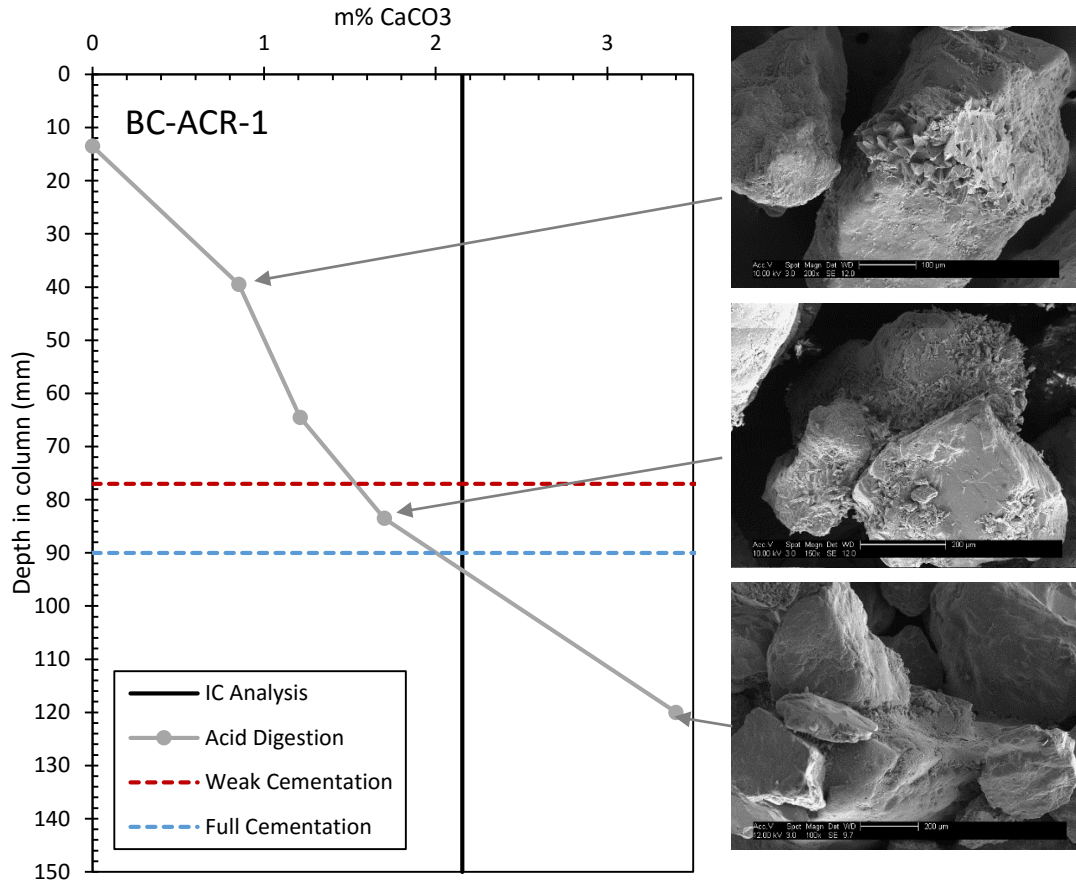


**Fig. 18.** Carbonate content (IC analysis and acid digestion) and SEM images with depth for Column OS-ACR-2.

As shown in Figure 18, the carbonate content in column OS-ACR-2 also increased with depth, with weak cementation observed around 30 mm depth and full cementation observed at around 85 mm depth. The SEM images show that in the uncemented zone there are some small calcite crystals present on the surfaces of soil particles. In the weakly cemented zone, there are a mixture of carbonate crystals on soil particles and bridging between

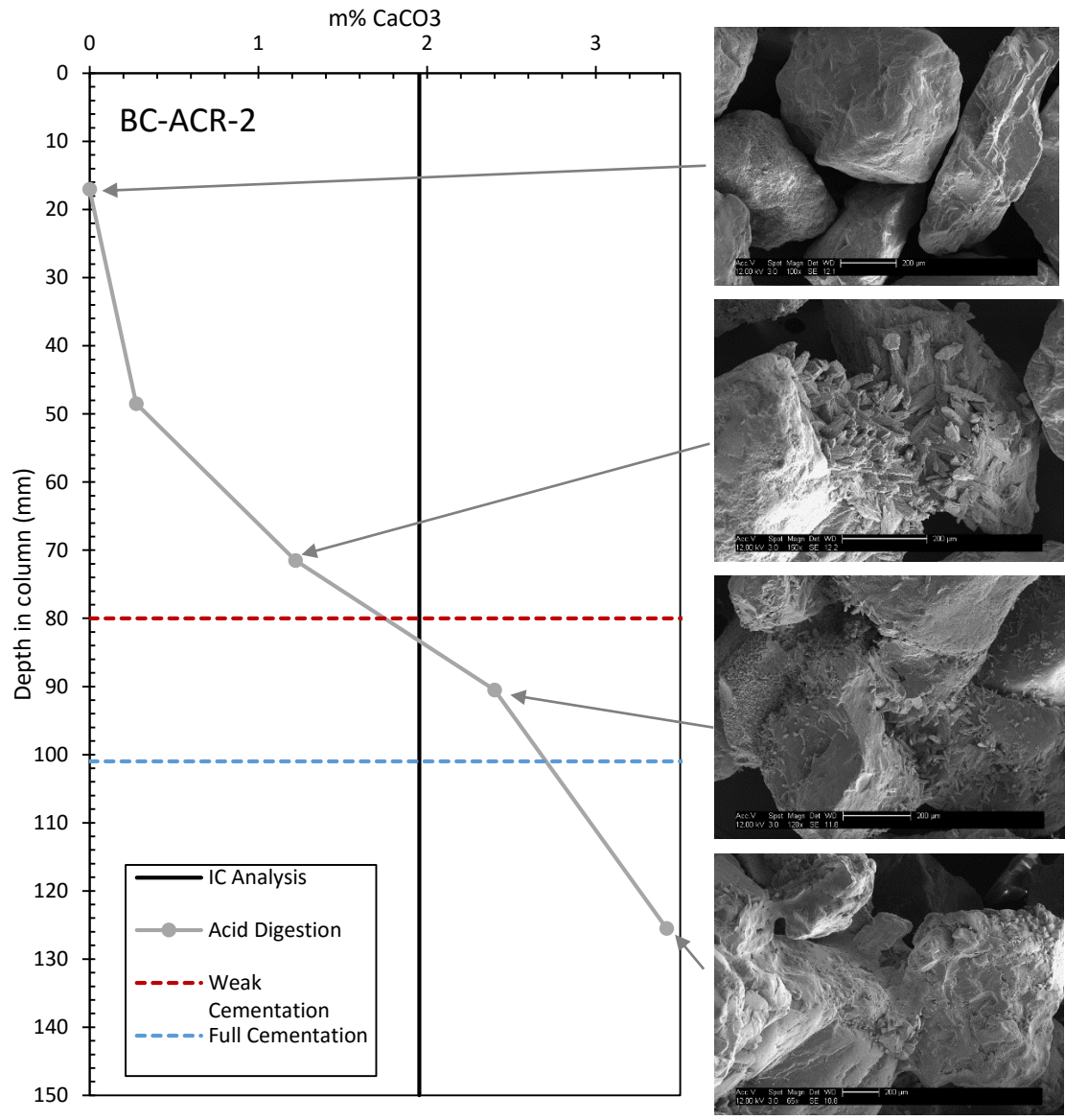
particles at particle contacts. This same trend is observed in the top of the cemented zone, but with more carbonate present at particle contacts. Finally, in the base of the cemented zone, carbonate can be seen filling void space between cemented sand particles. It is worth noting that in this column, weak cementation was observed at around a carbonate content of 2%, while full cementation was not achieved until a carbonate content of closer to 3%. As evidenced in Figures 17 and 18 the zone of weak cementation was larger in column OS-ACR-2 than in Column OS-ACR-1. This is most likely due to the fact that cementation was more concentrated at particle contacts in column OS-ACR-1 than in column OS-ACR-2.

Figures 19 and 20 show the carbonate content (from acid digestion and IC analysis) and SEM images of sand taken from Columns BC-ACR-1 and BC-ACR-2 respectively. Figure 19 shows that the carbonate content in column BC-ACR-1 increased with depth in the column, with no carbonate present in the top 15 mm. Weak cementation was observed in the column around 80 mm depth (roughly 1.5% carbonate) while full cementation was observed at about 90 mm depth (roughly 2% carbonate). As shown in the SEM images, near the top of the column, carbonate crystals were observed on soil particles. In the weakly cemented zone, carbonate was observed both on soil particles and bridging particles at particle contacts. Near the base of the column, carbonate was observed fully bridging and coating soil particles. In general, near the base of the column, the carbonate crystals were observed to have smooth and rounded edges. This is hypothesized as being due to carbonate crystallizing around trapped gas pockets in the base of the column.



**Fig. 19.** Carbonate content (IC analysis and acid digestion) and SEM images with depth for Column BC-ACR-1.

Figure 20 shows similar data for column on carbonate content versus depth for column BC-ACR-2.



**Fig. 20.** Carbonate content (IC analysis and acid digestion) and SEM images with depth for Column BC-ACR-2.

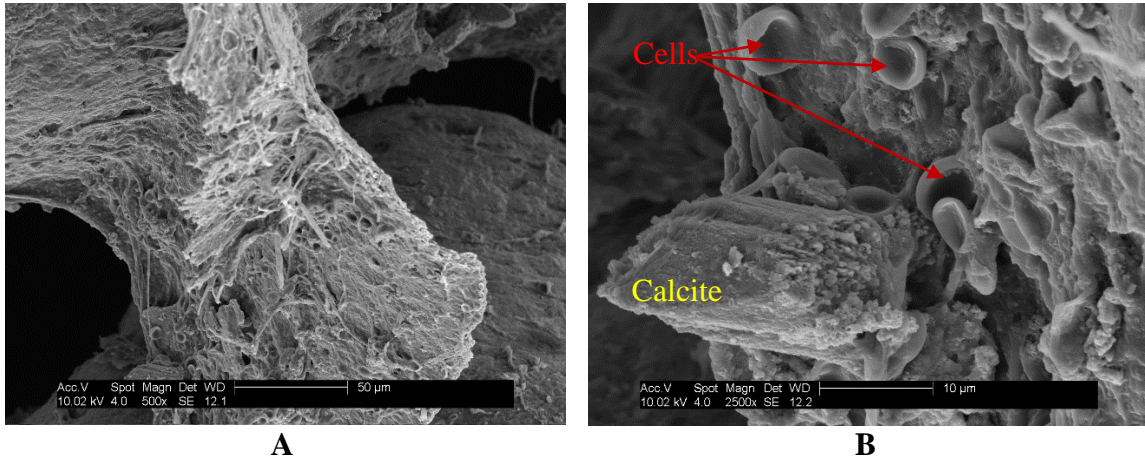
In Figure 20, for column BC-ACR-2, the carbonate content can be seen to increase with depth, with very little carbonate content from the top of the column to a depth of 50 mm. Weak cementation was observed at a depth of 80 mm (roughly 1.8% carbonate) while full cementation was observed at a depth of 100 mm (roughly 2.8% carbonate). As shown in the SEM images, no carbonate was observed on the soil particles in the top of the column.

In and near the weakly cemented zone, carbonate crystals were observed on soil particle surfaces and also at particle contacts. In the fully cemented zone, just as with column BC-ACR-1, carbonate, with a very smooth and rounded surface texture, was observed bridging and coating soil particles. The smooth, rounded texture of the carbonate in the fully cemented zone (near the base of the column) may be the result of carbonate crystallizing around trapped gas bubbles in the soil.

As shown in Figures 17, 18, 19, and 20, in the OS-ACR columns (Figures 17 and 18) carbonate is more evenly distributed throughout the columns when compared to the BC-ACR columns (Figures 19 and 20), in which there is no carbonate present in the tops of the columns. However, all columns display a trend of increasing carbonate content with depth. This is most likely because during each treatment cycle there was imperfect mixing between the fresh pore fluid (injected from the base of the column) and the stale fluid remaining in the columns. So, there were most likely more nutrients present in the bottoms of the columns than in the tops, leading to more biological activity and carbonate precipitation near the base of each column. This was confirmed through IC analysis of pore fluid samples taken from each of the sampling ports in the ACR columns. These results showed much lower nitrate concentrations in the tops of the columns compared to the bottoms even immediately following pore fluid replacement. The BC columns most likely showed a less uniform distribution of carbonate with depth when compared to the OS columns because the BC sand is slightly finer grained than the Ottawa sand, meaning that there was most likely even less mixing between fresh and stale pore fluid in these columns.



Further inspection of SEM images from near the top of column OS-ACR-2 revealed the interaction between biomass and carbonate precipitation in the soil. These images are shown in Figure 21 below.



**Fig. 21.** Biofilm bridging soil particles near the top of Column OS-ACR-2 (A). Interaction of biofilm, microbial cells and calcite (B).

As shown in Figure 21A, SEM imagery revealed a biofilm bridging two soil particles in column OS-ACR-2. By zooming in on the biofilm, it was revealed that it was composed predominantly of EPS, microbial cells, and calcite crystals (Figure 21B). While not labeled on the figure, the bulk of the biofilm (the stringy material seen in Figures 21A and 21B) is most likely composed of EPS. These images shed some light on the interactions between the microbial biomass, sand particles, and the calcite being precipitated in the column. It appears that the EPS produced by growing biomass forms on and between soil particles and provides a lattice on which cells can attach and calcite can begin to precipitate. This interaction requires further investigation as it may provide some interesting insights into the micro-scale processes of MICP via denitrification.

### Mechanical Testing

Table 3 below shows the initial relative densities, final relative densities, initial shear wave velocities and final shear wave velocities for all of the columns.

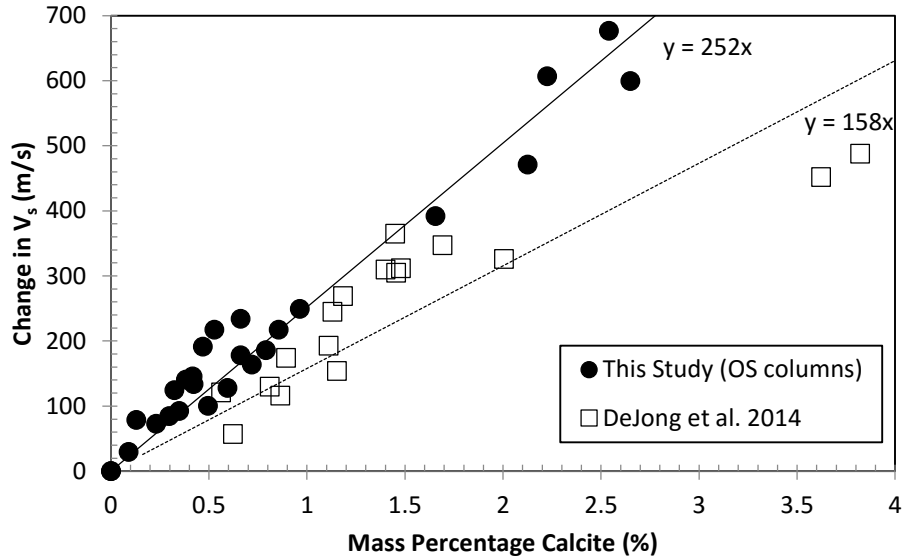
**Table 3.** Initial and final relative densities, initial and final shear wave velocities, and carbonate content (from IC analysis) for each of the columns tested.

Column	Type of sand	Initial $D_r$ (%)	Final $D_r$ (%)	$(Vs)_i$ (m/s)	$(Vs)_f$ (m/s)	Carbonate Content (%)	Number of Treatments
OS-TRX-1	Ottawa 20-30	51.3	31.8	150	180	0.090	4
OS-TRX-2	Ottawa 20-30	43.1	35.5	284	385	0.495	9
OS-TRX-3	Ottawa 20-30	49.4	44.5	228	462	0.662	13
OS-TRX-4	Ottawa 20-30	51.1	43.6	208	457	0.963	17
OS-TRX-5	Ottawa 20-30	41.6	15.5	156	548	1.66	21
OS-TRX-6	Ottawa 20-30	24.3	29.2	184	555	2.18	26
OS-TRX-7	Ottawa 20-30	30.6	20.3	245	852	2.65	30
OS-TRX-8	Ottawa 20-30	21.0	19.4	238	915	2.54	30
BC-TRX-1	Bolsa Chica	66.3	40.0	110*	N/A	2.10	30
BC-TRX-2	Bolsa Chica	66.9	32.9	110*	347	2.09	30
BC-TRX-3	Bolsa Chica	62.6	25.9	110*	N/A	2.11	30
OS-SS-1	Ottawa 20-30	37.5	46.0	124	291	0.418	5
OS-SS-2	Ottawa 20-30	40.0	36.4	124	341	0.856	10
OS-ACR-1	Ottawa 20-30	48.5	48.5	N/A	N/A	1.65	30
OS-ACR-2	Ottawa 20-30	32.5	32.5	N/A	N/A	2.30	30
BC-ACR-1	Bolsa Chica	62.3	62.3	N/A	N/A	2.04	30
BC-ACR-2	Bolsa Chica	68.0	68.0	N/A	N/A	1.85	30

As shown in Table 3, in almost all of the TRX and SS columns, the relative densities of the specimens decreased during treatment. This is most likely due to gas formation in the specimens and the low vertical effective stresses (weight of top cap) in each column. As gas formed in the columns and built up pressure, it most likely liquefied the soil and forced it into a less dense configuration. The ACR columns did not experience this same effect because the top caps were rigidly connected to the columns and thus there was no opportunity for expansion of the soil column as gas was generated. These results indicate that shallow soil deposits with low vertical effective stress may not be eligible for

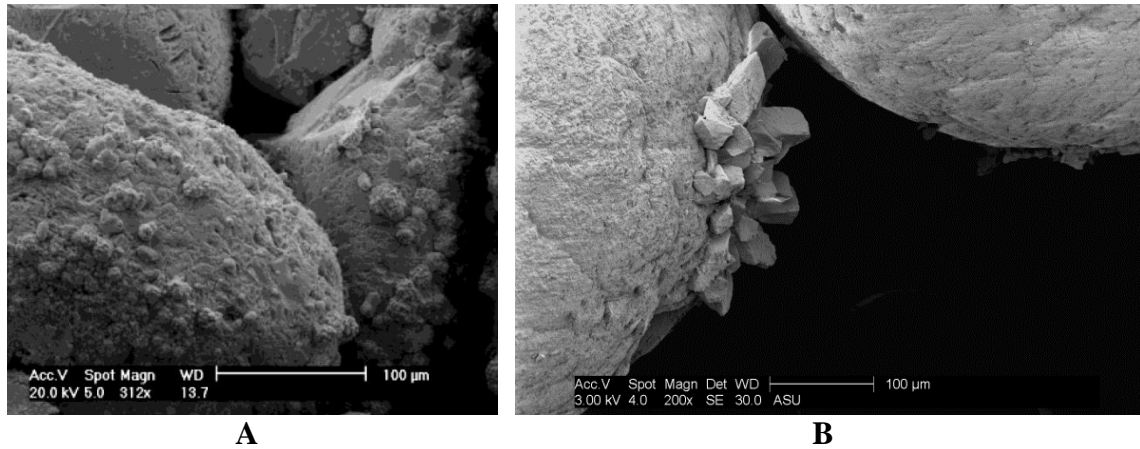
liquefaction mitigation via denitrification, as gas production can significantly loosen the soil (perhaps making it more susceptible to liquefaction) during treatment. However, it is anticipated that field overburden pressures should be sufficient to suppress this effect in all but the top foot or two of soil.

Table 3 also shows the change in shear wave velocity with the number of treatment cycles. As shown in the table, initial shear wave velocities for OS columns ranged anywhere from 124 m/s in the SS columns to 284 m/s in column OS-TRX-2. In general, the change in shear wave velocity was proportional to the number of treatment cycles, with final shear wave velocities ranging from 180 m/s to 915 m/s in the OS columns depending on treatment time. The initial shear wave velocities in the BC-TRX columns had to be estimated using dry soil columns at similar initial relative densities, as the bender elements used to measure shear wave velocity in these columns did not work under saturated conditions. The only BC column with functioning bender elements recorded a final shear wave velocity of 347 m/s. The reason that the Ottawa sand samples exhibited larger increases in shear wave velocity is likely that these samples began in denser configurations ( $e \sim 0.65$ ) compared to the Bolsa Chica sand columns ( $e \sim 0.75$ ). Figure 22 below shows the change in shear wave velocity versus carbonate content for the Ottawa sand samples (initial  $e \sim 0.65$ ) treated via denitrification along with data from Nevada sand samples (initial  $e \sim 0.60$ ) treated via ureolysis from DeJong et al. (2014).



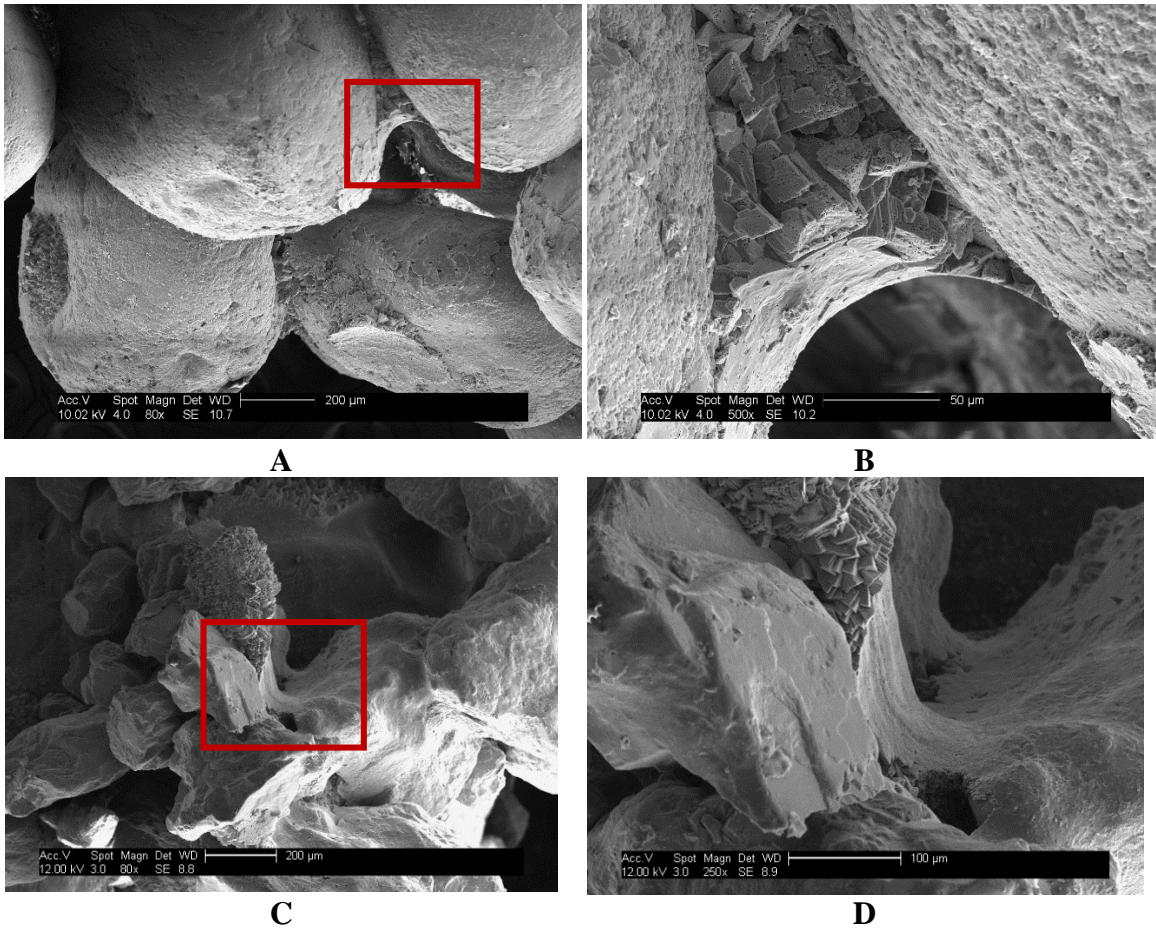
**Fig. 22.** Change in shear wave velocity for OS soil columns ( $e_{\text{initial}} \sim 0.65$ ) versus carbonate content as compared with Nevada sand samples ( $e_{\text{initial}} \sim 0.60$ ) from DeJong et al. (2014).

As shown in Figure 22, the soil columns treated via denitrification showed substantially greater rates of improvement (as measured using shear wave velocity) than those treated via ureolysis at similar carbonate contents. There are a variety of potential explanations for this. First, denitrification is a slower process than ureolysis. Slower rates of MICP have been shown to result in larger carbonate crystals. Soil with larger carbonate crystals after MICP treatment has, in turn, exhibited improved properties when compared to soil with smaller carbonate crystals after treatment (Cheng et al. 2014). It seems reasonable that larger crystal sizes would lead to increased bridging between particles, leading to improved shear wave velocities at lower carbonate contents. Figure 23 shows that carbonate crystals precipitated via denitrification (from this study) are much larger than those precipitated via ureolysis (from Cheng et al. 2014).



**Fig. 23.** Carbonate crystals precipitated via ureolysis (A) from Cheng et al. (2014) and carbonate crystals precipitated via denitrification from this study (B).

Another possible reason why soil treated via denitrification exhibits greater improvements in shear wave velocity when compared to ureolysis is the role of gas and partial desaturation on carbonate precipitation in the soil. When a soil is partially desaturated, gas occupies the larger void spaces and the pore water is forced into a film around soil particles and at particle contacts. During MICP, this desaturation effect could concentrate the precipitation of carbonates at particle contacts, leading to greater amounts of soil improvement in MICP via denitrification (which induces desaturation) compared to MICP via ureolysis (little to no gas production). The cylindrical bridging of precipitated carbonate around soil particle contacts was observed in both Ottawa sand and Bolsa Chica sand (columns OS-ACR-1, and BC-ACR-1), as shown in Figure 24.

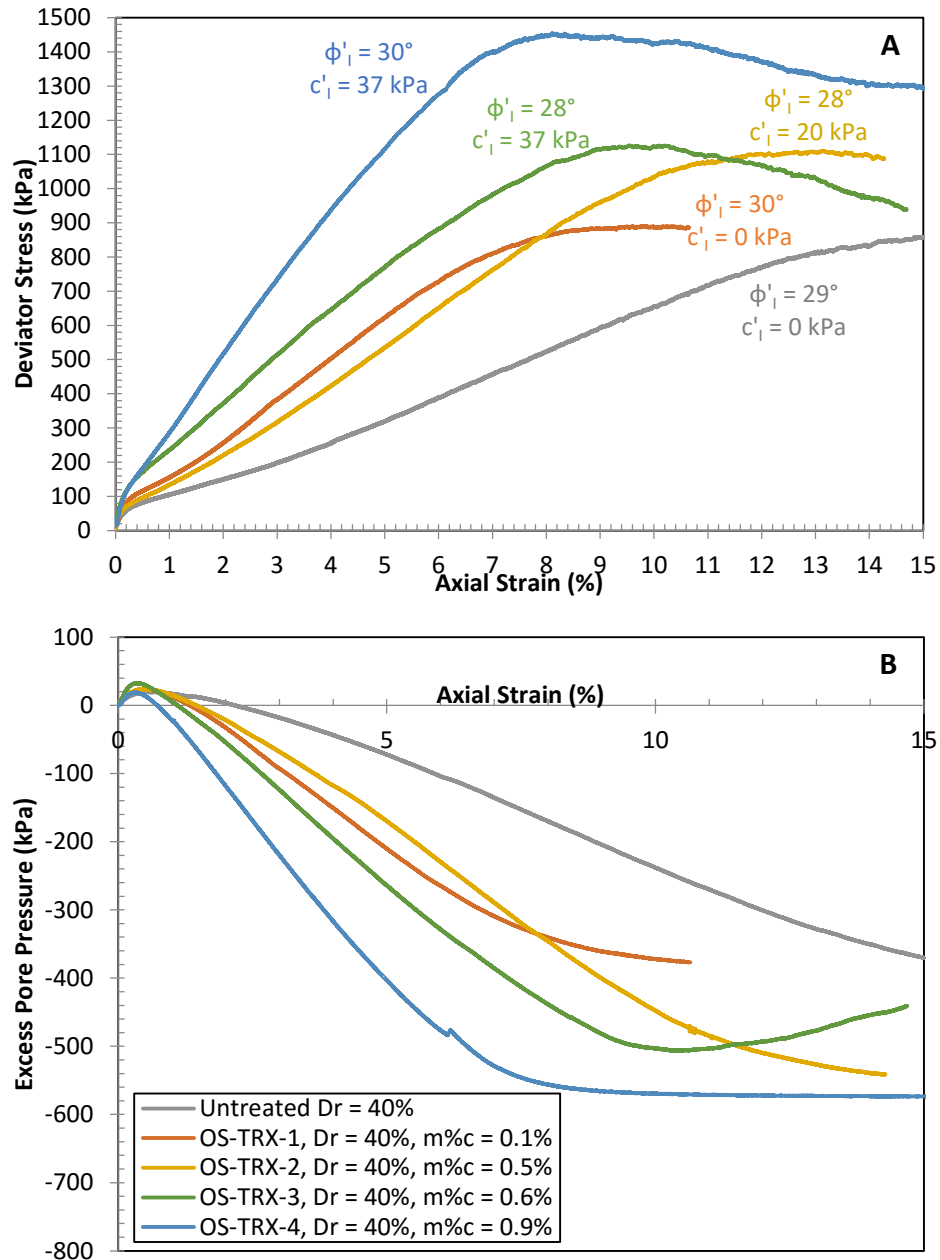


**Fig. 24.** SEM images showing the interaction between gas bubbles and carbonate precipitation in column OS-ACR-1 (A, B) and column BC-ACR-1 (C, D).

As shown in Figure 24, carbonate precipitation was found to occur in rounded, smooth formations between soil particles in samples of cemented OS and BC soils. The shape and location of this cementation (rounded and at particle contacts) suggests, as noted above, that desaturation played a role in localizing carbonate precipitation at particle contacts as cementation occurred around existing gas bubbles. This suggests that the interaction between gas production and MICP in soils treated via denitrification may result in greater soil improvement when compared with soils treated via ureolysis.

The undrained triaxial results for the OS-TRX specimens at an initial relative density of 40% are shown in Figure 25. For each column, the friction angle and cohesion were interpreted by plotting a linear trend line through the asymptotic portion of the p-q curves. The slope of these trend lines was used to estimate the interpreted friction angle ( $\phi'_1$ ), while the intercept was used to estimate the cohesion ( $c'_1$ ). For all untreated soil columns, this resulted in estimated cohesion values very close to zero (between -3 and -5 kPa), indicating that this may be a viable method to interpret the cohesion.

As shown in Figure 25, even very low denitrification-induced carbonate content (Column OS-TRX-1), can notably improve the stiffness and dilatant behavior of the soil when compared to an untreated soil specimen. With additional treatment, i.e., greater carbonate content (Columns OS-TRX-2, OS-TRX-3, and OS-TRX-4), the stiffness, dilatant behavior, and strength of the soil continue to improve through MICP via denitrification. These results indicate that very little carbonate precipitation is necessary to improve the undrained response of a liquefiable soil. Although no cementation was observed in any of the treated soil columns, there was a general increase in the interpreted cohesion of the soil columns with increasing carbonate content (Figure 25A), indicating that weak cementation was achieved. However, as the carbonate content in these columns was below the level at which cementation was observed in disassembled columns (see Figures 17, 18, 19, and 20), the predominant form of soil improvement in these columns may simply be particle roughening caused by the precipitation of carbonate on soil particle surfaces.



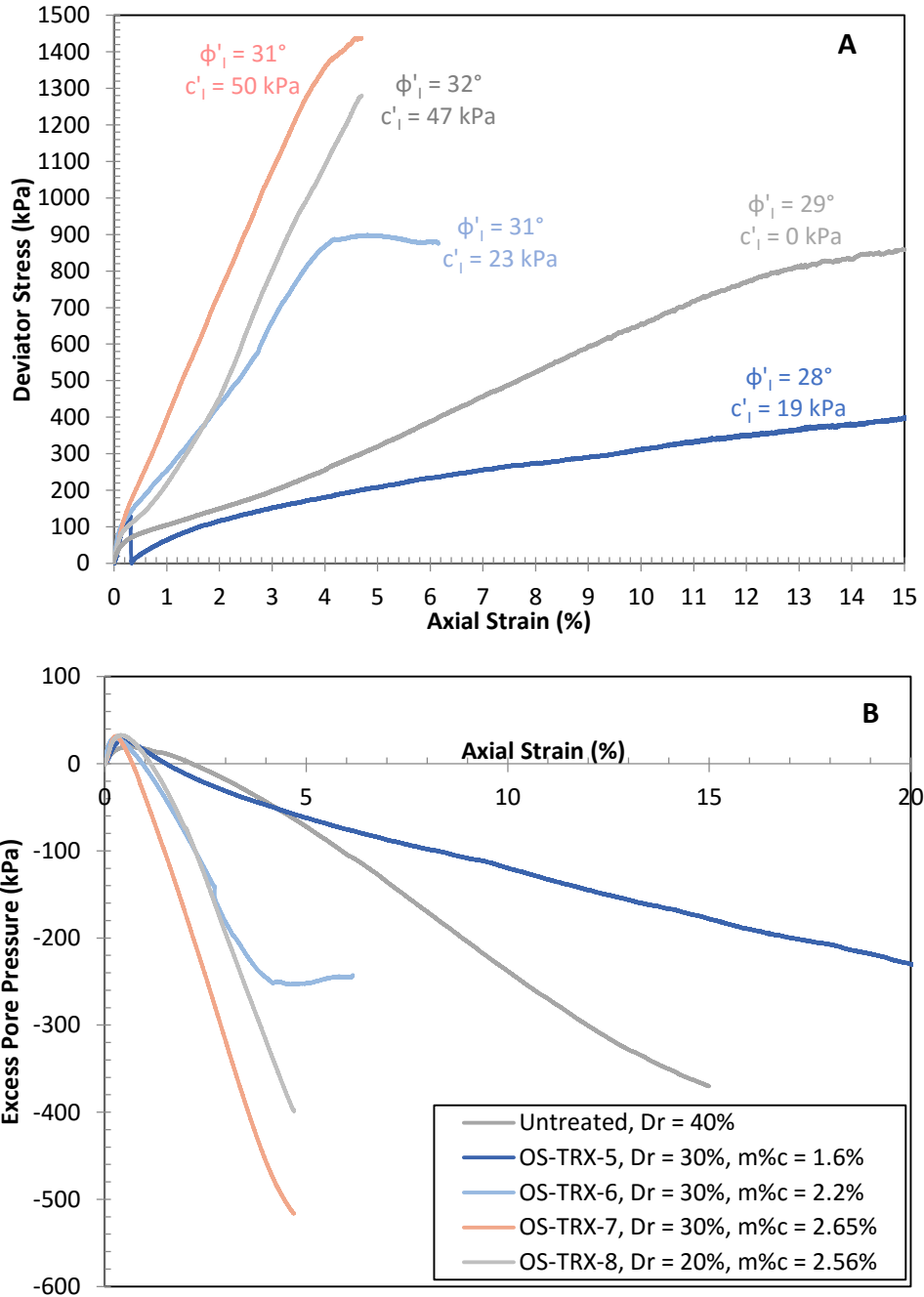
**Fig. 25.** Deviator stress (A) and excess pore pressure (B) from undrained testing of OS-TRX specimens at an initial relative density of 40% and a confining stress of 100 kPa.

Figure 26 shows the undrained response of the OS-TRX columns at an initial relative density of 30%. While attempts were made to generate an untreated soil column at a relative density of 30% using the same soil preparation procedure (air pluviation of dry



soil) for comparison with these results, the loosest sample obtained was at a relative density of 40%. So, this soil column ( $D_r = 40\%$ ) is used for comparison. Three of the treated columns (OS-TRX-6, OS-TRX-7, OS-TRX-8) experienced leakage between the specimen and the cell during testing, forcing the tests to be cut short. Hence, not all of the specimens were tested to 15% strain. Small cemented chunks of soil were found near the base of each of these columns, indicating that weak cementation may be responsible for some of the observed soil improvement.

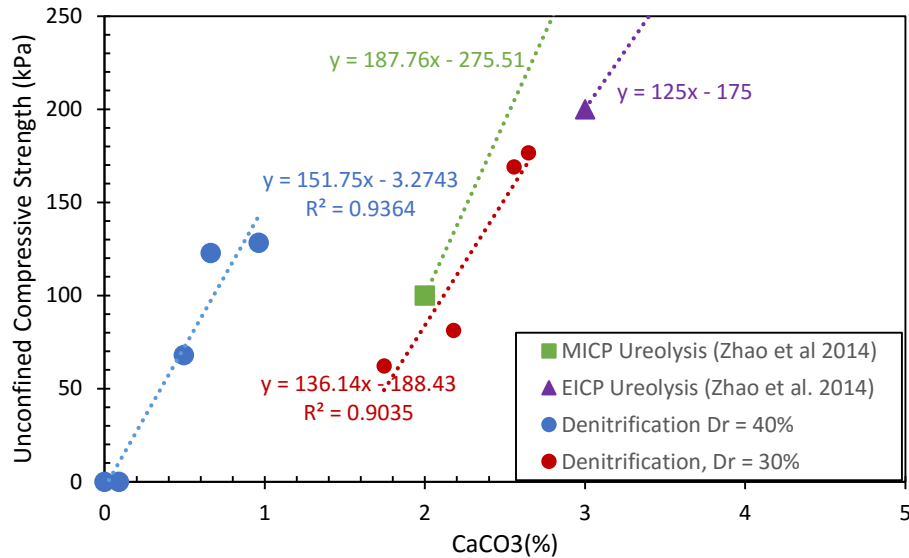
As shown in Figure 26, greater carbonate content results in increases in stiffness, strength, and dilatant behavior for the treated columns. Specimens also exhibited higher interpreted cohesion and friction angles with increased treatment. While three of the columns (OS-TRX-6, OS-TRX-7, OS-TRX-8) displayed improvements in strength, stiffness, and dilatant behavior compared to the untreated soil ( $D_r = 40\%$ ), Column OS-TRX-5 proved to be slightly less stiff and less dilatant than the untreated specimen. This is most likely due to the fact that the final relative density of this column was only 15.5% (Table 3) at the time of testing. Again, this shows that soils under very low confinement may actually become more susceptible to liquefaction following treatment via denitrification, as gas pressures can significantly loosen the soil. However, as no untreated columns at an initial relative density of 30% were tested, it remains unclear if the mechanical properties of Column OS-TRX-5 actually worsened following treatment.



**Fig. 26.** Deviator stress (A) and excess pore pressure (B) from undrained testing of OS-TRX specimens at an initial relative density of 30% and a confining stress of 100 kPa.

Using the interpreted undrained friction angles and apparent cohesion values calculated for each soil column, the unconfined compressive strength ( $UCS_I$ ) was estimated for all of

the treated OS-TRX columns. This data was then compared with data for Ottawa 20-30 sand treated via ureolysis (both MICP and EICP) from Zhao et al. (2014) as seen in Figure 27.



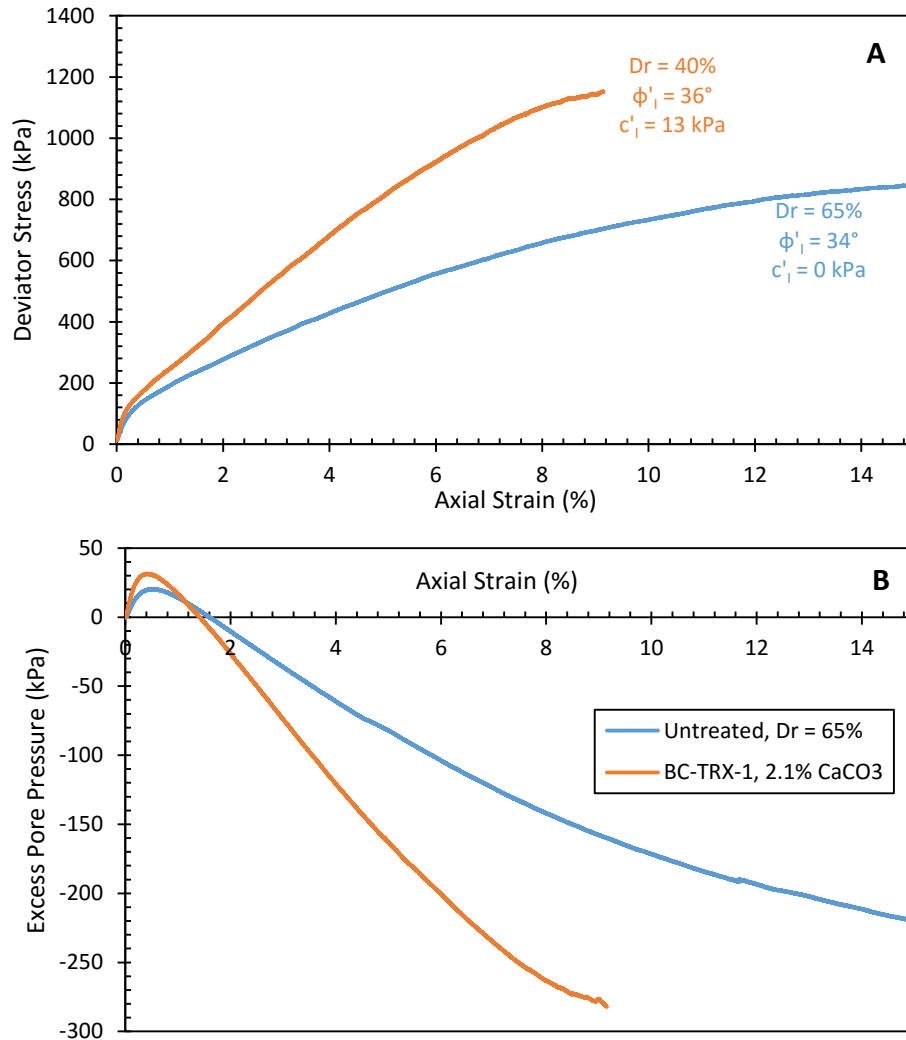
**Fig. 27.** Interpreted unconfined compressive strength ( $UCS_I$ ) of Ottawa 20-30 sand treated via denitrification (this study) at initial relative densities of 30% and 40% compared with UCS of Ottawa sand specimens ( $D_r = 42 - 50\%$ ) treated with MICP via ureolysis and EICP via ureolysis from Zhao et al. (2014).

As shown in Figure 27, Ottawa sand specimens treated via denitrification at an initial relative density of 40% (similar to those of Zhao et al. 2014) exhibited improvement in unconfined compressive strength at lower carbonate contents than specimens treated via ureolytic MICP or EICP (as indicated by the intercept value). However, the rate of increase in strength with carbonate content is slightly lower for the denitrification treated specimens than for the specimens treated via ureolytic MICP. It is hypothesized that denitrification specimens show greater improvement at lower carbonate contents than ureolytic specimens because of the interaction of gas and MICP evidenced in Figure 24. As noted previously,

if gas production forces carbonate to precipitate predominantly at particle contacts, this should lead to cementation and improved UCS at lower carbonate contents in specimens treated via denitrification. It is likely that the rate of increase of UCS with increasing carbonate content is lower for denitrification treated specimens than for ureolysis treated MICP specimens because of the loosening effect of the denitrification columns caused by gas production. If the soil columns were maintained at higher confining stresses during treatment, it is possible that they would exhibit higher UCS values. The denitrification specimens at an initial  $D_r$  of 30% showed a slightly lower rate of improvement with increasing carbonate content and a much lower apparent cohesion intercept than specimens at an initial  $D_r$  of 40%. The data indicates that strength improvement does not occur in the  $D_r \approx 30\%$  specimen until a carbonate content of roughly 1.3% (versus 0.02% for the  $D_r \approx 40\%$  specimens).

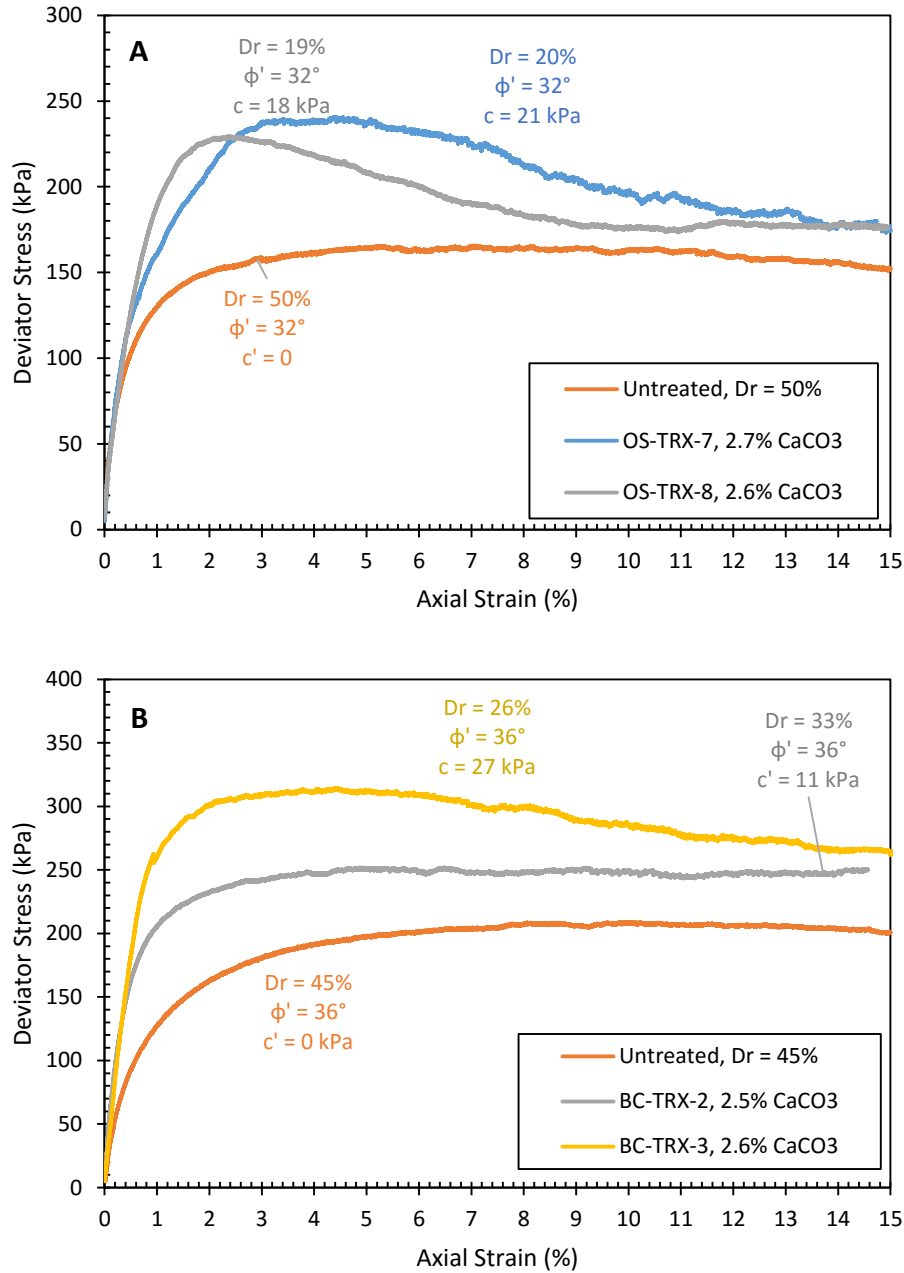
The undrained triaxial results for column BC-TRX-1 are presented in Figure 28. As shown in Figure 28, column BC-TRX-1 exhibited improved stiffness, strength, and dilatant behavior when compared to the untreated column at the same initial relative density. Additionally, column BC-TRX-1 showed improvements in the interpreted friction angle and cohesion. These results demonstrate the ability of MICP to improve the undrained response of the natural Bolsa Chica soil. However, while the treated soil does exhibit improvement compared to the untreated soil, the degree of improvement is not as pronounced as for the Ottawa sand samples. There are at least two possible reasons for this result. First, the initial void ratio of the Bolsa Chica soil was considerably higher (0.75) than the Ottawa sand samples (0.65). This means that more carbonate needs to be precipitated in order to bridge the void space between sand grains and improve the soil

properties. Also, the Bolsa Chica soil is generally much more angular than the Ottawa sand, so increased particle roughening caused by carbonate precipitation may have a lesser effect on Bolsa Chica soil properties than for the Ottawa sand.



**Fig. 28.** Deviator stress (A) and excess pore pressure (B) from undrained testing of column BC-TRX-1 and an untreated specimen at an initial relative density of roughly 65% and a confining stress of 100 kPa.

The results of drained testing of columns OS-TRX-7, OS-TRX-8, BC-TRX-2, and BC-TRX-3 compared to untreated soil are shown in Figure 29.

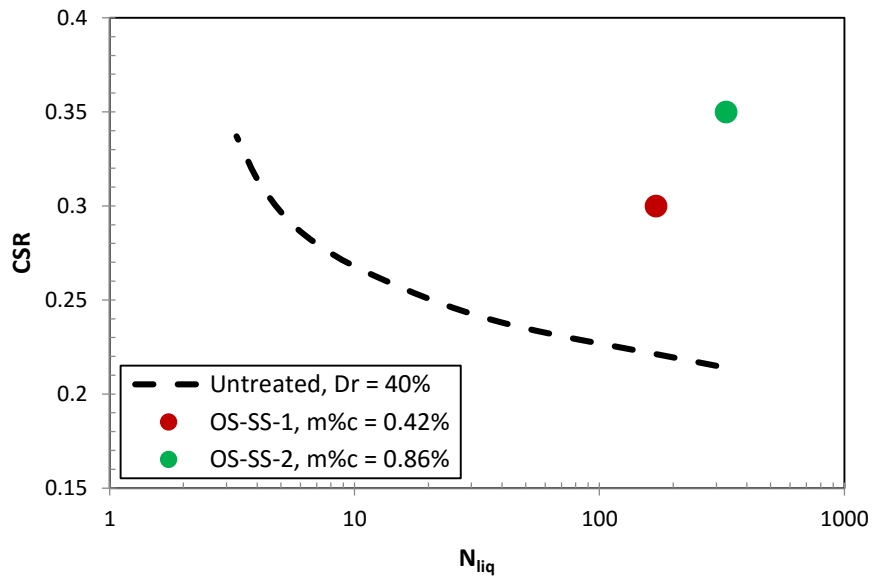


**Fig. 29.** Deviator stress versus axial strain for drained testing of Ottawa sand samples (A) and Bolsa Chica sand samples (B) at a confining stress of 75 kPa.

As shown in Figure 29, treated soils exhibited significantly higher drained strengths (both peak and residual) and cohesion values than untreated soils. To calculate the drained

cohesion for each soil, it was assumed that the treated soils exhibited the same friction angle as the untreated soils.

The results of cyclic direct simple shear testing of columns OS-SS-1 and OS-SS-2 are shown in Figure 30.

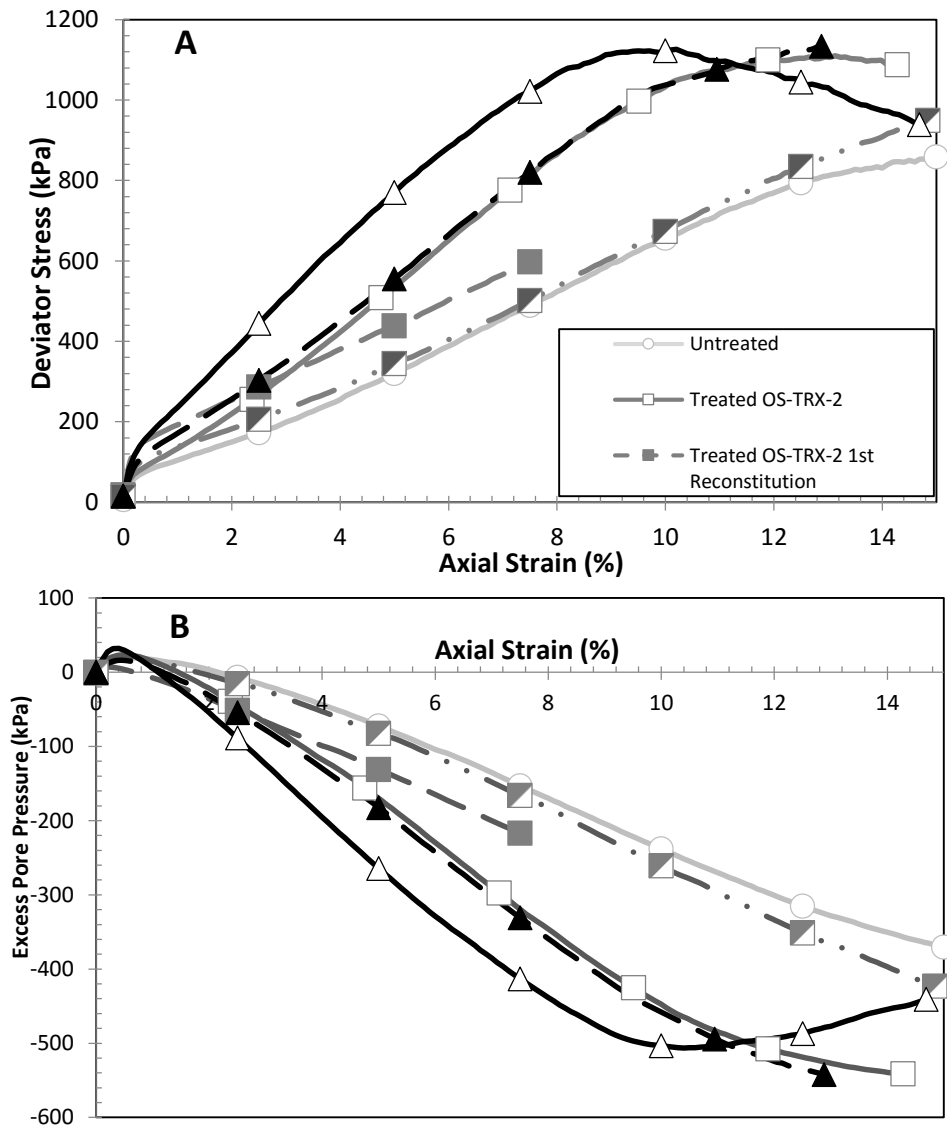


**Fig. 30.** Cyclic direct simple shear testing of untreated Ottawa sand, column OS-SS-1 and column OS-SS-2.

As shown in Figure 30, the cyclic resistance of the soil increased dramatically with relatively small carbonate content (less than 1%), and increased with increasing carbonate content. Although no cementation was visible in the soil columns after testing, the improvements to cyclic resistance may be due to a combined effect of weak cementation and particle roughening. In any case, the data represented in Figure 30 show that very little carbonate is necessary to dramatically improve the cyclic resistance, and hence the liquefaction resistance, of the soil.

## Reconstituted Specimens

Triaxial results from reconstituting column OS-TRX-2 and OS-TRX-3 are shown in Figure 31. In total, 1.05 g of biomass was removed from Column OS-TRX-2 prior to reconstituting the column, while 1.4 g of biomass was removed from Column OS-TRX-3.

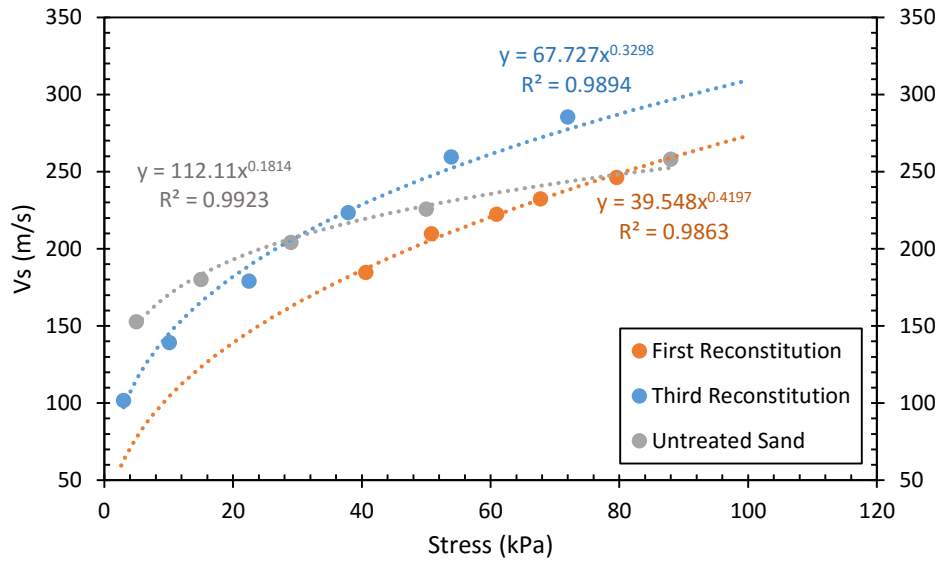


**Fig. 31.** Deviator stress (A) and excess pore pressure (B) with axial strain for untreated, treated, and reconstituted specimens.



As shown in Figure 31, with one reconstitution, both columns exhibit a deterioration in stiffness and dilatant behavior compared to the treated column, but still show significant improvement in strength, stiffness, and dilatant behavior when compared to the untreated soil. Similarly, after two reconstitutions, Column OS-TRX-2 shows a deterioration in stiffness and dilatant behavior when compared to the first reconstitution such that the properties after two reconstitutions are almost identical to those of the untreated specimen. These results imply that interparticle cementation is not necessary for MICP to induce significant improvements in the stiffness and dilatant behavior of a soil. The data in Figure 31 shows that some of the observed improvements in soil properties following MICP are the result of particle roughening as carbonate crystals coat sand particles. The observed degradation in soil properties (stiffness, strength, and dilatant behavior) with multiple reconstitutions is most likely the result of the removal of carbonate crystals from particle surfaces caused by abrasion during triaxial testing.

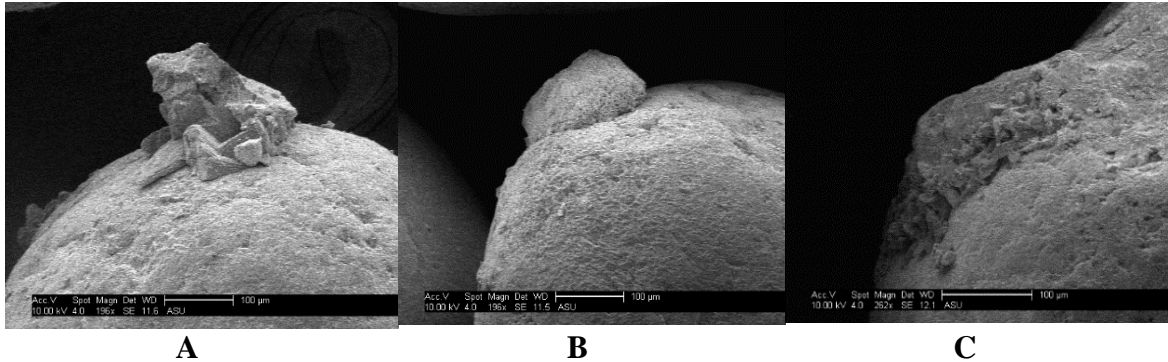
Santamarina and Cascante (1998) showed that particle surface roughness can drastically improve the strength and moderate strain stiffness of a particulate material. They also demonstrated that increased roughening led to a decrease in shear wave velocity under low confining pressures but an increased sensitivity of shear wave velocity to increasing confinement. The relationship between shear wave velocity and confining pressure for untreated soil and soil from column OS-TRX-3 after multiple reconstitutions is shown in Figure 32.



**Fig. 32.** Shear wave velocity as a function of confining stress for untreated soil and soil from Column OS-TRX-3 after one reconstitution and three reconstitutions. All samples are at a relative density of 40%

As shown in Figure 32, at low confining pressures the shear wave velocity of soil from column OS-TRX-3 is the lowest after only one reconstitution and slightly higher after three reconstitutions and the untreated soil displays the highest shear wave velocity. This trend is reflected in the coefficient on the power functions fitted to each data set. Also shown in Figure A, and reflected in the exponent on the power functions fitted to each data set, is that the shear wave velocity is most sensitive to confining pressure after one reconstitution, slightly less sensitive after three reconstitutions, and least sensitive for the untreated sand. As per Santamarina and Cascante (1998), these results indicate that the untreated soil is the least rough, while the soil is most rough after one reconstitution. These results further indicate that soil improvement in the reconstituted specimens is the result of particle roughening, with a degradation in properties with multiple reconstitutions caused by the abrasion and removal of carbonate crystals from treated soil.

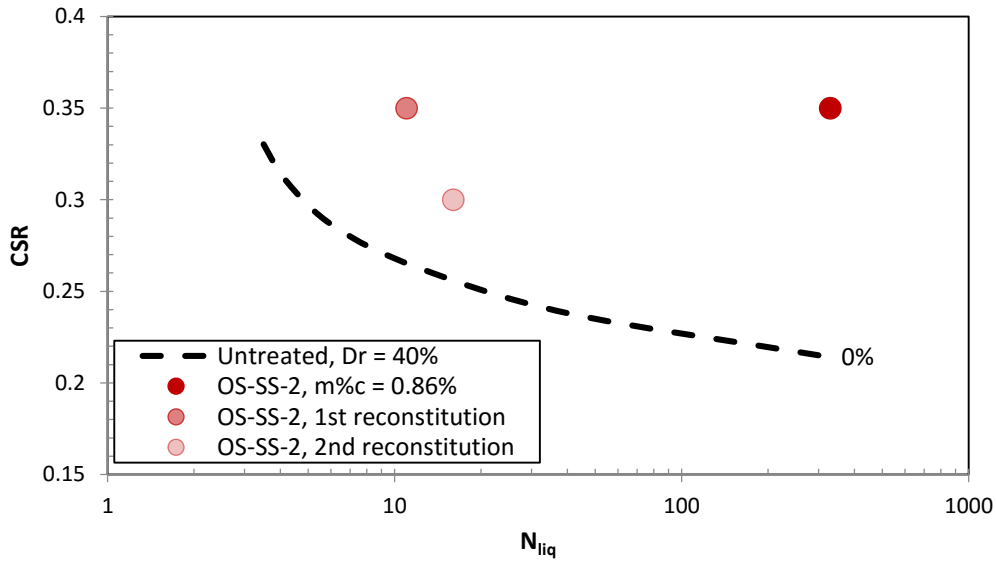
SEM images of sand from column OS-TRX-3 after multiple reconstitutions is shown in Figure 33.



**Fig. 33.** SEM images of sand taken from column OS-TRX-3 after zero reconstitutions (A), one reconstitution (B) and three reconstitutions (C).

As shown in Figure 33A, with no reconstitutions, calcite crystals found on the surfaces of sand particles from column OS-TRX-3 are very angular. After one reconstitution (Figure 33B), the calcite crystals were observed to be slightly more rounded, and after three reconstitutions (Figure 33C), the calcite crystals appeared to have been nearly completely abraded from the surfaces of sand particles. These images are further evidence that soil particles are significantly roughened due to treatment via MICP. Furthermore, these images show that carbonate crystals can be abraded from soil particle surfaces after multiple shearing events.

Results of cyclic direct simple shear testing of soil from Column OS-SS-2 subject to multiple reconstitutions are shown in Figure 34. In total, 1.5 g of biomass was removed from Column OS-SS-2 prior to reconstituting and retesting the soil.



**Fig. 34.** Cyclic resistance of untreated soil compared to column OS-SS-2 after treatment and two reconstitutions.

As shown in Figure 34, the cyclic resistance of soil from column OS-SS-2 degrades toward the untreated state with multiple reconstitutions. This suggests that particle roughening alone (no cementation) via MICP can significantly improve the cyclic resistance of a liquefiable soil. However, as with the triaxial results, it appears that abrasion and subsequent removal of carbonate from soil particles leads to the degradation in cyclic improvement of the soil with multiple shearing events.

## CONCLUSIONS

Testing of semi-stagnant soil columns shows that denitrification holds promise for liquefaction mitigation as a two-stage process, wherein desaturation provides mitigation in Stage 1 and carbonate precipitation provides mitigation in Stage 2. P-wave velocity and dialysis bag measurements in the denitrification column tests showed that desaturation occurs very quickly after the onset of denitrification (one to three days). Abiotic testing

results on untreated soil showed that the extent of desaturation achieved in these soil columns (82% – 95%) is enough to measurably increase the liquefaction resistance of the soil. Measurement of carbonate content through IC analysis and acid digestion revealed that denitrification induces the precipitation of calcium carbonate fairly slowly (roughly 2% over the course of a year). However, mechanical testing of the denitrification-treated soil revealed that very little calcium carbonate (as low as 0.1%) can lead to significant improvements in the stiffness, strength, cyclic resistance, and dilatant behavior of a soil. Testing of reconstituted sand specimens from treated columns revealed the role of particle roughening in improvement via MICP. Specifically, it was found that uncemented, reconstituted treated soil displayed improvements in stiffness, strength, dilatant behavior, and cyclic resistance when compared to untreated soil. However, testing of sand subjected to multiple reconstitutions suggests that the degree of soil improvement provided by particle roughening is reduced with multiple shearing events.

While the data gathered from testing of semi-stagnant soil columns strongly suggests the applicability of denitrification as a two-stage process for liquefaction mitigation, these soil columns do not accurately represent field conditions. In the field, this method will need to be applied to saturated soil with continuous groundwater flow. Therefore, it is necessary to conduct tests of soil columns suggested to continuous flow to demonstrate the applicability of denitrification for liquefaction mitigation in real world scenarios.

## **CHAPTER 5**

# **LIQUEFACTION MITIGATION VIA MICROBIAL DENITRIFICATION: A LABORATORY STUDY USING SOIL COLUMNS SUBJECTED TO CONTINUOUS FLOW**

### **INTRODUCTION**

Testing of semi-stagnant denitrification columns described in the previous chapter showed the ability of denitrification to mitigate the liquefaction potential of a soil as a two phase process, with desaturation providing short term mitigation and carbonate precipitation providing long term mitigation. However, due to their semi-stagnant nature, these tests did not simulate field conditions. The implementation of denitrification for liquefaction mitigation in the field will require introduction of the necessary nutrients and possibly a calcium source into the treatment area. One way to achieve this is to use the natural flow of the groundwater to carry the necessary nutrients and calcium source injected up-gradient into the treatment area. Alternatively, the necessary nutrients and substrate could be injected continuously into the treatment area. In either case, natural ground water flow will also remove waste products from the treatment zone. The semi-stagnant column tests did not simulate either the continuous supply of nutrients and substrate to the treatment zone or the removal of waste products. Additionally, the semi-stagnant columns relied on an initial inoculation with exogenous microbes and so did not demonstrate the potential for soil improvement via biostimulation of native microorganisms. In order to more closely simulate field conditions, additional soil columns were tested under continuous flow conditions and without an initial inoculation of exogenous microbes.

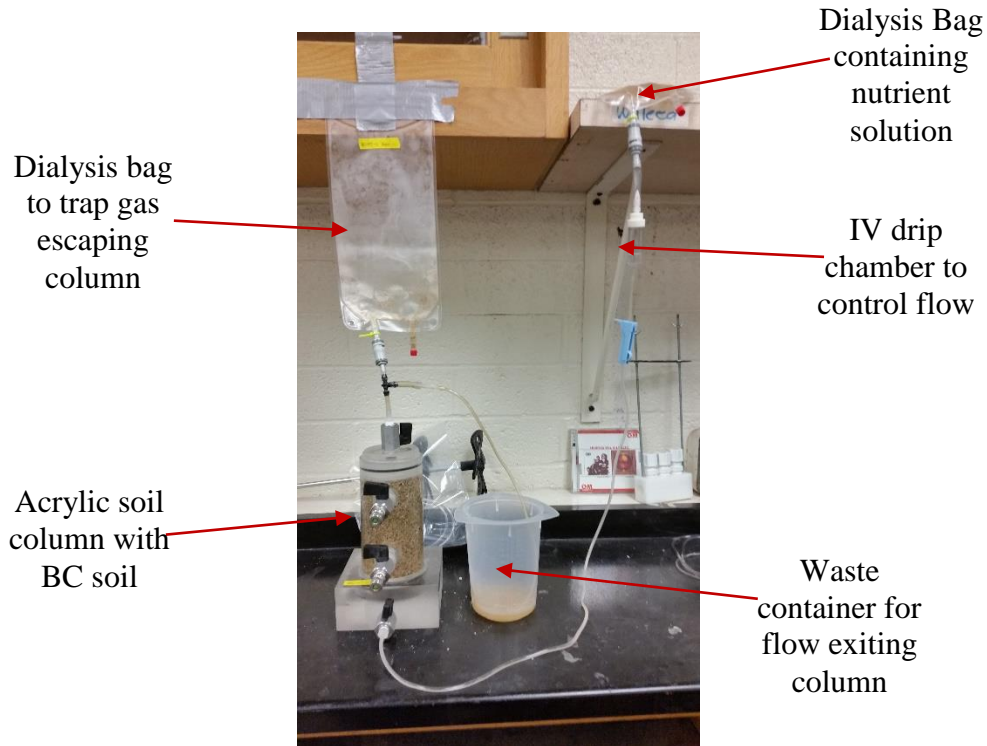
## MEANS AND METHODS

### Initial Tests

Three sets of continuous-flow soil columns were tested. The first set of tests involved four soil columns. Two of the soil columns were prepared using dry Ottawa 20-30 sand air-pluviated to a relative density of 45% (OS-CF-1 and OS-CF-2). The other two columns were prepared using a dry soil from Bolsa Chica State Beach in Huntington Beach California, air pluviated to a relative density of 50% (BC-CF-1, BC-CF-2). Two columns, OS-CF-1 and BC-CF-1, were prepared in 150 mm-tall, 73 mm-diameter clear acrylic columns. The other two soil columns, OS-CF-2 and BC-CF-2, were prepared using 70 mm-diameter triaxial base and top caps in a rigid jacket lined with a latex membrane under very low (weight of top cap) normal stress (roughly 3 kPa) for the duration of treatment. The acrylic columns were subjected to similarly low normal stresses during treatment. After pluviating, each of the columns was flushed with  $N_{2(g)}$  to minimize  $O_{2(g)}$  in the soil pores and create an environment suitable for denitrification.

To begin treatment, each of the four columns was flooded from the bottom upwards with an autoclaved nutrient solution consisting of 37.5 mM  $Ca(NO_3)_2$ , 75 mM  $Ca(CH_3COO)_2$ , 137.5 mM  $CaCl_2$ , 2.0 mM  $MgSO_4$ , 0.75 g/L tryptic soy broth (TSB), and 0.5 mL/L of a trace metals solution consisting of 0.5% (w/v)  $CuSO_4$ ,  $FeCl_3$ ,  $MnCl_2$ ,  $Na_2MoO_4 \cdot 2H_2O$ . Following flooding, each column was configured for flow of nutrients from the top of the column downward using a 1 L dialysis bag containing sterile nutrient solution (same as above) and an IV drip chamber (60 drips/mL) to control flow. The flow rate of fluid through the columns was set to approximately 1.5 – 2 mL/hr, corresponding to a flux of 0.035 ft/day. After six weeks of treatment in this manner, it was found that

flow was inhibited by escaping gas bubbles, and the columns were reconfigured for flow from the bottom upwards for the following four weeks. A picture of the experimental setup with flow from the bottom upwards is shown in Figure 35.



**Fig. 35.** Diagram of experimental setup for first generation continuous flow soil columns.

Following treatment, each of the four columns was flushed with approximately four pore volumes of deionized water to remove residual salts. Each column was then taken apart and inspected for cementation. Cemented soil chunks as well as loose sand from each column were then oven dried for forty eight hours at 105°C. Samples of cemented soil were taken for analysis under a scanning electron microscope (SEM). The remaining cemented sand and loose material from each column was exposed to strong acid, washed, and dried again to quantify the carbonate content in each column through the acid digestion method.



## Second Generation Tests

Following the success of the initial set of column tests, a soil column was prepared using dry Ottawa 20-30 sand air pluviated to a relative density of 40% (OS-CF-3). The column was prepared inside of a 150 mm-tall, 73 mm-diameter acrylic column equipped with sampling ports located 50 mm and 125 mm from the base of the column. Following sand placement, the column was flushed with  $N_{2(g)}$  to minimize the amount of  $O_{2(g)}$  in the system and create an environment suitable for denitrification to occur.

After flushing with  $N_{2(g)}$ , the column was flooded from the bottom with an autoclaved nutrient solution consisting of 37.5 mM  $Ca(NO_3)_2$ , 75 mM  $Ca(CH_3COO)_2$ , 137.5 mM  $CaCl_2$ , 2.0 mM  $MgSO_4$ , 0.75 g/L tryptic soy broth (TSB), and 0.5 mL/L of a trace metals solution consisting of 0.5% (w/v)  $CuSO_4$ ,  $FeCl_3$ ,  $MnCl_2$ ,  $Na_2MoO_4 \cdot 2H_2O$ . Following flooding, the column was configured for flow from the bottom upwards as seen in Figure 1 above using a sterile 250 mL dialysis bag to hold the nutrient fluid and an IV drip chamber to control the flow rate. The flow rate was set to approximately 37.5 mL/day for the five weeks of treatment.

At one week intervals during treatment, approximately 3 mL samples were taken from the dialysis bag containing the fresh media, the bottom port on the column, and the top port on the column. The pH of the samples was taken immediately following their removal from the column. Approximately 2 mL of each sample was then filtered through a 0.2  $\mu$ m filter and stored at 4°C until the end of the five week treatment period. Following the end of the treatment period, the filtered samples were diluted by a factor of 200 with DI water and analyzed using ion chromatography (Dionex ICS-2000). Using this method,

concentrations of nitrate, nitrite, acetate, carbonate, and calcium were determined at various points in space and time in the column.

Following treatment, the column was flushed with approximately four pore volumes of DI water to rinse away any residual salts. The sand was then removed and oven dried. Samples of cemented sand were kept for inspection under the SEM, while loose sand and the remaining cemented chunks were acid digested to quantify the carbonate content of the treated sand.

### **Third Generation Tests**

The third series of continuous flow tests was performed using dry Ottawa 20-30 sand air pluviated to a relative density of 45%. Two columns were tested. The first column was prepared using a 150 mm-tall, 73 mm-diameter clear acrylic column with sampling ports located at the base of the column, 50 mm from the base of the column, 125 mm from the base of the column, and at the top of the column (OS-CF-4). The second column was prepared using 100 mm-diameter simple shear base and top caps equipped with bender elements for the measurement of P-wave and S-wave velocity (OS-CF-5). This column was encased in a rigid jacket lined with a latex membrane for the duration of testing. Both columns were treated at very low confining stresses ( $< 3$  kPa). As with all of the other columns described in this chapter, these columns were purged with  $N_{2(g)}$  before treatment to facilitate denitrification.

Before treatment began, the columns were flooded from the bottom with a solution designed to simulate natural groundwater consisting of 184 ppm  $CaCl_2$ , 69 ppm  $NaHCO_3$ , and 63 ppm  $MgSO_4$  at a pH of 6.32. Flow was then induced through the columns using a peristaltic pump at a flow rate of 87.5 mL/day, corresponding to a flux of 0.075 ft/day.

Each column was first treated for approximately six hours with synthetic groundwater before switching to a sterile treatment solution consisting of 37.5 mM  $\text{Ca}(\text{NO}_3)_2$ , 75 mM  $\text{Ca}(\text{CH}_3\text{COO})_2$ , 137.5 mM  $\text{CaCl}_2$ , 2.0 mM  $\text{MgSO}_4$ , 0.75 g/L tryptic soy broth (TSB), and 0.5 mL/L of the trace metals solution detailed previously. Each column was treated for a total of six weeks with this treatment solution, followed by one week with simulated groundwater.

During the course of treatment, approximately 3.5 mL samples were drawn from each of the four sampling ports on the acrylic column (OS-CF-4) at one week intervals. The pH of each sample was taken immediately, at which point approximately 1.5 mL was used to find the total nitrogen content (TN) using a Hach TNT826 kit and 2 mL was filtered through a 0.2  $\mu\text{m}$  filter and stored at 4°C for the duration of column treatment. Following the end of the column treatment period, each sample was diluted by a factor of 200 and analyzed for ionic makeup using ion chromatography.

Every day for the duration of testing, the P-wave and S-wave velocity was measured in Column OS-CF-5 in order to analyze the degree of saturation and small strain stiffness of the soil in the column with time.

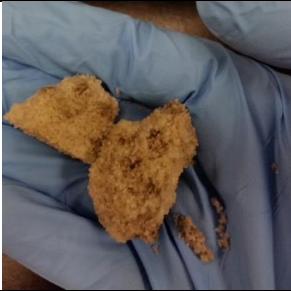
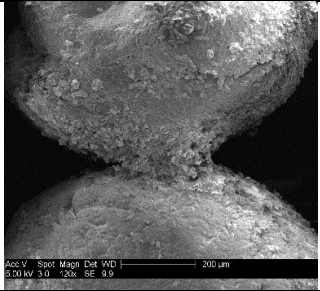

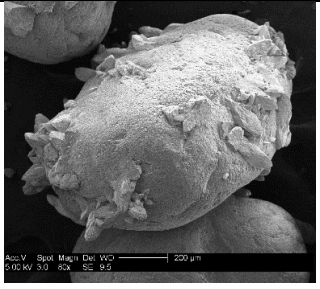
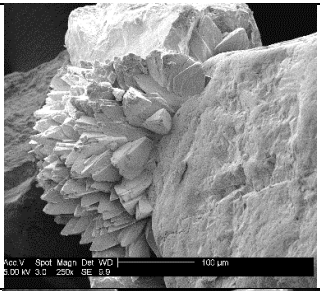

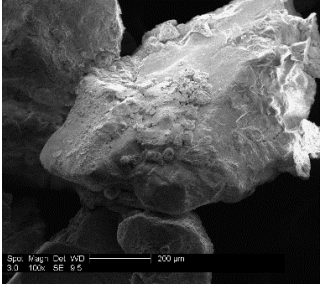
Following treatment, both of the columns were rinsed with approximately four pore-volumes of DI water to remove any residual salts. The sand from Column OS-CF-4 was then acid digested in layers to determine the carbonate content of the sand with depth, while the sand from Column OS-CF-5 was acid digested all together to get an overall carbonate content for the column. Samples from each column were saved for analysis via SEM.

## RESULTS

### Initial Tests

The results of the initial continuous flow tests are presented in Table 4.

**Table 4.** Results of initial continuous flow column tests (all columns treated for 10 weeks)

Column	CaCO <sub>3</sub> content (%)	Images of cemented soil	SEM Image of soil and carbonate
OS-CF-1	Uncemented sand: 0.457%  Cemented sand: 1.53%		
OS-CF-2	Uncemented sand: 0.268%  Cemented sand: 1.03%		
BC-CF-1	Uncemented sand: 0.109%	No observed cementation	
BC-CF-2	Uncemented sand: 0.223%  Cemented sand: too small to acid digest separately		

As shown in Table 4, cemented soil was observed in three of the four soil columns. This result is interesting because it shows that significant soil improvement (i.e. cementation) can occur within a matter of weeks after the onset of treatment in a continuously flowing system (contrary to the slower rate of cementation in the semi-stagnant columns). In all of the columns which exhibited cementation, the cemented chunks of soil were found at the tops of the columns. As the direction of fluid flow was from the tops of the columns to the bottoms for most of the duration of testing (6 out of 10 weeks), it makes sense that cementation would predominantly appear near the tops of the columns, as this is the location in which microbial growth would be the most likely to be stimulated as this is the location with the highest nutrient concentration.

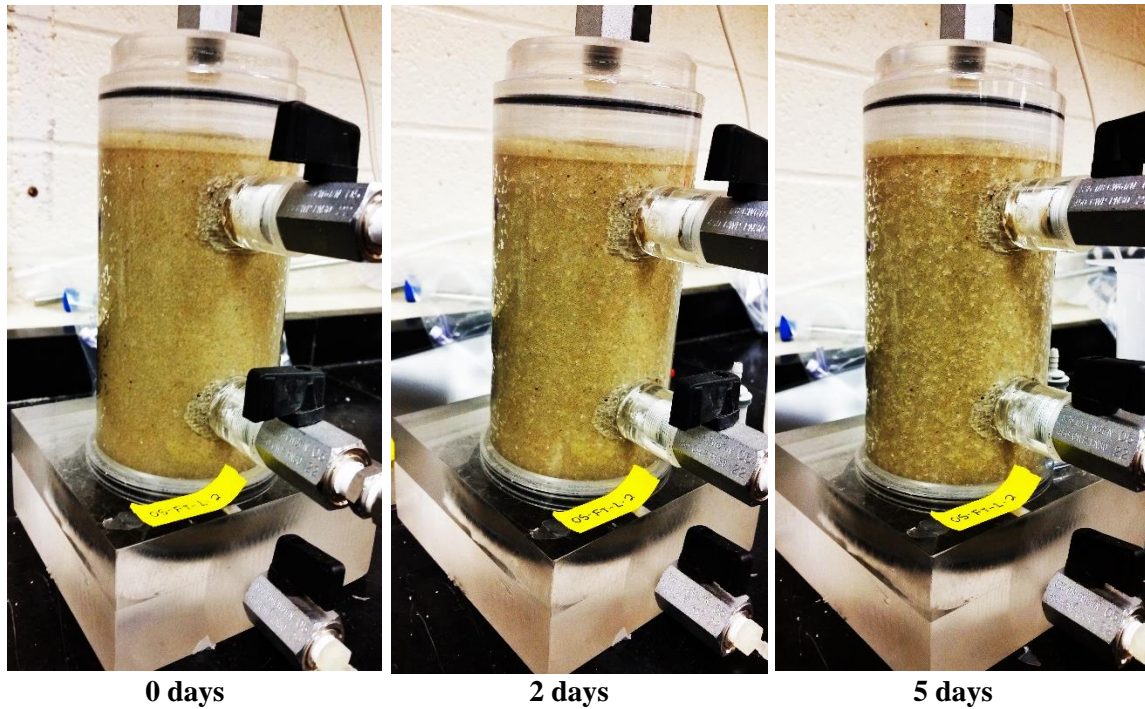
Also shown in Table 4, columns with Ottawa sand exhibited more extensive cementation than those with the natural Bolsa Chica sand. This is most likely due to the fact that there was less carbonate precipitation in the Bolsa Chica sand than in the Ottawa sand. The reason as to why there is less precipitation of carbonate in the Bolsa Chica sand is unclear, as IC analysis was not performed on these initial columns. However, it may be that nitrite accumulation slowed down the rate of biological activity and hence carbonate precipitation in these Bolsa Chica columns. The lack of cementation in the Bolsa Chica columns may also have something to do with the initial void ratios for each of the sands. The Bolsa Chica sand had a considerably higher void ratio ( $e = 0.77$ ) as compared to the Ottawa sand ( $e = 0.65$ ). Thus, it follows that more carbonate precipitation would be necessary to sufficiently bridge the voids between particles to induce cementation. In either case, less carbonate precipitation was observed in the columns with Bolsa Chica sand than in those with Ottawa sand.

Also shown in Table 4 are the carbonate content of cemented and uncemented sand and the SEM images of cemented soil from each column. It is interesting to note that Column OS-CF-2 exhibited more uniform and greater cementation than Column OS-CF-1, but with lower carbonate content in both the cemented and uncemented sections of the column. One potential reason for this is that larger carbonate crystals were precipitated in Column OS-CF-2 than in Column OS-CF-1. As shown in the SEM images of each column, carbonate crystal sizes are much smaller in Column OS-CF-1 than in Column OS-CF-2. Larger crystal sizes may lead to increased cementation at lower carbonate contents, as large crystals can more easily bridge gaps between sand particles. It remains unclear as to why one column exhibited larger crystals than the other, as both columns were treated in an identical fashion. Also, no IC analysis was performed on these columns, so it is unclear how the pore fluid chemistry may have influenced carbonate crystal size.

It is also interesting to note that significant carbonate precipitation was achieved in these columns without any inoculation with exogenous microbes. This result indicates that, in a field setting, it should be possible to stimulate native denitrifying organisms for soil improvement.

### **Second Generation Tests**

While the results of the initial continuous flow columns were promising, more data were necessary to fully characterize the biogeochemistry of the MICP process in continuous flow conditions as well as the potential for desaturation. Therefore, a second generation column was tested in which pore fluid samples were taken periodically and analyzed using ion chromatography. Figure 36 below shows the progression of desaturation in Column OS-CF-3 with time.

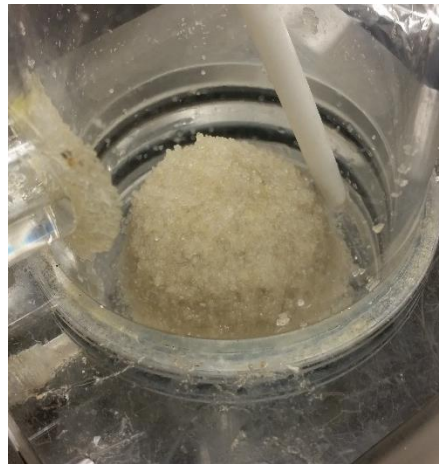


**Fig. 36.** Observed desaturation with time in column OS-CF-3

As shown in Figure 36, desaturation as evidenced by gas bubbles visible in the soil pores, occurs within days of stimulation of native organisms. Additionally, the gas bubbles were observed throughout the column, indicating that desaturation via denitrification is relatively uniform in nature. This suggests that liquefaction mitigation via desaturation could begin in a matter of days in natural conditions.

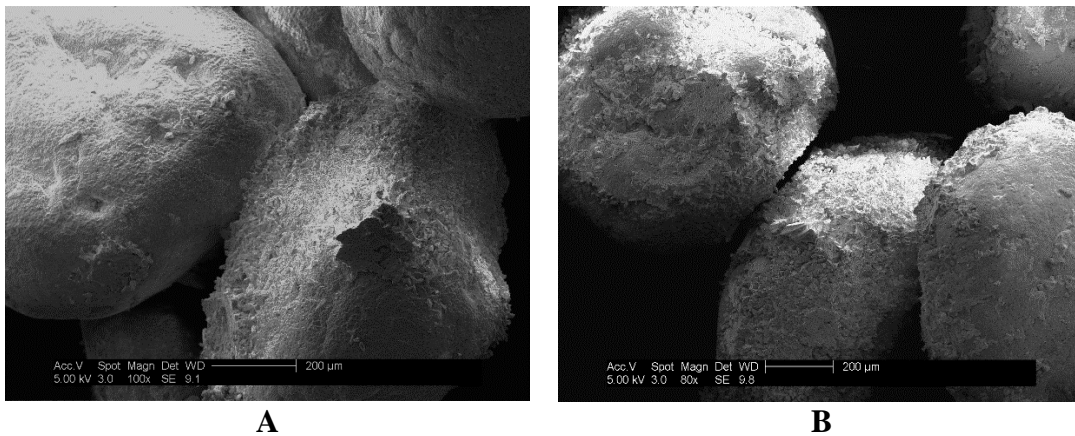
Carbonate precipitation and soil cementation were also shown to occur within the five weeks of treatment in Column OS-CF-3, as shown in Figure 37 below. As shown in Figure 37, a fairly large zone of soil cementation was visible at the base of Column OS-CF-3 after only five weeks of treatment. Acid digestion revealed that this cemented zone contained roughly 2.37% carbonate by weight. This result indicates that significant soil improvement via carbonate precipitation is possible within a matter of weeks to months after stimulation of native microorganisms. These results also show the advantages of continuous flow over

semi-stagnant conditions for carbonate precipitation, as it took roughly a year of treatment to achieve similar amounts of cementation in the semi-stagnant columns. The uncemented sand located in the upper parts of Column OS-CF-3 were found to contain 0.386% carbonate by weight.



**Fig. 37.** Cemented sand at base of column OS-CF-3

SEM images of treated sand from Column OS-CF-3 can be seen in Figure 38.



**Fig. 38.** SEM images showing interparticle cementation (A) and particle roughening (B) of treated soil from Column OS-CF-3.

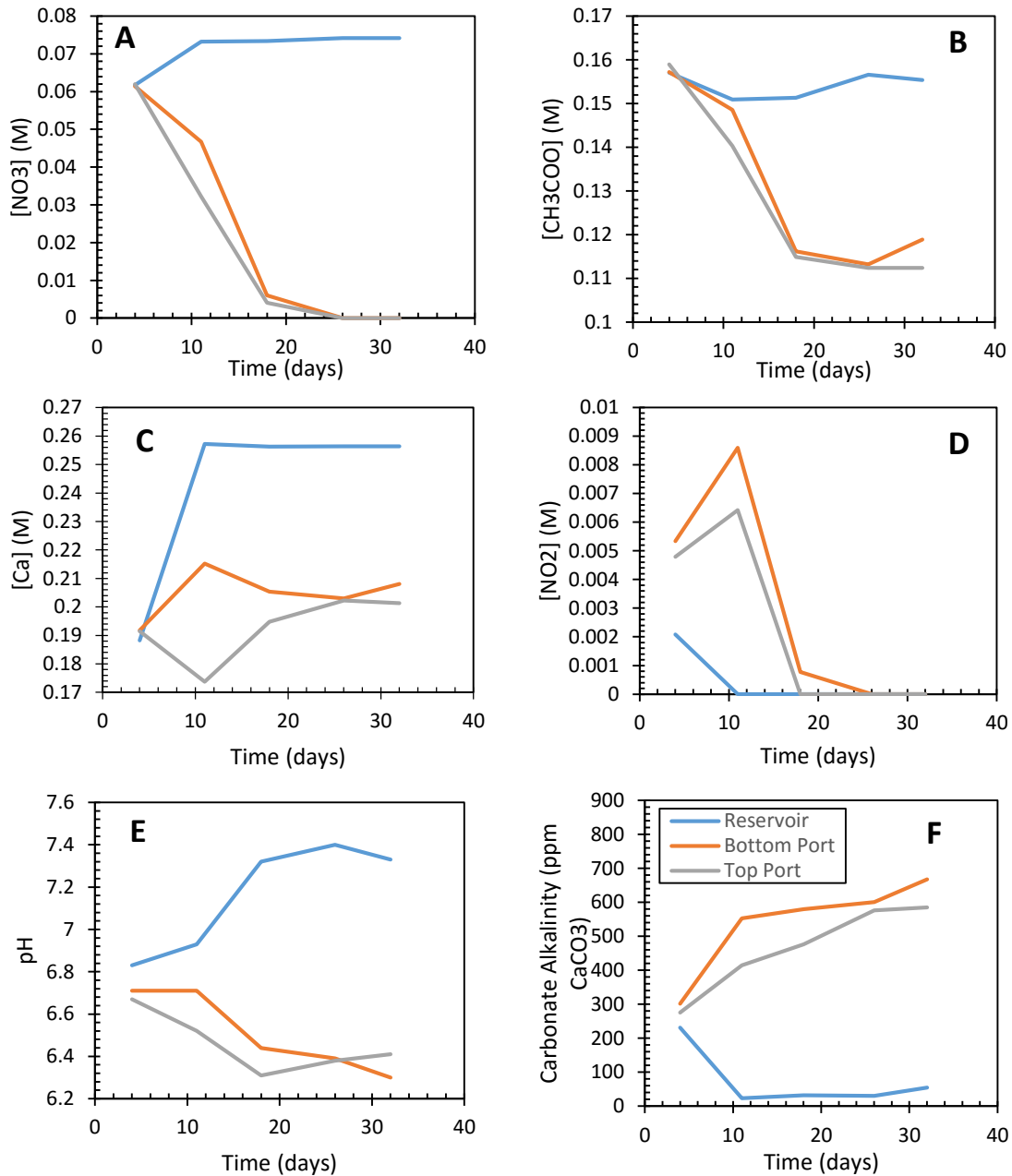
As shown in Figure 38, interparticle cementation as well as significant amounts of carbonate cladding on the sand particles were observed in SEM images of the cemented



sand from Column OS-CF-3. It is also interesting to note that, while the extent of carbonate precipitation on the soil particles is quite high, the carbonate crystals themselves are fairly small, especially when compared with Column OS-CF-2 (Table 1).

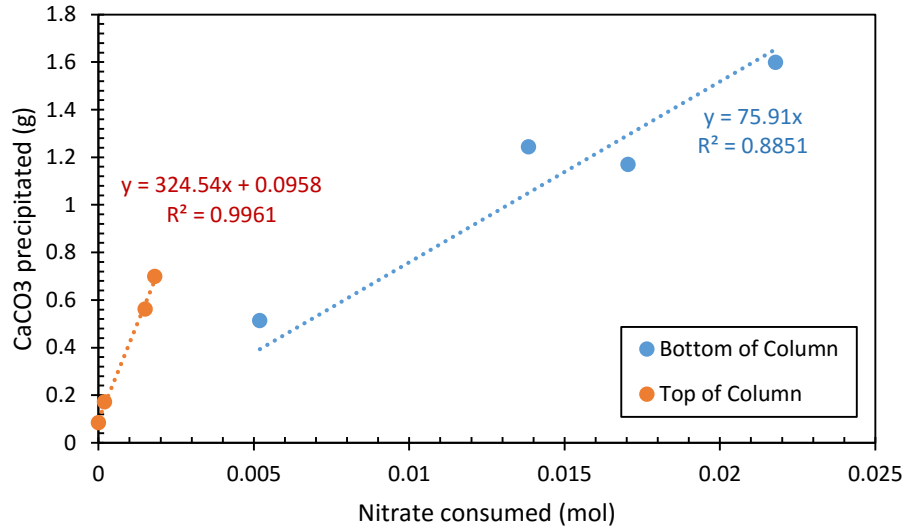
The results of IC analysis for column OS-CF-3 are shown in Figure 39 below. As shown in Figure 39A, the nitrate concentration begins to decrease significantly with space in the column after only 11 days of treatment, with full nitrate removal occurring within the column after 18-24 days. This result indicates rapid stimulation of denitrifying organisms. Also, the fact that nitrite accumulation in all parts of the column effectively ends after 18 days (Figure 39D), indicates that full denitrification is occurring and that microbial growth is not inhibited due to nitrite accumulation. Figure 39A and 39B indicate that microbial activity is highest in the bottom of the column, with most of the nitrate and acetate removal occurring between the reservoir and the bottom part of the column. Figure 39C shows that calcium concentrations are decreasing from the bottom to the top of the column for the first 10 days. This indicates that carbonate precipitation is occurring at all points in the column, but that more precipitation is occurring in the bottom of the column.

As shown in Figure 39E, there is a general decrease in pH from the base of the column to the top, indicating carbonate precipitation throughout the column. Finally, the increase in carbonate alkalinity between the reservoir and the bottom of the column shown in Figure 39F, followed by a decrease in alkalinity between the bottom and top of the column indicates that there is more biological activity occurring in the base of the column (i.e. increase in carbonate alkalinity), with comparably more carbonate precipitation occurring in the top of the column (i.e. decrease in carbonate alkalinity). So, it appears that there is a time delay between denitrification and carbonate precipitation in the column.



**Fig. 39.** Nitrate (A), acetate (B), calcium (C), nitrite (D), pH (E), and carbonate alkalinity for column OS-CF-3. The blue curve represents fluid taken from the reservoir of fresh nutrient solution directly upgradient of the column base, the orange curve represents fluid taken from the lower sampling port of the column (50 mm from base) and the grey curve represents fluid taken from the top sampling port of the column (125 mm from base of column).

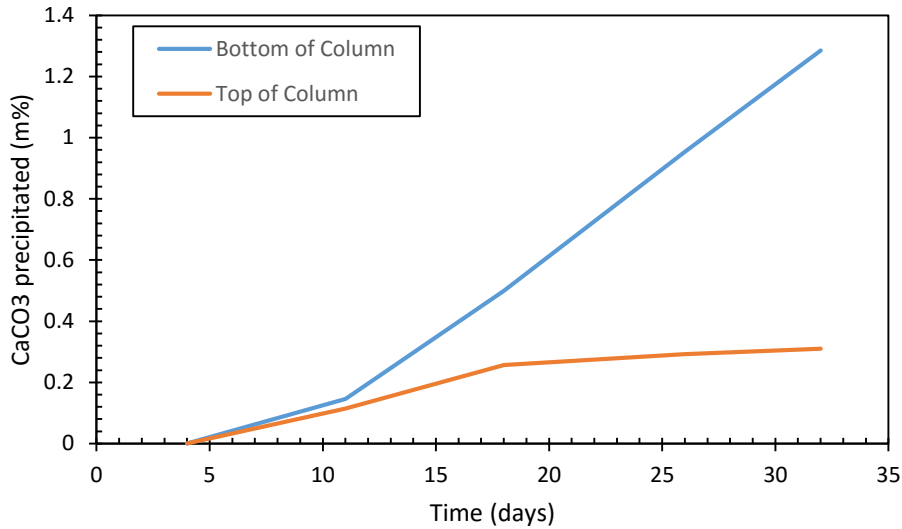
This difference in precipitation between the bottom and top of the column is further illustrated in Figure 40.



**Fig. 40.** Mass of carbonate precipitated versus mols of nitrate consumed for Column OS-CF-3.

As shown in Figure 40, the amount of carbonate precipitated per mol of nitrate consumed is greater in the top half of the column than in the bottom half. This indicates that there is more biological activity in the base of the column (as there is more nitrate consumed), but more carbonate precipitation in the top of the column. So, there must be a time lag between the microbial process of denitrification and the chemical process of carbonate precipitation occurring across the column. This time delay between biological activity and carbonate precipitation is important to understand if soil improvement via denitrification is implemented in the field.

Figure 41 shows the total amount of carbonate precipitated in the bottom and top halves of the column.



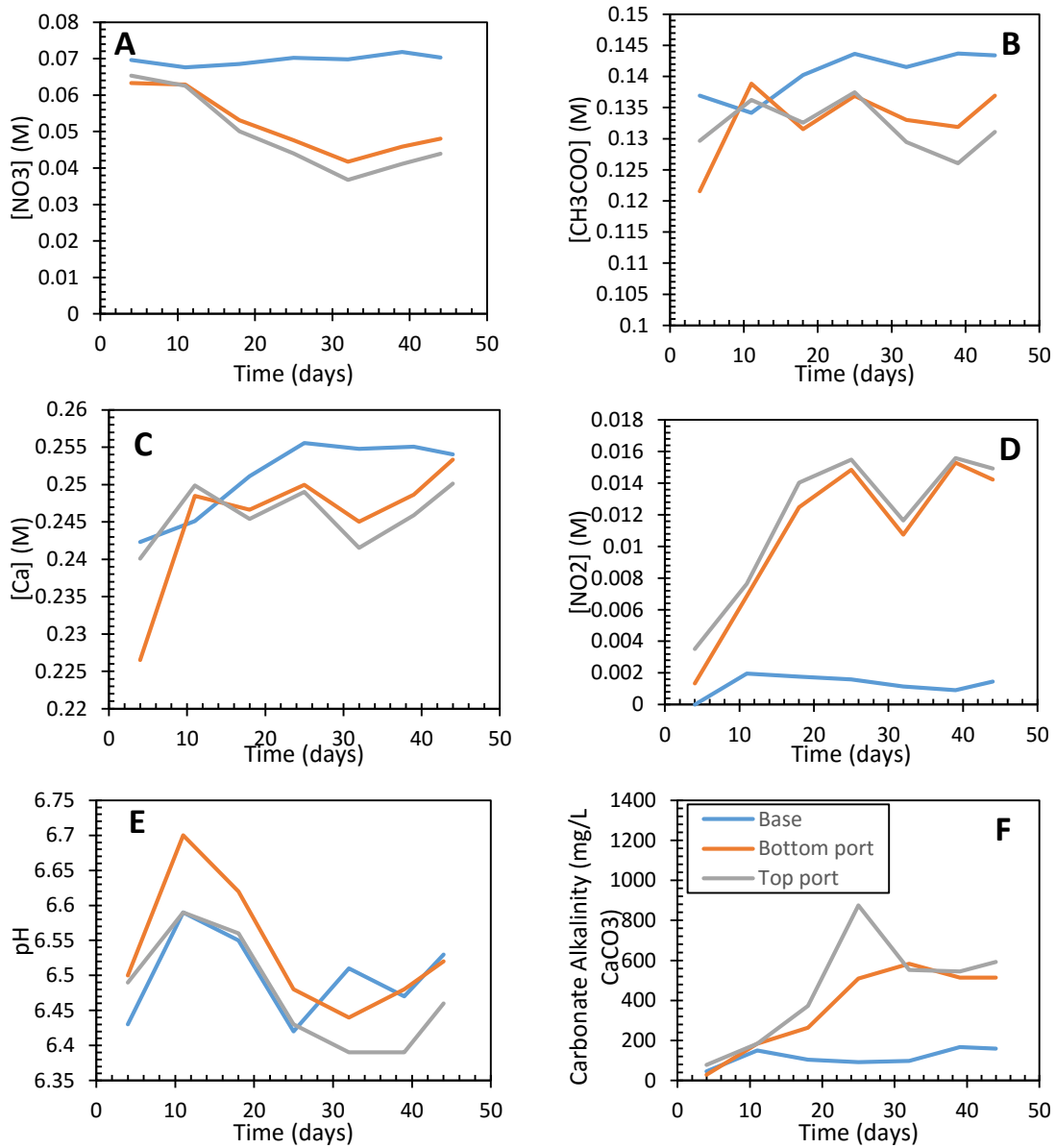
**Fig. 41.** Mass percentage of carbonate precipitated from IC analysis for Column OS-CF-3.

As shown in Figure 41, the rates of carbonate precipitation in the bottom and top of Column OS-CF-3 are initially very close, but carbonate precipitation begins to occur more quickly in the bottom of the column after 11 days of treatment, and carbonate precipitation in the top of the column slows down considerably after 18 days of treatment. This result indicates that microbial growth concentrates near the nutrient inflow (bottom of column) with time. This result is to be expected. The average amount of carbonate precipitation in the bottom half of the column is approximately 1.3% after 32 days, but only 0.3% in the top half of the column in the same time period.

### Third Generation Tests

Due to problems maintaining continuous flow with the roller clamp and IV drip setup used in the first two generations of continuous flow column tests, the third generation columns were conducted using a peristaltic pump to maintain constant flow. The flow rate was also increased to 87.5 mL/day (a flux of 0.075 ft/day) for these columns in an effort to achieve more uniform carbonate precipitation across the column. The third generation tests

were also initially flooded with the simulated groundwater to represent field conditions as closely as possible. The results of IC analysis from Column OS-CF-4 are shown in Figure 42.

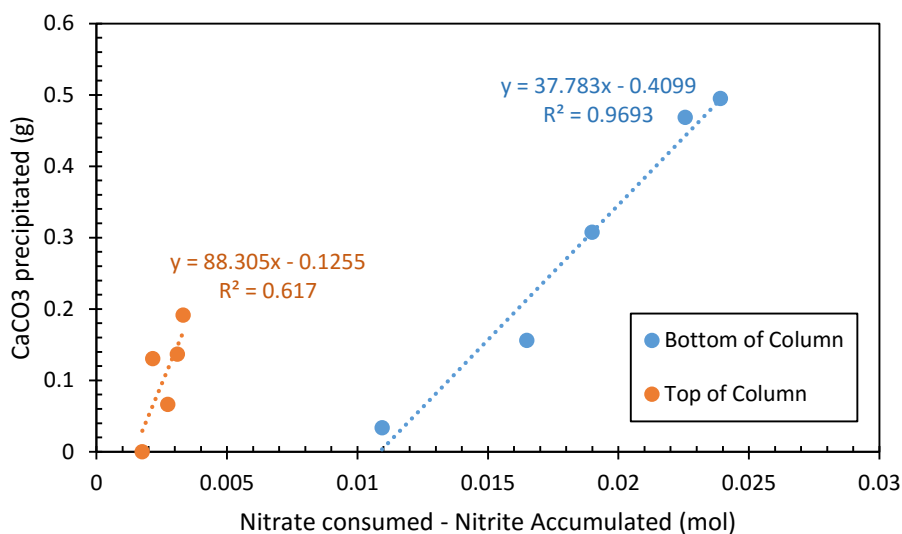


**Fig. 42.** Nitrate (A), acetate (B), calcium (C), nitrite (D), pH (E), and carbonate alkalinity (F) with time in column OS-CF-4

As shown in Figure 42A, the nitrate concentration begins to decrease in the column after 11 days of treatment, but then stalls at roughly 50% nitrate removal after 32 days. This result indicates rapid stimulation of denitrifying organisms followed by stagnation of microbial growth. This result is echoed in the acetate concentrations presented in Figure 42B. This inhibition of microbial growth is most likely the result of nitrite accumulation in the columns. As shown in Figure 42D, the nitrite concentration rises rapidly and then stagnates at around 15 mM after 18 days of treatment. It is widely recognized that nitrite, or more specifically nitrous acid, acts as an uncoupling inhibitor to cell growth (Sijbesma et al. 1996). It is most likely that more nitrite accumulation was observed in Column OS-CF-4 than in Column OS-CF-3 because of the higher flow rate in Column OS-CF-4. Figure 42A and 42B indicate that microbial activity is highest in the bottom of the column, with most of the nitrate and acetate removal occurring between the base and the bottom port of the column.

Figure 42C shows that calcium concentrations are generally decreasing from the base to the top of the column. This indicates that carbonate precipitation is occurring at all points in the column, but that more precipitation is occurring in the bottom of the column. However, the magnitude of calcium removal is much less in all parts of the column than for Column OS-CF-3, most likely due to partial denitrification and nitrite accumulation. As shown in Figure 42E, there is an initial increase in pH between the base of the column and the bottom port, followed by a decrease in pH from the base of the column to the top. This result indicates microbial activity in the base of the column is driving the pH upwards, followed by carbonate precipitation and less microbial activity in the top of the column causing the pH to drop. The increase in carbonate alkalinity between the reservoir and the

bottom of the column shown in Figure 42F, with little to no change in alkalinity between the bottom and top of the column, indicates that there is more biological activity occurring in the base of the column (i.e., more carbonate generation) with comparably more carbonate precipitation occurring in the top of the column (evidenced by the loss of carbonate). So, as with Column OS-CF-3, it appears that there is a time delay between denitrification and carbonate precipitation in Column OS-CF-4. This effect is further illustrated in Figure 43.

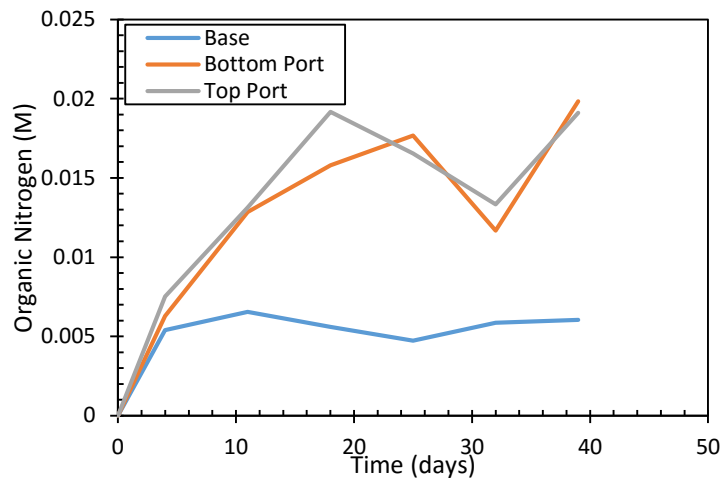


**Fig. 43.** Mass of carbonate precipitated versus mols of nitrate consumed for Column OS-CF-4.

As shown in Figure 43, the amount of carbonate precipitated per mol of nitrate consumed is higher in the top half of the column than in the bottom half of the column. This indicates a time lag between biological nitrate consumption and chemical carbonate precipitation from the bottom to the top of the column. It is also interesting to note that the amount of carbonate precipitated per mol of nitrate consumed is considerably lower in both the top and bottom of Column OS-CF-4 than in Column OS-CF-3. This is most likely due

to nitrite accumulation in Column OS-CF-4. More alkalinity is generated when nitrite is reduced to nitrogen gas than when nitrate is reduced to nitrite. Since there is less nitrite reduction in Column OS-CF-4, there is comparably less carbonate precipitation.

The amount of biological activity in each part of the column is further illustrated by the change in organic nitrogen between the different parts of the column presented in Figure 44.

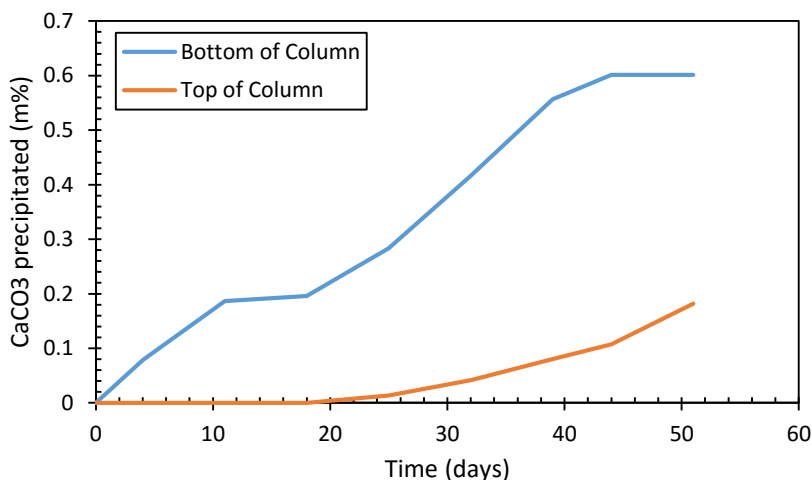


**Fig. 44.** Organic nitrogen concentrations Column OS-CF-4 with time.

As shown in Figure 44, the organic nitrogen concentration increases considerably between the base of the column and the bottom port, indicating an increase in microbial biomass. However, the organic nitrogen concentration barely increases between the bottom port and the top port of the column, indicating a stagnation in microbial growth in the top part of the column. This is further evidence that microbial activity is much higher in the bottom part of the column.

Figure 45 shows the cumulative amount of carbonate precipitated in the top and bottom parts of the column with time.

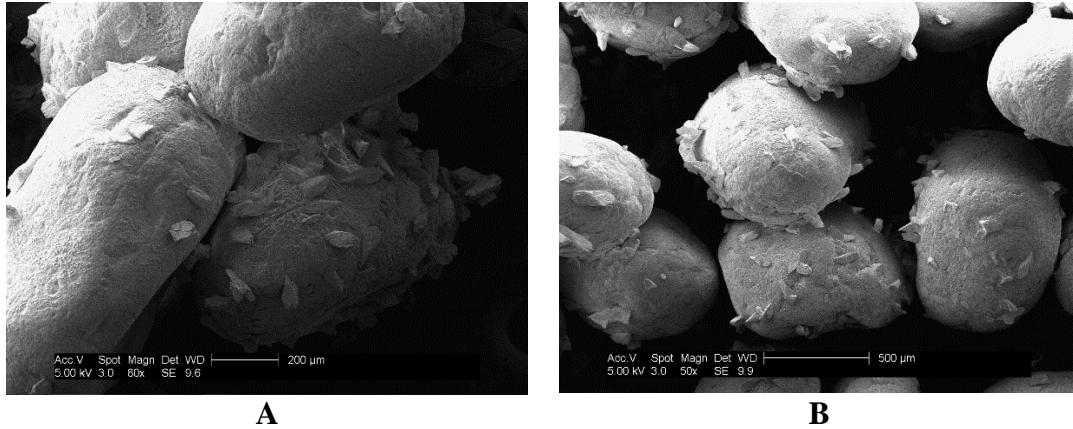




**Fig. 45.** Mass percentage carbonate precipitated from IC analysis for Column OS-CF-4.

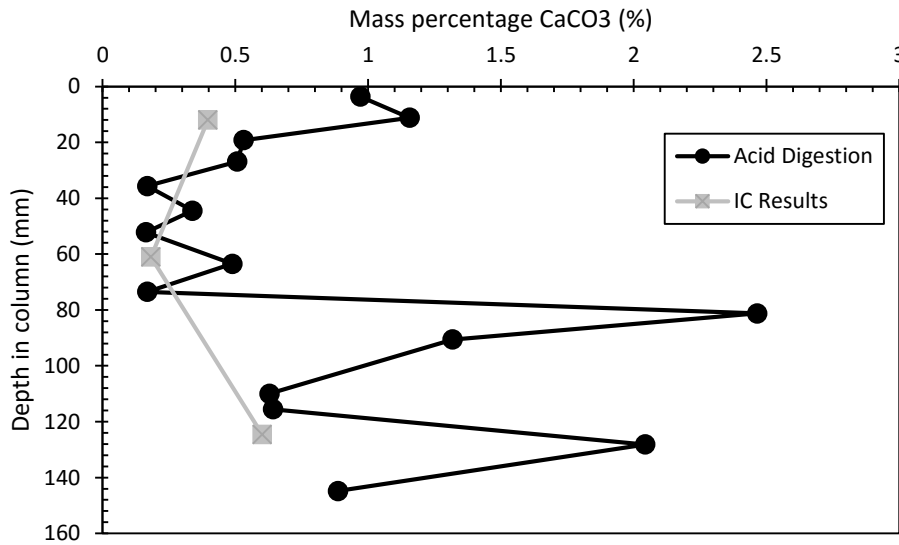
As shown in Figure 45, considerably more carbonate was precipitated in the bottom of Column OS-CF-4 than in the top of the column. However, after 39 days of treatment, the rate of carbonate precipitation begins to increase in the top of the column, with a simultaneous decrease in the bottom of the column. This may be due in part to the growth of nitrite resistant bacteria in the top of the column that are capable of performing denitrification at high nitrite concentrations. Data on the composition of the microbial community at the top of the column is necessary to confirm this hypothesis (Chapter 6).

SEM images showing interparticle cementation and particle roughening in Column OS-CF-4 are shown in Figure 46 below. As shown in Figure 46, both interparticle cementation and particle roughening were observed in soil taken from Column OS-CF-4. The SEM images show that carbonate precipitated in very large, discrete crystals along the particle surfaces. This is much different from the precipitation pattern observed in Column OS-CF-3, but reminiscent of the precipitation pattern observed in Column OS-CF-2. The larger crystal sizes may be due to slower precipitation caused by nitrite accumulation in the column.



**Fig. 46.** SEM images of treated soil from Column OS-CF-4 showing interparticle cementation (A) and particle roughening (B).

A comparison of the carbonate content with depth derived from IC analysis to that derived from acid digestion is shown in Figure 47.



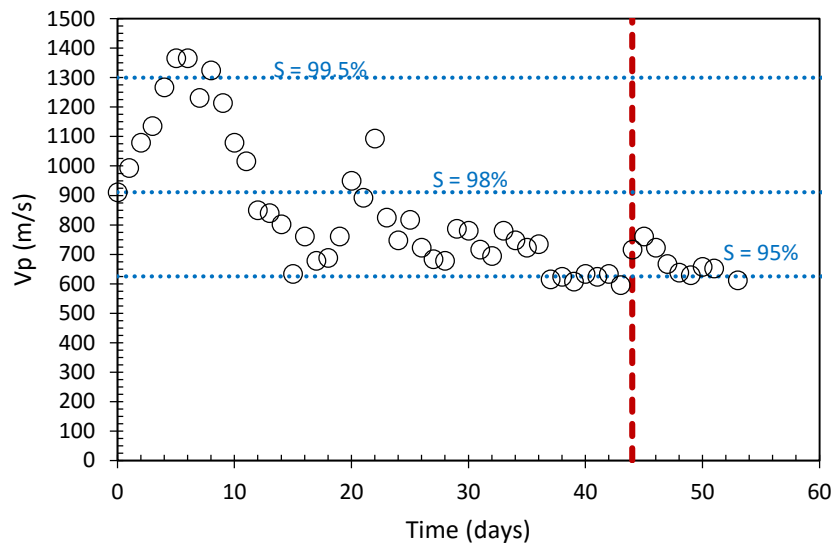
**Fig. 47.** Carbonate content in Column OS-CF-4 from IC analysis and acid digestion.

As shown in Figure 47, both acid digestion and IC analysis show an hourglass pattern of carbonate precipitation in the column, with most of the precipitation occurring at the

bottom, a small amount occurring in the middle, and a moderate amount occurring near the top of the column. However, the IC results for carbonate content are generally lower than those from acid digestion. This may be due to sand loss during acid digestion which results in a higher apparent mass percentage of carbonate. As this column was digested in small pieces, sand loss may have a large impact on the apparent carbonate content. As an example, in this column, a loss of only 0.5 g of sand would result in an apparent increase in carbonate content of upwards of 1%. It should also be noted that the decrease in carbonate content at a depth of roughly 100 mm from acid digestion corresponds to the location where a small cemented sample of sand was removed from the column for SEM analysis. The removal of this cemented chunk most likely resulted in lower carbonate contents at this point in the column when the remaining, uncemented sand was acid digested.

The P-wave velocity results from Column OS-CF-5 is presented in Figure 48. As shown in Figure 48, at the start of treatment, the P-wave velocity in Column OS-CF-5 corresponds to a degree of saturation of 98%. As treatment commences, the P-wave velocity and degree of saturation increase, indicating a degree of saturation of roughly 99.5% after six days. This increase in saturation is most likely due to the removal of residual gas from the soil pores due to continuous flow conditions. After the sixth day of treatment, the P-wave velocity begins to decrease considerably to a value corresponding to a degree of saturation of roughly 96% by the seventeenth day of treatment. This most likely is attributable to gas production caused by the stimulation of denitrifying microorganisms. Following the seventeenth day of treatment, there is a slight rise in P-wave velocity to a corresponding degree of saturation of roughly 98.5%. The small peak in P-wave velocity may have been

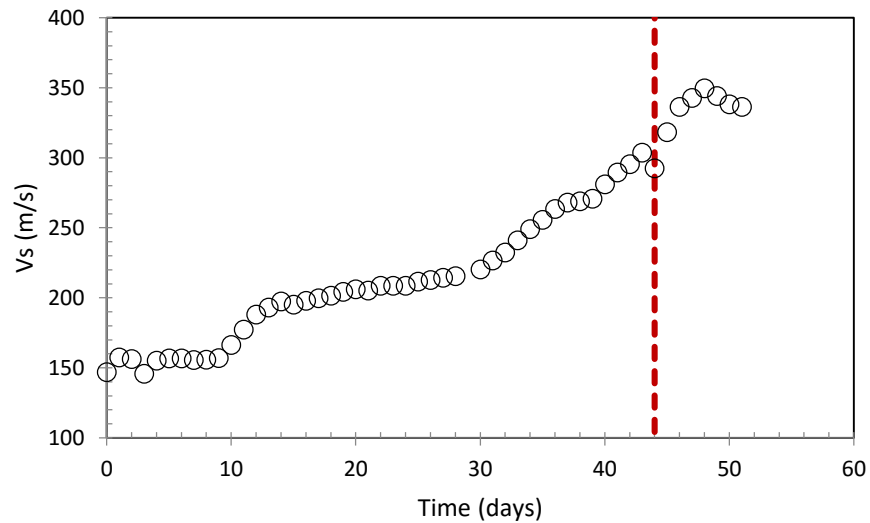
due to an accumulation of nitrite and a corresponding decrease in microbial activity and gas production. However, it appears that this period of nitrite inhibition did not last long, as the P-wave velocity dropped again and stabilized to a corresponding degree of saturation of roughly 95-96% after twenty eight days of treatment. These results indicate that desaturation occurs fairly quickly after the stimulation of native organisms in continuous flow conditions. It also suggests that the degree of saturation will fall to and stabilize at a degree of saturation suitable for significant liquefaction mitigation.



**Fig. 48.** P-wave velocity with time for Column OS-CF-5. The red dashed line indicates the termination of treatment, while the blue lines indicate the corresponding degree of saturation in the column from Figure 6 (Chapter 3).

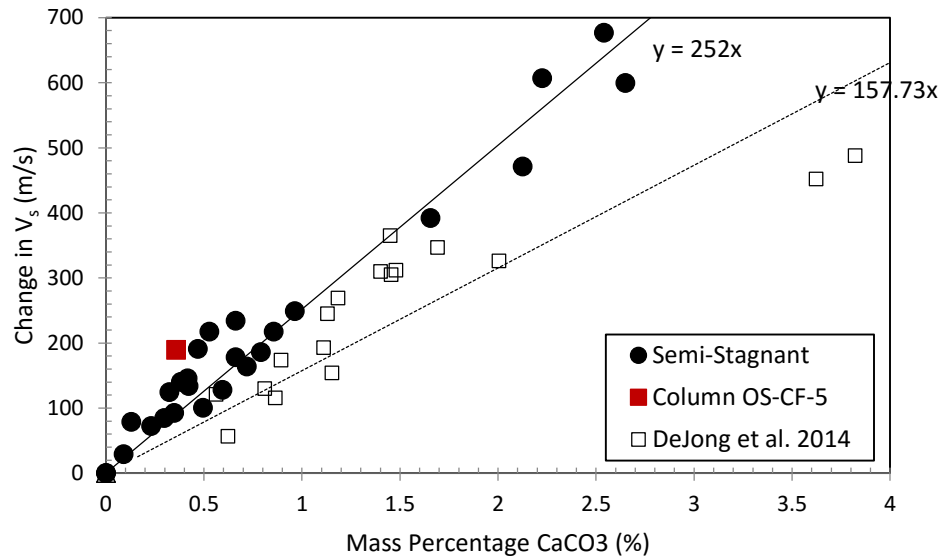
The shear wave velocity with time for Column OS-CF-5 is shown in Figure 49. As shown in Figure 49, the shear wave velocity in Column OS-CF-5 begins at roughly 150 m/s, a value consistent with that of a loose, liquefiable sand. After 10 days of treatment, the shear wave velocity begins to rise quickly to a value of roughly 200 m/s after 14 days of treatment. This may correspond to the onset of carbonate precipitation in the column.

If carbonate precipitation does begin 10 days after the onset of denitrification (as possibly indicated by the P-wave velocity), it would further support the contention that there is a time lag between biological activity and the chemical precipitation of carbonates in the column. After fourteen days of treatment, the shear wave velocity increases very slowly until roughly thirty days of treatment. This period of what may be slower carbonate precipitation in the column corresponds well with the small spike in P-wave velocity seen in Figure 48. After thirty days of treatment, the shear wave velocity begins to increase at a higher rate until four days following the termination of treatment. The final shear wave velocity in the column is roughly 340 m/s, well above the accepted range for a liquefiable soil (Andrus and Stokoe 1997). However, it should be noted that the limits set by Andrus and Stokoe (1997) are for uncemented soils and may not apply to the liquefaction resistance of MICP treated soil.



**Fig. 49.** Shear wave velocity with time for Column OS-CF-5. The red dashed line corresponds to the termination of treatment.

Following treatment, the carbonate content of Column OS-CF-5 was determined to be 0.36% via acid digestion. Figure 50 shows how the change in shear wave velocity in Column OS-CF-5 compares with the change in  $V_s$  from the semi-stagnant denitrification columns from Chapter 4 as well as from soil treated via ureolysis (DeJong et al. 2014).



**Fig. 50.** Change in shear wave velocity versus carbonate content for Column OS-CF-5, semi-stagnant denitrification columns, and soil treated via ureolysis by DeJong et al. (2014).

As shown in Figure 50, the change in shear wave velocity with carbonate content is higher in Column OS-CF-5 than in either the semi-stagnant columns or the soil treated via ureolysis. As discussed previously, soil treated via denitrification generally develop larger carbonate crystals than soil treated via ureolysis due to the slower rate of carbonate precipitation during denitrification, resulting in a larger increase in shear wave velocity for the same carbonate content (Chapter 4). This effect is not as dramatic in the semi-stagnant columns. However, the semi-stagnant columns may have been disturbed due to the constant draining and refilling, resulting in a reduction in shear wave velocity.

## CONCLUSIONS

Testing of soil columns subjected to continuous flow showed the applicability of denitrification as a two stage process for liquefaction mitigation under field conditions. The results showed that, following the inception of denitrification, desaturation occurs quickly and to an extent capable of providing a significant reduction in cyclic resistance of the soil. In addition, carbonate precipitation on and between soil particles in the continuous flow columns was found to occur much more quickly than previously observed in semi-stagnant column tests. In fact, it was found that cementation and particle roughening could be induced within a matter of weeks following inception of denitrification in continuous flow columns. Finally, results of the continuous flow column tests indicated that biostimulation of denitrifying organisms in-situ should be achievable. However, the flow rate and initial concentrations of nitrate play a large role in the rate and amount of soil improvement via denitrification, as higher concentrations and higher flow rates can result in nitrite accumulation and inhibition of microbial growth.

**CHAPTER 6**  
**CHARACTERIZATION AND ANALYSIS OF MICROBIAL COMMUNITIES**  
**FOR SOIL IMPROVEMENT VIA DENITRIFICATION**

**INTRODUCTION**

Testing of semi-stagnant and continuous-flow soil columns demonstrated the ability of native soil microbes to mitigate the potential for liquefaction through denitrification (Chapters 4, 5). This chapter describes the makeup of the stimulated microbial communities in these columns. This chapter also explores the question of whether stimulating native microbes in the soil (biostimulation) or adding exogenous microbes (bioaugmentation) is more effective for soil treatment via denitrification. If mitigation of earthquake-induced soil liquefaction via denitrification is to be applied in the field, it is important to know what kind of microbes will be stimulated in the soil and how the members of the stimulated microbial community interact to generate gas and induce MICP for soil improvement. It is also important to understand if and how inoculation of soil sites with exogenous microbes will affect soil improvement via denitrification.

This chapter characterizes the microbial communities stimulated in the semi-stagnant and continuous-flow soil columns as a means to understand how different treatment regimens (i.e., semi-stagnant vs. continuous flow, biostimulation vs. bioaugmentation) affect the makeup of the microbial community and the effectiveness of soil improvement via denitrification. It also presents a comparison of denitrification and carbonate precipitation in an uninoculated soil column and soil columns inoculated with pure culture and mixed culture to determine the most effective method for soil treatment.



## MEANS AND METHODS

### Initial Column Tests

Three acrylic soil columns (73 mm diameter, 150 mm tall) were prepared to determine the effectiveness of microbial inoculation for inducing denitrification in a clean sand. Each of the soil columns was initially exposed to a 70% solution of ethanol to disinfect the testing equipment. Following disinfection, 210 mL of pore fluid consisting of 50 mM  $\text{Ca}(\text{NO}_3)_2$ , 100 mM  $\text{Ca}(\text{CH}_3\text{COO})_2$ , 2.0 mM  $\text{MgSO}_4$ , 100 mM  $\text{CaCl}_2$ , and 0.5 mL/L trace metals (0.5% (w/v)  $\text{CuSO}_4$ ,  $\text{FeCl}_3$ ,  $\text{MnCl}_2$ ,  $\text{Na}_2\text{MoO}_4 \cdot 2\text{H}_2\text{O}$ ) were added to each column. The solution was autoclaved prior to its addition to the columns in an attempt to avoid extraneous microorganisms.

Following the addition of pore fluid to the columns, 990 g of Ottawa 20-30 silica sand was rained into the columns to a relative density of 30%. The sand also was autoclaved prior to its addition to the columns. Following placement of the sand in the columns, top caps (ethanol disinfected) were placed on tops of the soil columns and secured in place using silicone glue.

One of the soil columns, meant to serve as an uninoculated control, then received 40 mL of an autoclaved solution of nutrient broth (Difco, 8 g/L) through an injection port at the base of the column. However, as microbial growth was found to occur in this column during the treatment period, it will hereunto be referred to as the “Uninoculated column” rather than a control column. The other two soil columns received a 40 mL inoculation of either a mixed microbial culture (the Mixed Culture column) or a pure culture of *Pseudomonas denitrificans* (the Pure Culture column). The mixed microbial culture was grown by adding 5 g of soil and 5 mL of water, both of which were obtained from Bolsa

Chica State Beach in Huntington Beach, CA, to 85 mL of a solution containing nutrient broth (Difco 8 g/L), 25 mM  $\text{Ca}(\text{NO}_3)_2$ , and 25 mM  $\text{Ca}(\text{CH}_3\text{COO})_2$  and incubating the mixture under anaerobic conditions for 48 hours ( $\text{OD}_{600}$  0.567). The pure microbial culture was prepared in the same manner, but instead of adding sand and water from Bolsa Chica State Beach, a 2 mL inoculum of a pure culture of *P. denitrificans* was added ( $\text{OD}_{600}$  0.614 after 48 hours incubation). Following the addition of inoculum (or nutrient broth for the Uninoculated column), each column received 10 mL of extra pore fluid to raise the fluid level to the tops of each of the columns.

Pore fluid from each of the soil columns was then sampled (3 mL) at ten time intervals (0, 0.8, 1.8, 2.8, 3.8, 4.8, 5.8, 9.8, 12.8, 17.8, 28.8 days) from a sampling port located 5 cm from the base of each column. The pore fluid samples were then tested for pH, ionic makeup (Ion chromatography – Dionex ICS-2000), and total alkalinity (Hach TNT 870). Mass balance of the concentration of nitrate, nitrite, and calcium with time was used to assess the amount of denitrification and calcium carbonate precipitation in each of the columns. Following treatment, acid digestion was also used to quantify the amount of carbonate precipitation.

### **Analysis of Microbial Community in Semi-Stagnant and Continuous-Flow Columns**

Samples of pore fluid (5.5 mL) were extracted from two sampling ports (5 cm from base of column, 2.5 cm from top of column) in all four semi-stagnant acrylic columns (OS-ACR-1, OS-ACR-2, BC-ACR-1, BC-ACR-2) detailed in Chapter 4 on the fifth day of the 16<sup>th</sup> treatment cycle. Immediately following extraction, a 0.5-mL sample of the pore fluid taken from each sampling port was filtered through a 0.2- $\mu\text{m}$  syringe filter and stored at 4°C for two weeks before being analyzed using ion chromatography (IC) (Dionex ICS-

2000) to obtain an ionic spectrum at both sampling points in each column. The remaining 5-mL sample from each sampling port was used to assess the microbial ecology in the column. Pore fluid samples (5 mL) were also extracted at three different times ( $t = 16, 30, 44$  days after inception) from all four sampling ports (base of column, 5 cm from base of column, 2.5 cm from top of column, top of column) from continuous flow column OS-CF-4, detailed in chapter 5, to assess the evolution of the microbial ecology with space and time in the column. Separate samples were taken two days prior to each of the three pore fluid extractions described above for IC and pH measurement.

Immediately following extraction, each of the 5 mL pore fluid samples taken for assessment of microbial ecology was transferred into an autoclaved, sterile micro-centrifuge tube. These samples were then centrifuged at 13,200 g for 15 minutes. The supernatant was removed from each sample, and the pellets were stored at  $-20\text{ }^{\circ}\text{C}$ . After storing the biomass pellets for no more than 4 weeks, a MO-BIO Powersoil DNA isolation kit was used to isolate the DNA in each sample. Following DNA isolation, 16S rRNA genes were amplified using Polymerase Chain Reaction (PCR) and sent for Illumina sequencing at the Microbiome Analysis Laboratory in the Swette Center for Environmental Biotechnology at Arizona State University. QIIME (Caporaso et al. 2010), an open source bioinformatics program, was then used to analyze the raw sequence data to determine the diversity of microbial ecology in each sample. Specifically, the taxonomy of the microbial community in each sample was assessed from the phylum through genus level, phylogenetic diversity was estimated using the Faith method (Faith 1992), and the number of species present in each sample was estimated using the Chao1 index.

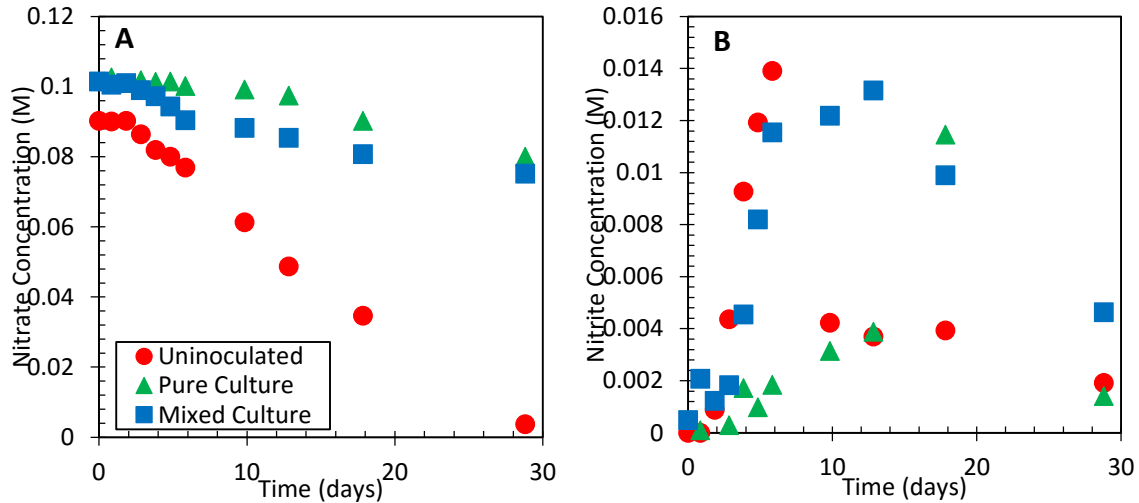
## RESULTS

### Initial Column Tests

Figure 51 plots the nitrate and nitrite concentrations with time in each of the three initial soil columns. The uninoculated column showed the fastest rate of nitrate removal, followed by the column inoculated with a mixed culture. The column inoculated with a pure culture of *P. denitrificans* showed the slowest rate of nitrate reduction. The fact that the uninoculated column, which was initially ethanol disinfected and filled with autoclaved sand and fluid, demonstrated the highest rate of nitrate removal shows that naturally occurring denitrifying bacteria are extremely resilient and were able to grow very quickly even after disinfection. It also demonstrates that biostimulation of these organisms is a more effective strategy than bioaugmentation (i.e. inoculating with exogenous microbes) for inducing denitrification in a soil deposit.

One reason that the uninoculated column demonstrated faster denitrification rates than the augmented columns is evidenced by the nitrite concentration shown in Figure 51B. The uninoculated and mixed-culture columns had rapid accumulation of nitrite to levels of 12-14 mM 3-6 days after the inception of the experiment. However, the nitrite concentration in the uninoculated column quickly decreased (roughly to 4 mM) within 8 days after inception. The mixed culture column, however, still had elevated nitrite concentrations 18 days after inception. It is possible that the prolonged period of nitrite accumulation inhibited the growth of denitrifying microbes in the mixed-culture column, causing the rate of nitrate removal to be slower than in the uninoculated column (Sijbesma et al. 1996). Consistent with slow removal of nitrate, the nitrite concentration rose at a slow rate in the column inoculated with a pure culture of *P. denitrificans* until roughly 18 days of treatment.

It may be that growth of the microbial community in this column was inhibited by the initially high nitrate levels (roughly 100 mM), as *Pseudomonas* species have been shown to be inhibited by high nitrate levels (Saleh-Lakha et al. 2009). These results suggest that a biostimulated microbial community may be less susceptible to nitrate and nitrite inhibition than a bioaugmented community.

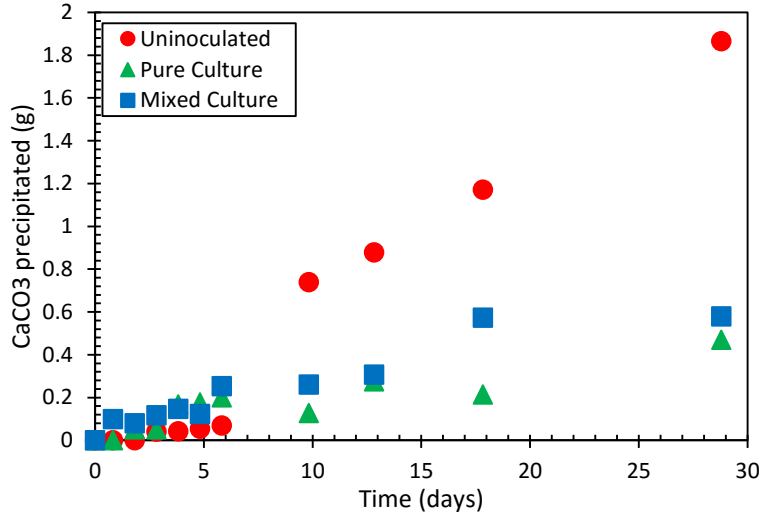


**Fig. 51.** Nitrate (A) and Nitrite (B) concentrations in the uninoculated column, the column inoculated with mixed culture, and the column inoculated with pure culture.

Figure 52 shows the amount of carbonate precipitation with time in each of the three acrylic columns. Consistent with the rate of denitrification (Fig. 51), the rate of carbonate precipitation was highest for the uninoculated, but biostimulated column and lowest for the column inoculated with a pure culture of *Pseudomonas denitrificans*.

Acid digestion of the sand from each column following treatment revealed that a total of 2.1 g, 1.2 g, and 1.0 g of calcium carbonate were precipitated in the uninoculated, mixed culture, and pure culture columns respectively. These carbonate contents, while slightly higher than those calculated from IC analysis and mass balance, confirm that the microbial

community formed from biostimulation is capable of performing MICP faster and to a greater extent than the communities formed from pure or mixed culture inoculation.



**Fig. 52.** Precipitation of calcium carbonate from IC analysis of  $\text{Ca}^{2+}$  and Ca mass balance for each of the three soil columns.

The results in Figures 51 and 52 and from the acid digests support that biostimulation of denitrifying microbes (uninoculated) may represent the most efficient method of inducing MICP in the field and that inoculation of any kind with exogenous microbes results in less efficient MICP via denitrification.

### **Semi-Stagnant Columns – Microbial Community Analysis**

The relevant concentrations of nutrients (electron donors and electron acceptors), pH and ionic strength at each sampling location for the four semi-stagnant columns described in Chapter 4 can be found in Table 5 below. All of these columns were initially inoculated with a mixed culture of bacteria enriched from sand and water taken from Bolsa Chica State Beach. Two of the columns (OS columns) were composed of Ottawa 20-30 silica sand, while the other two (BC columns) were composed of Bolsa Chica sand.

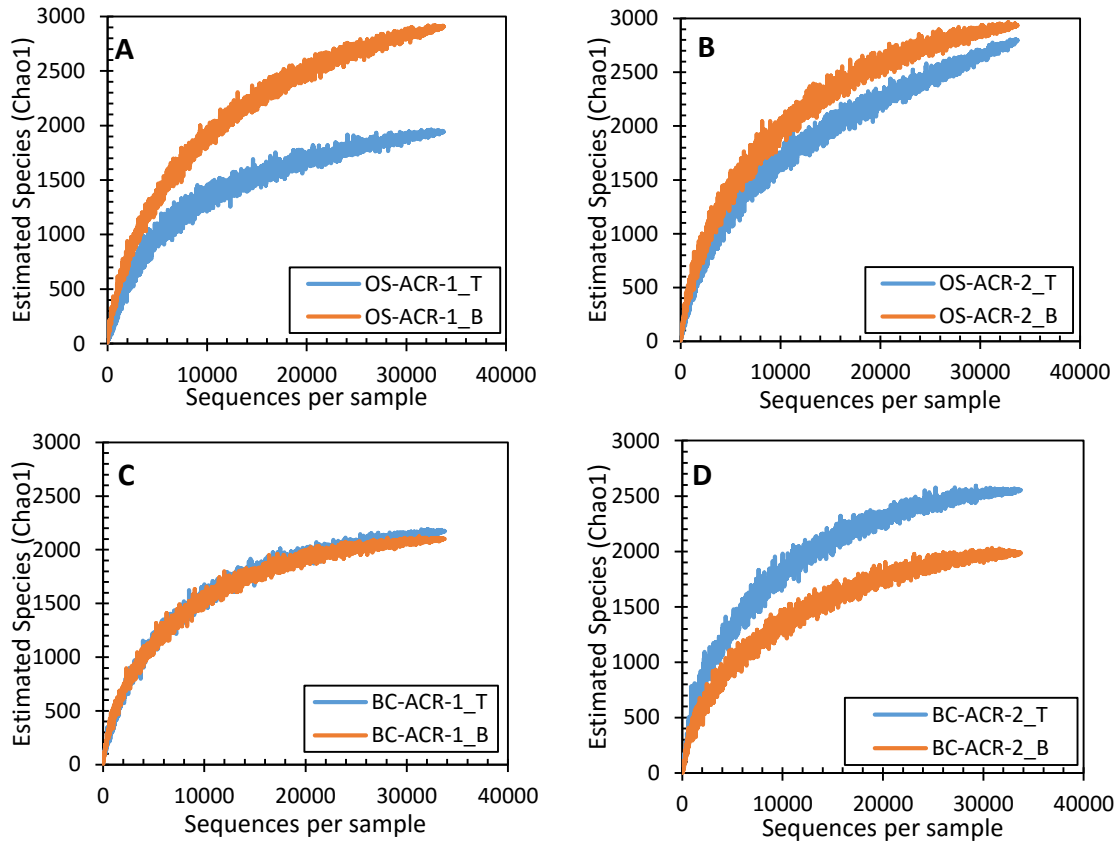
**Table 5.** Concentrations of major nutrients, pH, and ionic conductivity at each sampling location for semi-stagnant columns.

Column	Position	[NO <sub>3</sub> <sup>-</sup> ] (M)	[NO <sub>2</sub> <sup>-</sup> ] (M)	[SO <sub>4</sub> <sup>2-</sup> ] (M)	[CH <sub>3</sub> COO <sup>-</sup> ] (M)	pH	I (M)
OS-ACR-1	Top	0	0	0.0014	0.094	6.56	0.51
	Bottom	0.011	0.017	0.0017	0.127	6.41	0.59
OS-ACR-2	Top	0.0024	0.012	0.0015	0.116	6.58	0.56
	Bottom	0.011	3.2E-04	0.0015	0.124	6.43	0.56
BC-ACR-1	Top	N/A	N/A	N/A	N/A	N/A	N/A
	Bottom	0.0015	0	0.0011	0.083	6.38	0.47
BC-ACR-2	Top	0.0022	0.0015	0.0014	0.092	6.65	0.51
	Bottom	0.0025	0.0032	0.0015	0.115	6.46	0.53

As shown in Table 5, there was an abundance (greater than 10 mM) of nitrate in the bottoms of the OS-ACR columns at the time of sampling. Comparatively, there was considerably less nitrate (roughly 2 mM) in the bottoms of the BC-ACR columns. The tops of each column consistently showed low nitrate concentrations (roughly 0 - 2 mM). The sulfate concentrations at each sampling location in each column were consistently low (roughly 1.5 mM). The nitrite concentrations at each sampling location were generally low (0 – 3 mM) except in the bottom of column OS-ACR-1 and the top of column OS-ACR-2, where the nitrite concentration was above 10 mM. This indicates that there is a buildup of denitrification intermediates (aka nitrite) in these locations. The acetate concentration was very high across all sampling locations. Each column displayed a significantly higher pH in the top of the column than in the bottom of the column, with pH ranging from 6.56 – 6.65 in the tops of the columns and pH ranging from 6.38 – 6.46 in the bottoms of the columns. Similarly, the ionic strength tended to be slightly higher in the bottoms of the columns than in the tops of each column.

An estimated number of species (based on the Chao1 index) found in each column is shown in Figure 53 below. The Chao1 index is calculated based on the number of observed

taxonomic units, defined as a group of sequences with at least 97% similarity. It is important to note that the Chao1 index has been found to over-predict the number of species in samples sequenced using the Illumina platform (Caporoso et al. 2010). Therefore, this index is not meant to be used as an actual estimate of the number of species present, but only an indicator with which to compare species richness in each of the samples.



**Fig. 53.** Estimated number of species (Chao1 index) in column OS-ACR-1 (A), OS-ACR-2 (B), BC-ACR-1 (C), and column BC-ACR-2 (D).

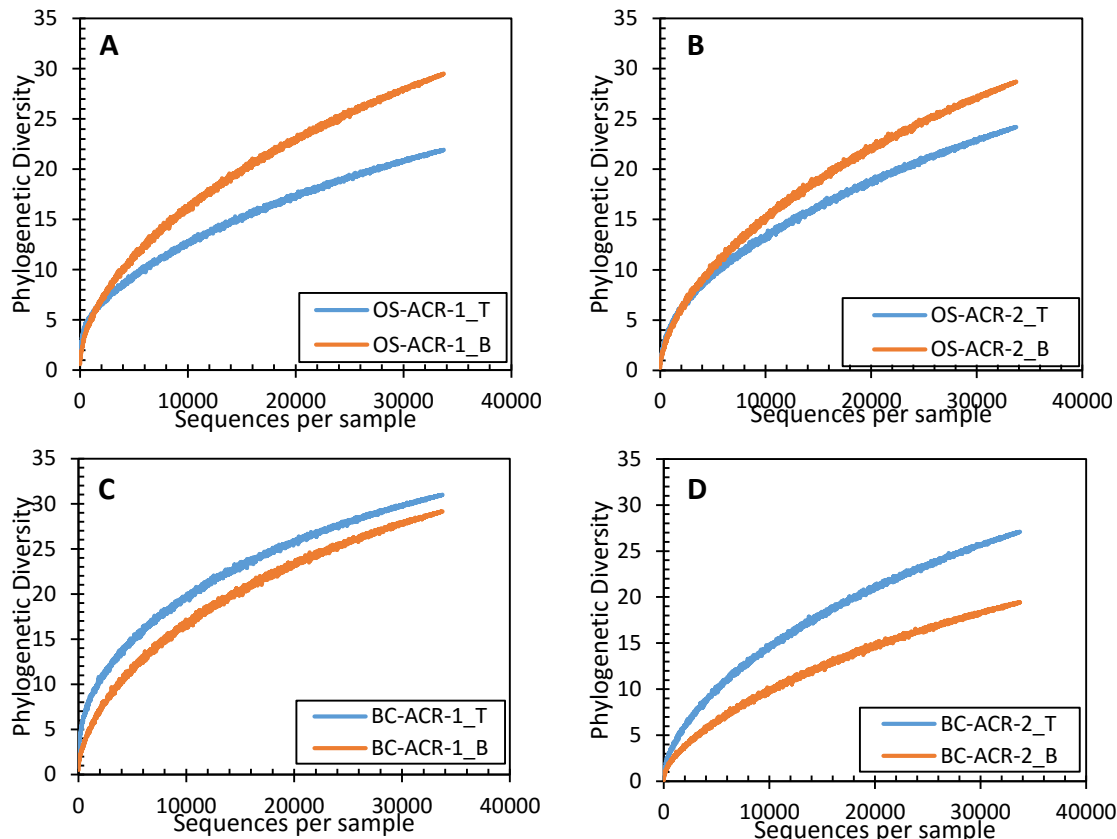
As shown in Figure 53, The OS-ACR columns generally contained a greater species richness than the BC-ACR columns. As shown in the figure, the estimated number of species was not very different between the tops of the columns (labeled with a T in the above figure) and the bottoms of the columns (labeled with a B), except in Column OS-



ACR-1, which displayed a greater number of species in the bottom of the column than the top. It is hypothesized that greater species richness is observed in the Ottawa sand columns due to the difference in nutrient availability between the columns. As a coarser soil, Ottawa sand should allow for more interconnectivity of soil voids and a more free flow of nutrients throughout the column than Bolsa Chica sand. As shown in Table 5 and Figure 53, the sampling locations with fewer species (especially in the BC columns) tended to have much lower concentrations of nitrate and nitrite. It is hypothesized that the lack of nutrients in these sampling locations (Table 5) may have limited the growth of some microbial species.

An estimated measure of phylogenetic diversity at each sampling location in each of the four semi-stagnant columns is found in Figure 54. Faith's phylogenetic diversity index is a sum of the lengths of individual branches of the phylogenetic tree for all of the species in the sample. So, the index is higher when the members of the microbial community are more distantly related. Thus, this indicator is a true measure of phylogenetic diversity, and not just species richness.

As shown in Figure 54, the phylogenetic diversity is higher in the bottoms of the OS-ACR columns than in the tops of the columns. It is hypothesized that imperfect mixing is occurring in the columns during drainage and refilling, leading to lower nutrient levels in the tops of each column than in the bottoms. This may have led to the development of more diverse communities in the bottoms of each column than in the tops. The opposite trend is found in the BC-ACR columns, with more diversity in the tops of the columns than in the bottoms. It may be that the lower ionic strengths and slightly higher pH conditions found in the tops of these columns led to more favorable conditions for microbial growth and hence greater diversity.

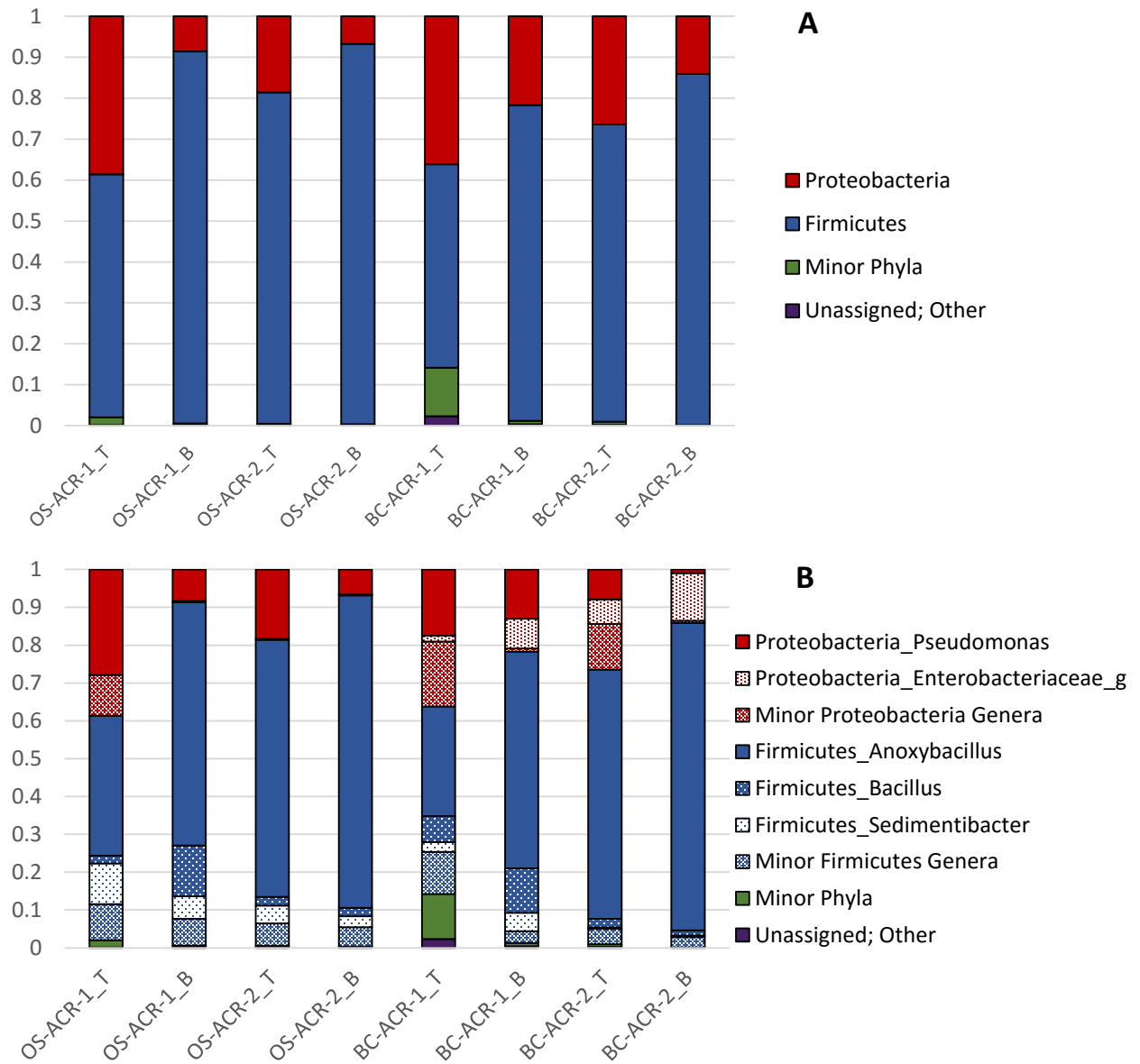


**Fig. 54.** Phylogenetic diversity (from Faith 1992) in columns OS-ACR-1 (A), OS-ACR-2 (B), BC-ACR-1 (C), and BC-ACR-2 (D).

A taxonomic breakdown of the microbial community structure in each sampling location by phylum and genus is shown in Figure 55 below.

As shown in Figure 55A, the predominant phyla in each sampling location in each column are overwhelmingly Firmicutes (roughly 60 – 85% of DNA present in the column) and Proteobacteria (roughly 15 – 40% of DNA present in the column). The breakdown to the genus level presented in Figure 55B shows that the predominant genus in each column is *Anoxybacillus* (30 – 80% of DNA) followed by *Pseudomonas* (1 – 28% of DNA), and *Bacillus* (2 – 14% of DNA). *Sedimentibacter* species are also found in many of the columns in significant amounts and Enterobacteriaceae genera are also found in significant

quantities in the BC-ACR columns. It should be noted that *Pseudomonas* species, while present in all sampling locations, tend to be more predominant in the tops of each soil column than the bottoms. Conversely, *Bacillus* species, while present in all sampling locations, tend to be more predominant in the bottoms of each soil column than the tops.



**Fig. 55.** Taxonomy of microbial ecology in each sample from Semi-Stagnant columns showing major phyla (A) and major genera (B).

Many *Bacillus* species have been found to be capable of performing full denitrification (reducing nitrate to nitrogen gas) or partial denitrification (accumulating intermediates such as nitrite and nitrous oxide) (Verbaendert et al. 2011). Some species of *Bacillus* have also been found to reduce nitrate to nitrous oxide in moderately saline environments above pH 5.5. These same *Bacillus* species have been found to perform denitrification even under very high nitrate and nitrite concentrations (up to 1.06 M nitrate, 0.58 M nitrite) (Denariáz et al. 1989). Based on these observations, it is hypothesized that the *Bacillus* species predominate in the bottoms of the columns, where nitrate loading, nitrite loading, and ionic strength are generally highest because they are capable of performing denitrification under high saline, high nitrate, and high nitrite conditions. However, as some *Bacillus* species are not capable of fully reducing nitrate to nitrogen gas, the presence of these species may be responsible for the accumulation of intermediates such as nitrite and nitrous oxide.

Many *Pseudomonas* species are capable of performing full denitrification of nitrate to nitrogen gas (Carlson and Ingraham 1983). However, at moderate to high salinity, high nitrate loading, and pH less than 7, *Pseudomonas* species have been found to accumulate nitrite and nitrous oxide. (Saleh-Lakha et al. 2009, Viswanathan et al. 2008, Almeida et al. 1994). Nitrite, or more specifically, nitrous acid, acts as an uncoupler in the metabolism of *Pseudomonas* species, leading to a drastic decline in cell growth (Sijisbesma et al. 1996). Based on these observations, it is hypothesized that the generally higher pH, lower ionic strength, and lower nitrate loading (from imperfect mixing) has allowed *Pseudomonas* species to grow more abundantly in the tops of each of the columns rather than the bottoms.

Some, but not all, *Anoxybacillus* species have been found to be capable of reducing nitrate to nitrite for respiration. In general, these *Anoxybacillus* species are mildly

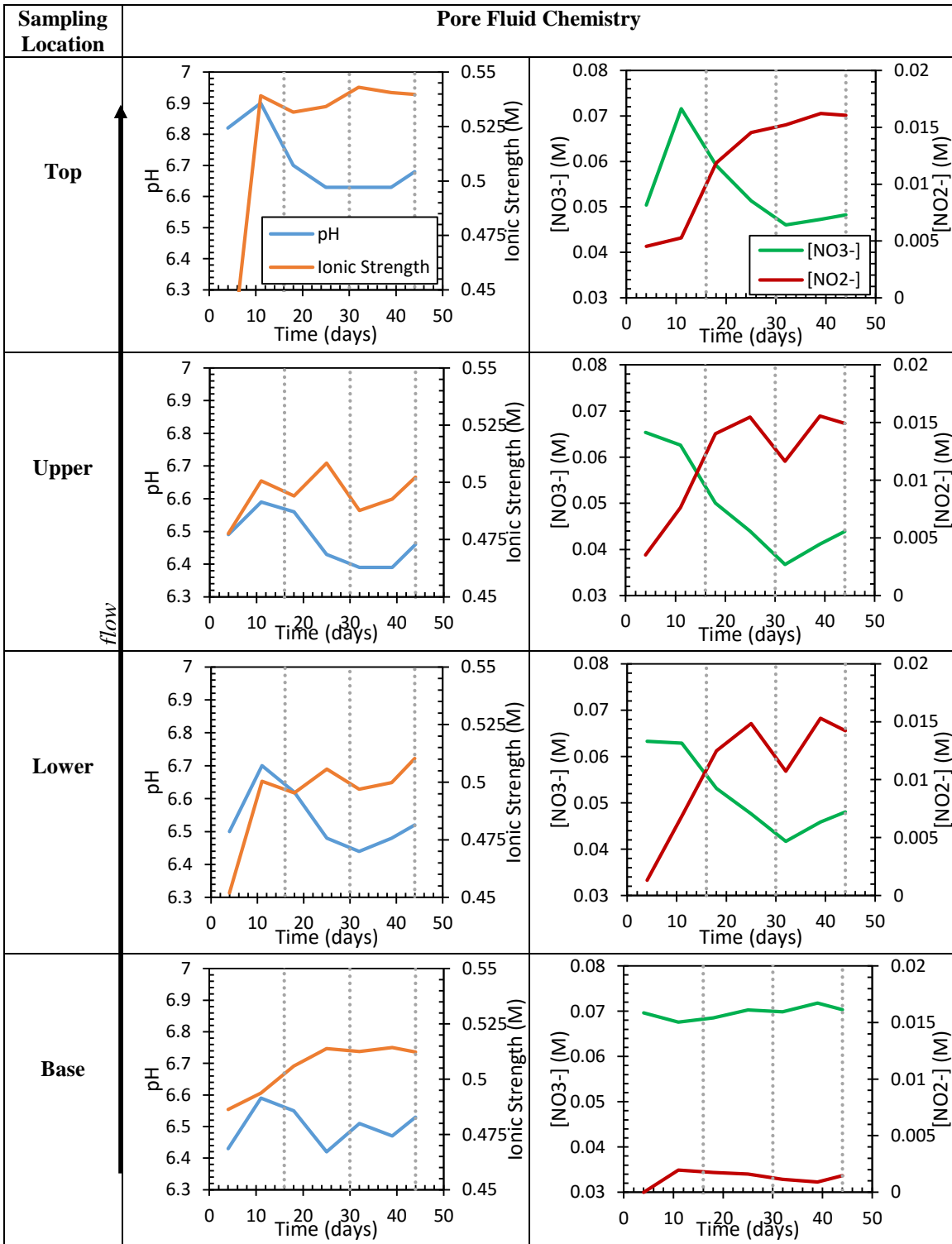
thermophilic, capable of surviving over a broad pH range and in saline environments. They are found predominantly in geothermal springs, manure, and milk-processing plants. Morphologically, *Anoxybacillus* species are gram positive, spore forming rods (Goh et al. 2014, Dulger et al. 2004, Poli et al. 2006, Zhang et al. 2011). It is hypothesized that the *Anoxybacillus* species are the predominant inhabitants of the semi-stagnant soil columns due to their ability to survive relatively extreme environments. These soil columns are subjected to feast-famine conditions, in which the microbes may go for long periods of time (weeks) without nutrients, as well as moderately high ionic strengths. The ability of *Anoxybacillus* species to reduce nitrate to nitrite and then form spores during periods with low nutrients probably accounts for their predominance in all sampling locations in all of the semi-stagnant soil columns.

Many members of Enterobacteriaceae genera are capable of reducing nitrate to nitrite, indicating that they are most likely surviving in the column using this metabolism (Warren 2007). *Sedimentibacter* species, while not necessarily capable of reducing nitrate, have been found to reduce thiosulfate to sulfide (Takii et al. 2007). It is possible, therefore, that these bacteria are involved in sulfate reduction in the soil columns.

### **Continuous Flow Columns – Microbial Community Analysis**

Table 6 shows the concentrations of nitrate and nitrite as well as pH and ionic strength with time for each sampling location in Column OS-CF-4. In this column, consisting of Ottawa 20-30 sand, native soil bacteria were stimulated for denitrifying organisms using a continuous flow of nutrient solution injected from the base of the column. Sampling times for microbial community analysis are shown with dashed grey lines.

**Table 6:** Nitrate and nitrite concentrations, as well as pH and ionic strength with time for each sampling location in Column OS-CF-4.



As shown in Table 6, the pH, ionic strength, nitrate concentration, and nitrite concentration remain fairly constant at the base of the column, indicating that there is not much denitrification occurring in the pore fluid before it reaches the soil column. At the lower sampling port, the ionic strength remains fairly constant over the course of microbial sampling, but the pH decreases from roughly 6.65 to 6.45 between the first and second sampling events, rebounding slightly to 6.5 at the last sampling event. The nitrate concentration at the bottom sampling port drops from roughly 55 mM to 42 mM between the first and second sampling event, but then rises to about 48 mM for the final sampling event. The nitrite concentration steadily rises for each sampling time in the bottom port, from roughly 9 mM for the first sampling event to roughly 14 mM at the final sampling event. These results indicate that denitrification is occurring in the bottom part of the column, but that nitrite is also accumulating in this region.

At the upper sampling port, the ionic strength remains relatively constant for all of the sampling events, while the pH decreases slightly from 6.57 to 6.4 between the first and second sampling events, rising slightly to 6.45 for the final sampling event. The nitrate concentration in the upper sampling port falls from roughly 52 mM to 38 mM between the first and second sampling events, but then rises to roughly 44 mM for the final sampling event. The nitrite concentration steadily rises in the upper sampling port from 9 mM to 15 mM between the first and last sampling events. These results indicate that there is some denitrification occurring in the middle of the column, but with nitrite accumulation as well.

At the top of the column, the ionic strength remains relatively constant while the pH drops slightly from the first to the final sampling event. Generally, the pH is highest at the top of the column compared to the other sampling locations, staying between about 6.72

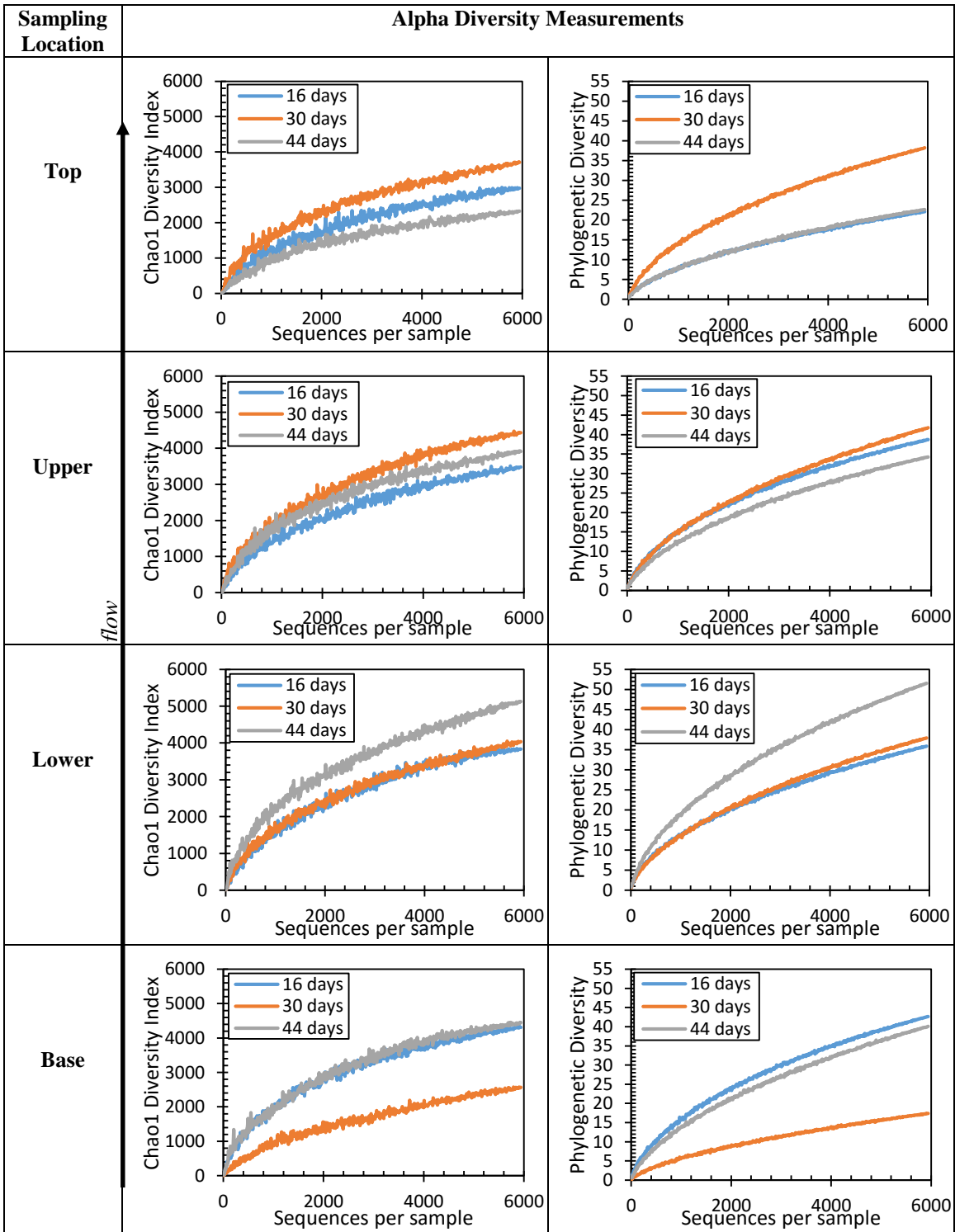
and 6.6 for all sampling events. The nitrate concentration generally decreases with time, while the nitrite concentration increases with time, from roughly 6 mM to 16 mM from the first to the final sampling event. It is hypothesized that the ionic strength and nitrate concentrations are higher at the top of the column than at the upper sampling port in the column because of evaporation effects at the outlet to the column (near the top).

The Chao1 index and the Faith index for phylogenetic diversity (both measures of alpha diversity in the microbial community) are shown in Table 7 for each sampling location and each sampling time for Column OS-CF-4.

As shown in Table 7, there is no clear trend with either the phylogenetic diversity or the Chao1 index (an estimate of the number of species present in the microbial community) with time at any of the sampling ports. However, in general, at each sampling time, the estimated number of species present at a given sampling location increases slightly between the base of the column and the lower sampling port, before decreasing between the lower sampling port, the upper sampling port, and the top of the column. The phylogenetic diversity index shows the same trend. This is most likely the result of the selection process. As the pore fluid enters the column from the base, the microbial communities present in the pore fluid mix with those present in the soil, increasing the diversity somewhat between the base and the bottom port. However, as certain denitrifying species are selected for growth in the soil column, other species begin to die out. This explains the general decline in diversity from the bottom sampling port to the top of the column.



**Table 7.** Alpha diversity (Chao1 and Faith's phylogenetic diversity index) for each sampling location and each sampling time in Column OS-CF-4.



However, it should be noted that at all times and all sampling locations, the alpha diversity, as measured by the Chao1 and Faith indices, is significantly higher in the continuous flow column than in any of the semi-stagnant columns (Figures 51, 52). This could be due to a variety of factors. First, at the time of sampling, the semi-stagnant columns had been treated for roughly 7 months. This is a lot of time for certain species to be selected against in the semi-stagnant columns. Also, the semi-stagnant columns are subjected to feast-famine conditions, so only those species that can survive for long periods without nutrients could thrive in those columns. This may further decrease the amount of diversity in the semi-stagnant columns as compared to the continuous flow columns. Finally, the fact that the semi-stagnant columns were inoculated with a mixed microbial community prior to treatment may have reduced the ability of native soil bacteria to compete in these columns, further reducing diversity.

Table 8 below shows the taxonomic breakdown of the microbial community to the genus level at each sampling time and location in the continuous flow column.

As shown in Table 8, before entering the soil column, the pore fluid is predominantly composed of Firmicutes genera (blue in color; 85 – 98% of total DNA in samples at each sampling time). However, between the base of the column and the lower sampling port, Proteobacteria genera, and specifically *Pseudomonas* species, are significantly enriched, with anywhere from 30 – 50% of the DNA in the sample belonging to the phylum Proteobacteria at all sampling times. It also seems that *Bacillus* species are enriched between the column base and the lower sampling port (30 – 40% of the DNA at all sampling times in the lower port). So, it is theorized that *Pseudomonas* and *Bacillus* species are the two main denitrifying organisms stimulated in the bottom of the column.



It is hypothesized that the proportion of *Bacillus* species to *Pseudomonas* species increases with time in the lower sampling port because of the decrease in pH and increase in nitrite concentration with time at this sampling location. As previously stated, *Pseudomonas* species are inhibited at  $\text{pH} < 7$  and high nitrite concentrations (Saleh-Lakha et al. 2009, Viswanathan et al. 2008, Almeida et al. 1994). Meanwhile, certain *Bacillus* species have been shown to be tolerant of lower pH values and higher concentrations of salt, nitrate, and nitrite (Denariáz et al. 1989) while performing full or partial denitrification (Verbaendert et al. 2011). So, it appears that, in the bottom of the soil column, environmental factors like pH and nitrite concentration are causing the microbial ecology to shift in favor of *Bacillus* species with time.

Also shown in Table 8, the taxonomy of the microbial communities remains roughly similar between the lower sampling port and the upper sampling port with time in the continuous flow column. However, there is a slightly higher proportion of *Pseudomonas* species (roughly 45 – 50% of DNA) and slightly lower proportion of *Bacillus* species (roughly 30 -35% of DNA) in the upper port compared to the lower port, especially at the second two sampling times. It is theorized that, as the nitrate concentrations and ionic strength decrease from the bottom to the middle of the column (with hardly any change in pH or nitrite concentration), *Pseudomonas* species are stimulated slightly more compared to *Bacillus* species in the middle of the column.

Finally, at the top of the continuous flow column, it appears that members of the Caulobacteraceae family, and specifically *Brevundimonas* species, are replacing *Pseudomonas* and, to a lesser extent, *Bacillus* species as the dominant species in the column with time. Studies have shown that many *Brevundimonas* species are capable of

performing denitrification (Kavitha et al. 2009; Tsubouchi et al. 2014). Kavitha et al. (2009) also found that *Brevundimonas diminutia* was capable of performing denitrification at nitrate levels as high as 10,000 ppm, indicating that *Brevundimonas* species are resistant to high nitrate concentrations. Although *Brevundimonas* species are known to perform denitrification even under high nitrate loading, it remains unclear as to why these species began to replace the *Pseudomonas* and *Bacillus* species as the primary denitrifiers in the top of the column, but not in any other column location. It is hypothesized that perhaps the increasing nitrite concentrations with time in the top of the column allowed *Brevundimonas* species to outcompete the *Pseudomonas* species at this location with time.

## CONCLUSIONS

Acrylic column testing showed that the rate of denitrification and carbonate precipitation was higher in a previously disinfected, uninoculated soil column than in soil columns inoculated with either a mixed or pure culture of denitrifying bacteria. Furthermore, the biostimulated community in the uninoculated column was found to be less susceptible to nitrite accumulation and growth inhibition when compared to the bioaugmented mixed and pure culture columns. These results demonstrate that, not only are naturally occurring denitrifying soil bacteria extremely resilient, but that biostimulation of native bacteria with a readily available electron donor and acceptor may be the most effective strategy for inducing denitrification for soil improvement in the field.

Analysis of the alpha diversity within the semi-stagnant and continuous flow soil columns showed that, at all points and times in the columns, the biostimulated continuous flow soil columns contained more diverse microbial communities measured using both the Chao1 and Faith indices. Although this could be a result of the flow conditions (semi-

stagnant versus continuous flow) and the difference in treatment time between the columns, this higher diversity may be a further indication that biostimulation results in a more diverse and versatile microbial community structure than bioaugmentation. Analysis of the alpha diversity in both column types also showed that diversity in a microbial community can vary over a large range over rather small variations in space and time within the same soil column. This indicates that the microbial communities stimulated for denitrification are very sensitive to small differences in environmental conditions.

Microbial taxonomy analysis showed that, in both biostimulated (continuous flow) and bioaugmented (semi-stagnant) microbial communities, members of the phyla Firmicutes and Proteobacteria were stimulated. In particular, *Pseudomonas* and *Bacillus* species were highly selected for denitrification (as well as *Brevundimonas* species, although these were only stimulated in the top of the continuous flow column). As *Pseudomonas* and *Bacillus* species are extremely common microbes, these results indicate that it should be easy to stimulate denitrifying microbial communities in the field regardless of location or soil conditions.

Further analysis of the microbial community data showed that the balance between *Bacillus* and *Pseudomonas* species is controlled by environmental conditions, with *Bacillus* species more common in areas of lower pH, higher ionic strength, and higher nitrate and nitrite concentrations, as these conditions are generally less favorable for the growth of *Pseudomonas* species. Similarly, it appears that *Brevundimonas* species are selected over *Pseudomonas* species under conditions with high nitrite concentrations. These results indicate that mixed microbial communities stimulated for denitrification are capable of adapting to changing chemical conditions in the subsurface, meaning that

biostimulation for soil improvement via denitrification may be applicable to a wide variety of sites with varying soil chemistry.

## CHAPTER 7

### A STOICHIOMETRIC MODEL FOR BIOGEOTECHNICAL SOIL IMPROVEMENT VIA MICROBIAL DENITRIFICATION

#### INTRODUCTION

Column testing has shown the ability for denitrifying organisms to mitigate the potential for earthquake-induced soil liquefaction via desaturation and carbonate precipitation. However, the relationships between input materials (e.g., calcium chloride, calcium nitrate, a carbon source), intermediate materials (e.g., nitrite, microbial biomass), and the outputs of interest (e.g., calcium carbonate, biogas) remain unclear. A stoichiometric model is presented herein to elucidate the interactions between inputs, intermediate products, and outputs in order to better understand the processes at work in MICP via denitrification. Once calibrated, the model will also be used to predict optimum ratios of calcium, nitrate, and carbon source for maximizing gas production and carbonate precipitation.

#### STOICHIOMETRIC MODEL

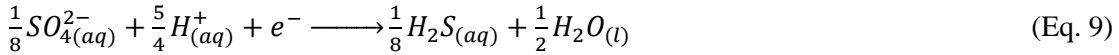
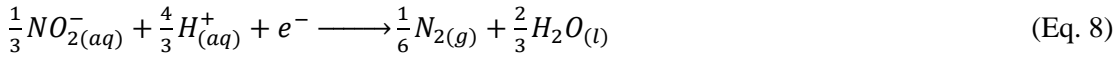
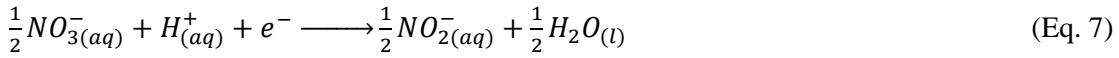
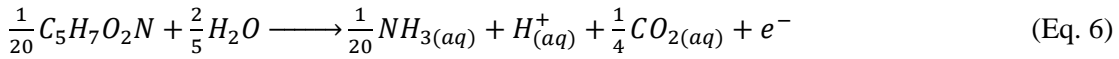
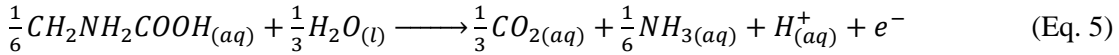
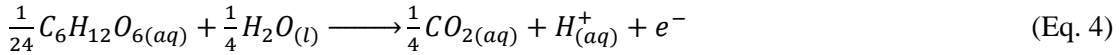
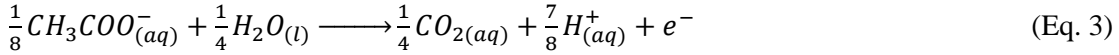
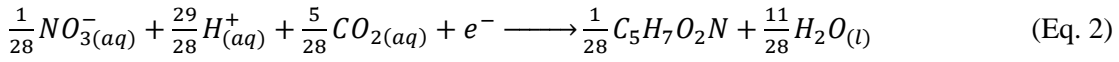
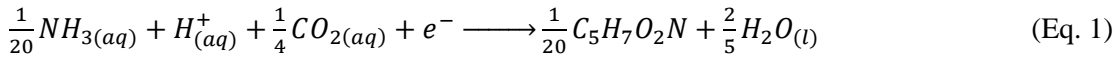
Stoichiometric modeling of MICP via denitrification involves three steps: obtaining balanced chemical equations, determining kinetic expressions, and coupling these to the thermodynamics of carbonate precipitation.

##### Balanced Chemical Equations

For MICP via denitrification, three types of half reactions were used to model microbial growth. Two cell synthesis half reactions were considered: ammonia ( $\text{NH}_3$ ) as a nitrogen source (Eq. 1) and nitrate ( $\text{NO}_3^-$ ) as a nitrogen source (Eq. 2). Four different electron donor half reactions were also considered: acetate (Eq. 3), glucose (Eq. 4), glycine (Eq. 5), and



endogenous decay of biomass (Eq. 6). Glucose and glycine were included due to the addition of small amounts of tryptic soy broth (TSB) in the experimental medium. TSB contains small amounts of glucose as well as significant amounts of peptides, which were in this case modeled using glycine, the simplest amino acid. Three different electron acceptor half reactions were considered: nitrate (Eq. 7), nitrite (Eq. 8), and sulfate (Eq. 9). Sulfate was considered due to evidence for sulfate reduction in the experimental results.



By pairing each of the four electron donor reactions (Eqs. 3-6) and the three electron acceptor reactions (Eqs. 7-9), twelve different microbial metabolisms were identified for this work. These pairings and the coefficients used in each half reaction are presented in Table 9.

**Table 9.** Microbial metabolisms considered in this model including coefficients used on each of the half reactions presented in Eqs. 1-9.

Metabolism (acceptor, donor)	Coefficients						
	Eq. 1	Eq. 2	Eq. 3	Eq. 4	Eq. 5	Eq. 6	Eq. 7
<b>Nitrate, Acetate</b>	$f_{s,1,1}^0 * (1 - f_a)$	$f_{s,1,1}^0 * f_a$	1	0	$1 - f_{s,1,1}^0$	0	0
<b>Nitrite, Acetate</b>	$f_{s,1,2}^0 * (1 - f_a)$	$f_{s,1,2}^0 * f_a$	1	0	0	$1 - f_{s,1,2}^0$	0
<b>Sulfate, Acetate</b>	$f_{s,1,3}^0 * (1 - f_a)$	$f_{s,1,3}^0 * f_a$	1	0	0	0	$1 - f_{s,1,3}^0$
<b>Nitrate, Glucose</b>	$f_{s,2,1}^0 * (1 - f_a)$	$f_{s,2,1}^0 * f_a$	1	0	$1 - f_{s,2,1}^0$	0	0
<b>Nitrite, Glucose</b>	$f_{s,2,2}^0 * (1 - f_a)$	$f_{s,2,2}^0 * f_a$	1	0	0	$1 - f_{s,2,2}^0$	0
<b>Sulfate, Glucose</b>	$f_{s,2,3}^0 * (1 - f_a)$	$f_{s,2,3}^0 * f_a$	1	0	0	0	$1 - f_{s,2,3}^0$
<b>Nitrate, Glycine</b>	$f_{s,3,1}^0 * (1 - f_a)$	$f_{s,3,1}^0 * f_a$	1	0	$1 - f_{s,3,1}^0$	0	0
<b>Nitrite, Glycine</b>	$f_{s,3,2}^0 * (1 - f_a)$	$f_{s,3,2}^0 * f_a$	1	0	0	$1 - f_{s,3,2}^0$	0
<b>Sulfate, Glycine</b>	$f_{s,3,3}^0 * (1 - f_a)$	$f_{s,3,3}^0 * f_a$	1	0	0	0	$1 - f_{s,3,3}^0$
<b>Nitrate, Biomass</b>	0	0	0	1	1	0	0
<b>Nitrite, Biomass</b>	0	0	0	1	0	1	0
<b>Sulfate, Biomass</b>	0	0	0	1	0	0	1

In Table 9, the coefficient  $f_{s,x,y}^0$  represents the fraction of electron equivalents used for cell synthesis from metabolism with electron donor “x,” and electron acceptor “y,” while the coefficient  $f_a$  represents the fraction of cell synthesis for which  $\text{NO}_3^-$ , as opposed to  $\text{NH}_3$ , is the nitrogen source. The coefficient  $f_{s,x,y}^0$  was calculated for each reaction based on the thermodynamic properties of the half reactions considered, as well as the efficiency of electron transfers within the cell (Rittmann and McCarty 2001). The metabolisms in which biomass is the electron donor represent the process of endogenous decay, in which cells oxidize themselves to meet energy requirements. For endogenous decay, there is no

cell synthesis, so  $f_{S,x,y}^0 = 0$ . The coefficient  $f_a$  was defined as a ratio of nitrate to ammonia in solution according to Eq. 10 below.

$$f_a = \frac{C_{NO_3}}{(C_{NO_3} + A_{NH_3} * C_{NH_3})} \quad (\text{Eq. 10})$$

$C_{NO_3}$  = concentration of nitrate (M)

$A_{NH_3}$  = constant to reflect the higher affinity of cells to use ammonia for cell synthesis as opposed to nitrate. This coefficient was used as a fitting parameter.

$C_{NH_3}$  = concentration of aqueous ammonia (M)

### Kinetics Expressions

The MICP system was modeled as a batch reactor, meaning there are no inputs or outputs to the system during the reaction. A dual-limitation kinetics model was applied, giving the rate expressions for the electron donor and the biomass concentration found in Eqs. 11 and 12 below (Bae and Rittmann 1996).

$$\frac{dC_d}{dt} = -\hat{q} * \frac{C_d}{K_d + C_d} * X_a * \frac{C_a}{K_a + C_a} \quad (\text{Eq. 11})$$

$C_d$  = concentration of electron donor (M)

$\hat{q}$  = maximum specific rate of electron donor utilization ( $t^{-1}$ )

$K_d$  = Monod half-maximum-rate concentration of electron donor (M)

$X_a$  = concentration of biomass (M)

$C_a$  = concentration of electron acceptor (M)

$K_a$  = Monod half-maximum-rate concentration of electron acceptor (M)

$$\frac{dX_a}{dt} = X_a * \left( \hat{q} * \frac{Y}{\left(1 + \frac{C_{NO_2}}{I_{NO_2}}\right)} * \frac{C_a}{K_a + C_a} * \frac{C_d}{K_d + C_d} - f_d * b * \left(1 + \frac{C_{NO_2}}{I_{NO_2}}\right) \right) \quad (\text{Eq. 12})$$

$Y$  = true yield (mol cells/mol electron donor)

$C_{NO_2}$  = concentration of nitrite (M)

$I_{NO_2}$  = nitrite inhibition constant (M)

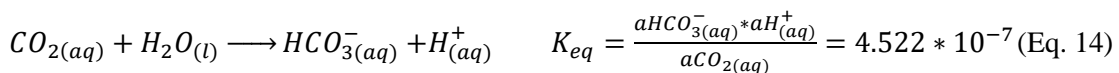
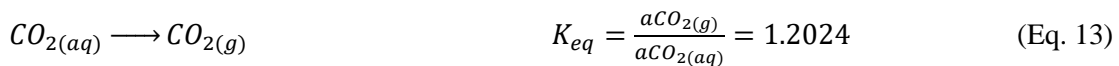
$f_d$  = fraction of active biomass that is biodegradable

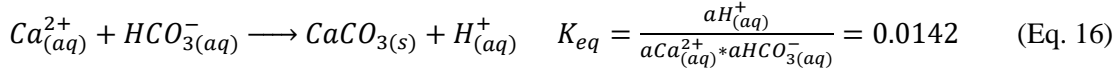
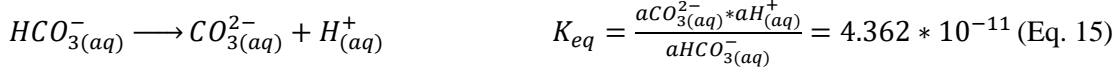
$b$  = endogenous decay coefficient ( $t^{-1}$ )

The value of  $\hat{q}$  was computed based upon the maximum electron flow to the electron acceptor and the temperature (assumed to be 20°C), and Y was calculated based upon the  $f_{s,x,y}^0$  values for each metabolism. The value of  $f_d$  was fixed at 0.8 (Rittmann and McCarty 2001). Values for  $C_a$  and  $C_d$  were calculated based upon Eq. 9 and stoichiometry from Eqs. 3-7 at each time step. The values of  $b$ ,  $K_d$ ,  $K_a$ , and  $I_{NO_2}$  were adjusted to fit the model to experimental data. Nitrite inhibition was included in the kinetics reaction due to overwhelming evidence that nitrite, or more specifically, nitrous acid, acts as a decoupling inhibitor to cell growth (Almeida et al. 1994, Sijbesma et al. 1996).

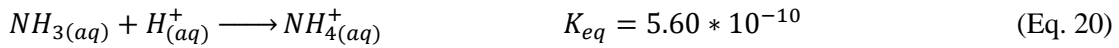
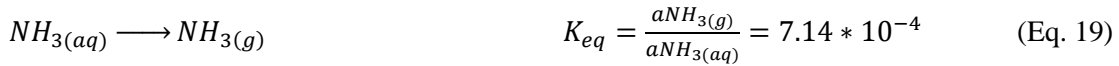
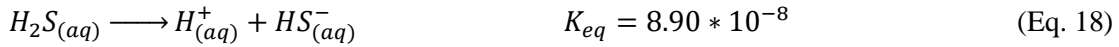
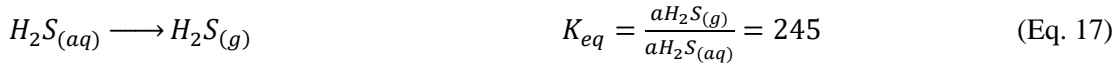
### Carbonate Equilibrium and Precipitation

Once the balanced equations and kinetics expressions were established, a mass balance approach coupled with the thermodynamics of carbonate speciation and precipitation was used to determine the amount of gas production and calcium carbonate ( $CaCO_3$ ) precipitation. Microbial denitrification produces carbon dioxide ( $CO_2$ ). The rate and amount of  $CO_2$  production was determined for each process based on the kinetics and stoichiometry of the reaction. Then, the thermodynamics of carbonate speciation and  $CaCO_3$  precipitation was used to determine how much carbon stayed in solution (as either dissolved  $CO_2$ , bicarbonate anion ( $HCO_3^-$ ), or carbonate anion ( $CO_3^{2-}$ )), precipitated as  $CaCO_3$ , or partitioned into the gas phase as gaseous  $CO_2$ . The equations of carbonate equilibrium are presented in Eqs. 13-16. The rate constants were obtained using the computer program CHNOSZ (Dick 2008).





As illustrated by Eqs. 13-16, inorganic carbon speciation and precipitation is intricately tied to the production and consumption of protons ( $H^+(aq)$ ) in solution and, hence, the pH. In order to determine the equilibrium pH at each time step, a mass balance approach was used based on all of the speciation and precipitation reactions involved. So, in addition to the carbonate reactions, it was necessary to consider the speciation of hydrogen sulfide, a byproduct of sulfate reduction (Eq. 17-18), and ammonia, a product of endogenous decay and glycine oxidation (Eq. 19 – 20). The rate constants for these equations were found using CHNOSZ (Dick 2008).



The activity coefficients for each of the charged chemical constituents involved in Eqs. 13-20 were determined from the ionic strength of the solution, the temperature, and the dielectric constant of water according to Davies Equation (Davies 1962).

## EXPERIMENTS

Four specimens were prepared in 150 mm-tall, 73 mm-diameter acrylic columns equipped with a drainage port at the base, a gas collection port at the top, and sampling ports located 5 cm from the base and 5 cm from the top. Two columns contained Ottawa 20-30 crystal silica sand at a relative density of 45% while the other two contained a beach

sand from Bolsa Chica State Beach, Huntington Beach, California at a relative density of 90%. The acrylic columns were alcohol sterilized (70% v/v ethanol) and the sand was autoclaved to minimize the potential for contamination of the columns with microbes. After sand placement, each column was purged from the top port with  $N_{2(g)}$  to minimize oxygen and promote denitrification.

Each column was then inoculated with 30 mL of a mixed culture of microbes enriched from sand and water collected from Bolsa Chica State Beach. The inoculum was prepared by mixing 2 g of Bolsa Chica sand, 5 mL of Bolsa Chica water, and 95 mL of growth solution containing 20 g/L nutrient broth (Difco, BD Brand), 12.5 mM  $Ca(NO_3)_2$ , and 12.5 mM  $Ca(CH_3COO)_2$  in deionized (DI) water and then incubating the resultant mixture for five days at 30°C. A separate solution containing 125 mM  $CaCl_2$ , 50 mM  $Ca(CH_3COO)_2$ , 25 mM  $Ca(NO_3)_2$ , and 2 mM  $MgSO_4$  in DI water was also prepared as the pore fluid for each of the acrylic columns. 0.5 mL/L of a trace metals solution consisting of 0.5% (w/v)  $CuSO_4$ ,  $FeCl_3$ ,  $MnCl_2$ ,  $Na_2MoO_4 \cdot 2H_2O$  was also added to the pore fluid solution in order to promote microbial growth. The pore fluid solution was then adjusted to  $pH \approx 8$  using 1 M NaOH. Following inoculation with 30 mL of mixed microbial culture, the pore fluid solution (roughly 230 mL) was slowly added to the bottom port of each column until fluid began to exit the top port.

The pore fluid in each column was drained at two week intervals and refilled with fresh pore fluid. As the pore fluid drained, it was displaced with  $N_{2(g)}$  in order to keep the columns anaerobic. For each refilling of the columns, the concentrations of  $NO_3^-$  and acetate in the pore fluid were slowly raised and the concentration of calcium chloride reduced until, after 36 weeks of treatment (18 pore fluid fillings), the pore fluid consisted

of 100 mM  $\text{Ca}(\text{CH}_3\text{COO})_2$ , 50 mM  $\text{Ca}(\text{NO}_3)_2$ , 2mM  $\text{MgSO}_4$ , and 100 mM  $\text{CaCl}_2$ . After twelve weeks of treatment, small amounts of tryptic soy broth (0.75 g/L) were added to the pore fluid in order to further promote microbial growth. A full accounting of pore fluid composition for the duration of treatment can be found in Table 2 (Chapter 4). In order to monitor the amount of gas generated, dialysis bags were connected to the top ports of each column to collect gas and displaced fluid during denitrification.

During the 20<sup>th</sup> refilling cycle (42 weeks after initial inoculation), the chemistry in each column was monitored by extracting roughly 3-4 mL of pore fluid at 0, 0.75, 1.5, 3.5, 6.5, and 9.5 days after refill from both the top and bottom sampling ports. For each sample, the pH was taken immediately after extraction, the Total Kjeldahl Nitrogen (TKN) was found through the use of a Hach TNT 880 kit, and the ionic makeup of the pore fluid was determined by filtering 1 mL of the sample through a 0.2  $\mu\text{m}$  filter. The filtered samples were stored at 4°C for two weeks before diluting them by a factor of 200 with DI water and analyzing the filtered, diluted samples using ion chromatography (Dionex ICS-2000). In this way, pH, TKN, nitrate, nitrite, sulfate, acetate, carbonate, ammonium, and calcium concentrations were determined at each sampling site in each column with time. The TKN data and ammonium concentrations were used to estimate the organic nitrogen content in each sample, which was used as a measure of biomass concentration.

During the 21<sup>st</sup> refilling cycle (44 weeks after initial inoculation), the amount of gas generated in each column was determined at 0, 1, 2, 3, 4, 5, 6.5, and 14 days after refill by measuring the volume change of the dialysis bag. It was assumed that the volume change was equal to the total volume of gas generated within the column.

## MODEL CALIBRATION AND VALIDATION

The IC and pH data from the column experiments indicated that the pore fluid was super-saturated with respect to  $\text{CaCO}_3$ , with a saturation index (SI) ranging from 10-15 at all times. This is most likely due to the high concentrations of acetate in solution, as acetate has been shown to inhibit the formation of  $\text{CaCO}_3$  (Haile 2011; Kitano et al. 1969). The model was adjusted to reflect this finding by changing the initial SI to 10 and the long term SI to 15. The values of  $K_a$ ,  $K_d$ , and  $b$  from Eqs. 9-10 were established by fitting the acetate and  $\text{NO}_3^-$  concentrations in the model to the experimental data. The value for microbial inhibition due to nitrite accumulation,  $I_{\text{NO}_2}$ , was also chosen as a fitting parameter. The fitted values for  $K_a$ ,  $K_d$ ,  $b$ , and  $I_{\text{NO}_2}$  can be found in Table 10.

**Table 10.** Kinetics coefficients used to fit model output to experimental data

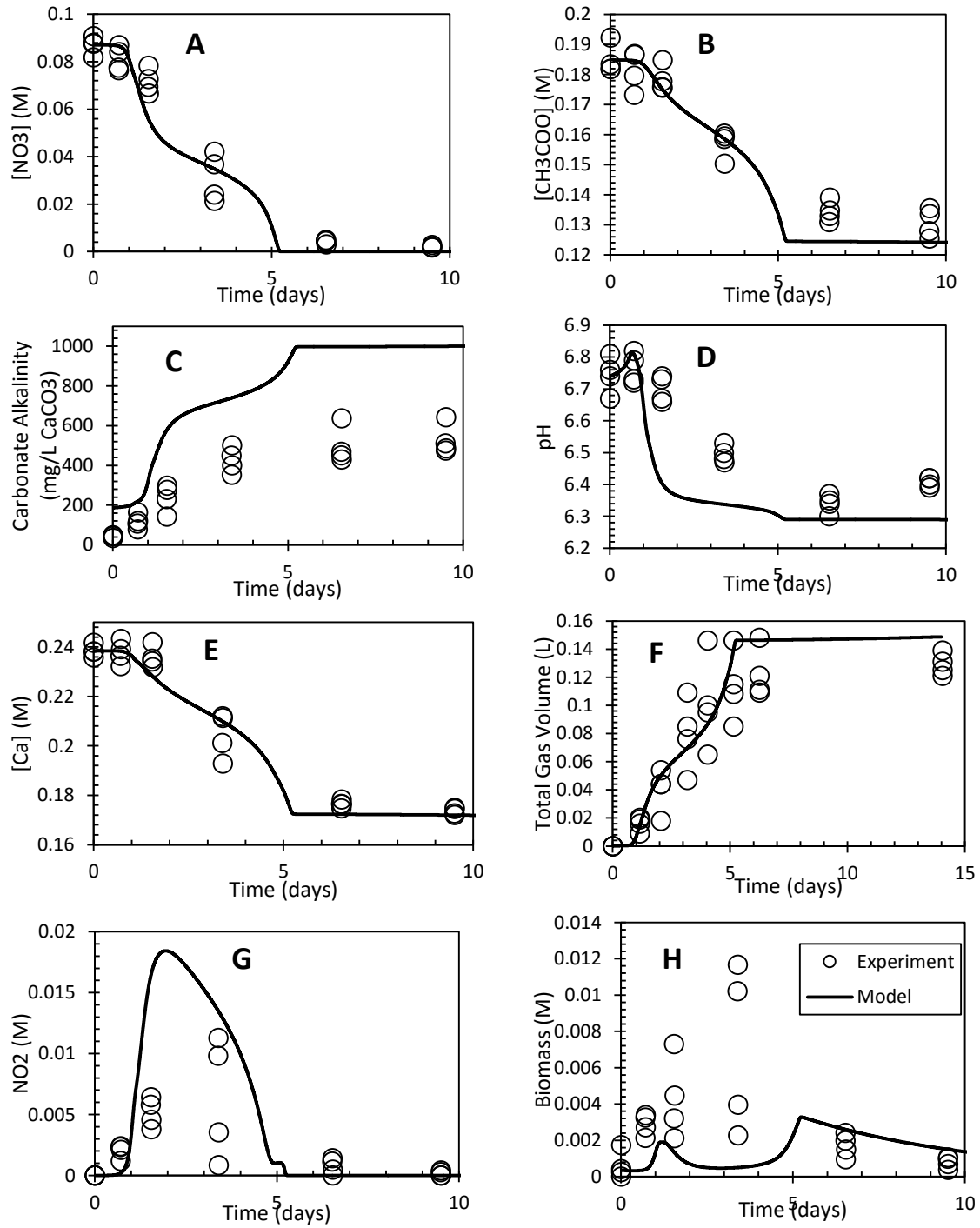
$K_{\text{NO}_3}$	$K_{\text{NO}_2}$	$K_{\text{SO}_4}$	$K_{\text{Acetate}}$	$K_{\text{Biomass}}$	$K_{\text{Glucose}}$	$K_{\text{Glycine}}$	$b_{\text{NO}_3}$	$b_{\text{NO}_2}$	$b_{\text{SO}_4}$	$I_{\text{NO}_2}$
0.001 M	0.001 M	$10^{-5}$ M	0.004 M	$2 \times 10^{-5}$ M	0.001 M	0.001 M	0.3 $\text{d}^{-1}$	0.3 $\text{d}^{-1}$	0.18 $\text{d}^{-1}$	0.01 M

The  $K$  values ( $K_a$ ,  $K_d$ ) for  $\text{NO}_3^-$ ,  $\text{NO}_2^-$ , acetate, glucose, and glycine in Table 10 are slightly higher than those reported in the literature (Rittmann and McCarty 2001). It could be the case that the values reported here are slightly higher than those reported previously due to mass transport resistance, i.e., the resistance of chemicals to flow in response to a concentration gradient. Since the experiments were not conducted in well mixed reactors, these resistances can be quite high. Ignoring these resistances in the model will therefore result in unusually high  $K$ -values (Rittmann and McCarty 2001). The  $b$  values used to fit the data lie within the expected range (Rittmann and McCarty 2001). The value for  $I_{\text{NO}_2}$



used to fit the data also lies within the expected range (Sijbesma et al. 1996). Comparisons between the fitted model output and experimental data are shown in Fig. 56.

The agreement between the model output and the experimental data shown in Fig. 56 is generally good, especially with regard to  $\text{Ca}^{2+}$  concentration and total gas volume (the sum of  $\text{N}_{2(\text{g})}$ ,  $\text{CO}_{2(\text{g})}$ , and  $\text{H}_2\text{S}_{(\text{g})}$  volumes), the outputs of greatest interest for soil improvement. The amount of  $\text{Ca}^{2+}$  lost from the system is directly proportional to the amount of  $\text{CaCO}_3$  precipitated, while the total gas volume is related to the final degree of saturation. Both of these values are necessary for determining the extent of soil improvement expected from microbial denitrification (Kavazanjian et al. 2015). The disparity between observed and expected carbonate alkalinity (Fig. 56C) is most likely due to sample preparation and subsequent IC analysis. The fluid samples taken from each column contain high amounts of dissolved  $\text{CO}_2$ . When they are exposed to the atmosphere, even for a short time, the dissolved  $\text{CO}_2$  will off-gas (Eq. 12). Since it was not possible to dilute and then analyze fluid samples for IC analysis without exposing them to the atmosphere, some inorganic carbon was most likely lost via this mechanism. The slight disparity between observed and expected pH is another reason why the model predicts a higher than observed carbonate alkalinity. At lower pH, much more bicarbonate can remain in solution without precipitating as calcium carbonate (Eq. 15). Since the model predicts a slightly lower pH than what was observed, it makes sense that it would also predict a slightly higher carbonate alkalinity. The observed disparity in pH may be the result of a buffer, such as phosphate, present in the TSB that was not included in the model. The model also does a fair job of predicting the nitrite concentration with time.



**Fig. 56.** Model output and experimental results for nitrate (A), acetate (B), carbonate alkalinity (C), pH (D), calcium (E), total gas volume ( $N_{2(g)}$ ,  $CO_{2(g)}$ , and  $H_2S_{(g)}$ ) (F), nitrite (G), and biomass (H) for microbial denitrification.

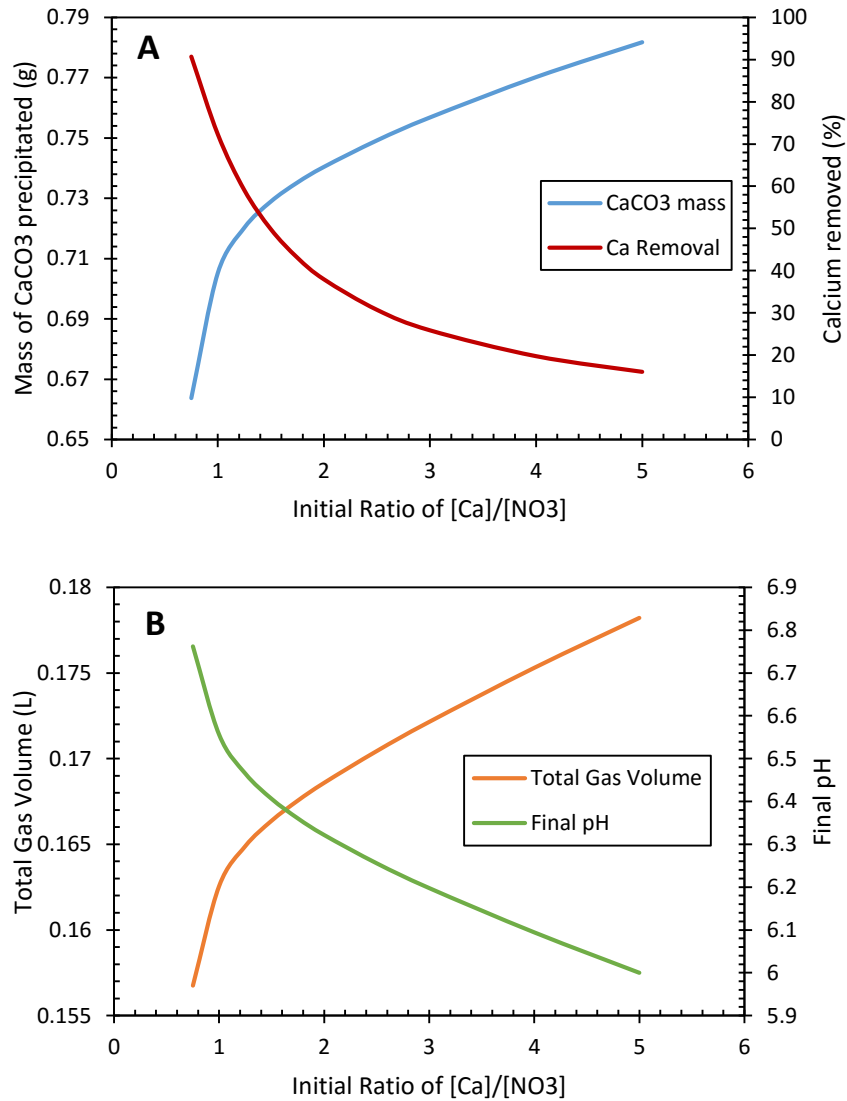
## **SENSITIVITY ANALYSIS**

Following model calibration to the experimental data, a sensitivity analysis was performed using the model to determine the optimum concentrations of constituents for carbonate precipitation and gas production. Specifically, the initial concentrations of calcium and acetate were varied to determine the optimum ratios of calcium to nitrate to acetate. The carbon source was also varied between glucose, acetate, and glycine to identify which among these carbon sources was optimum.

### **Varying Calcium Concentration:**

For analysis of the sensitivity of MICP via denitrification to calcium concentration, the initial concentrations of nitrate, acetate, sulfate, glycine, and glucose were maintained at 0.1 M, 0.25 M, 0.002 M, 0.0075 M, and 0.0025 M respectively while varying the initial calcium concentration from 0.075 to 0.5 M. The results of the analysis is presented in Figure 57.

As shown in Figure 57A, the total mass of carbonate precipitated rises continuously with an increasing ratio of initial calcium to nitrate concentration. However, the sensitivity of the total mass of carbonate precipitated to the calcium/nitrate ratio is much higher below an initial ratio of 1 than it is above a ratio of 1. In fact, the total precipitation at an initial ratio of 5 is only 10% greater than at an initial ratio of 1. This indicates that increasing the initial ratio of calcium to nitrate above 1 provides little benefit with respect to the amount of calcium carbonate precipitation.



**Fig. 57.** Results of sensitivity analysis. Total calcium carbonate mass and calcium removal from pore water (A) and total gas generated and final pH (B) versus initial ratio of calcium concentration to nitrate concentration.

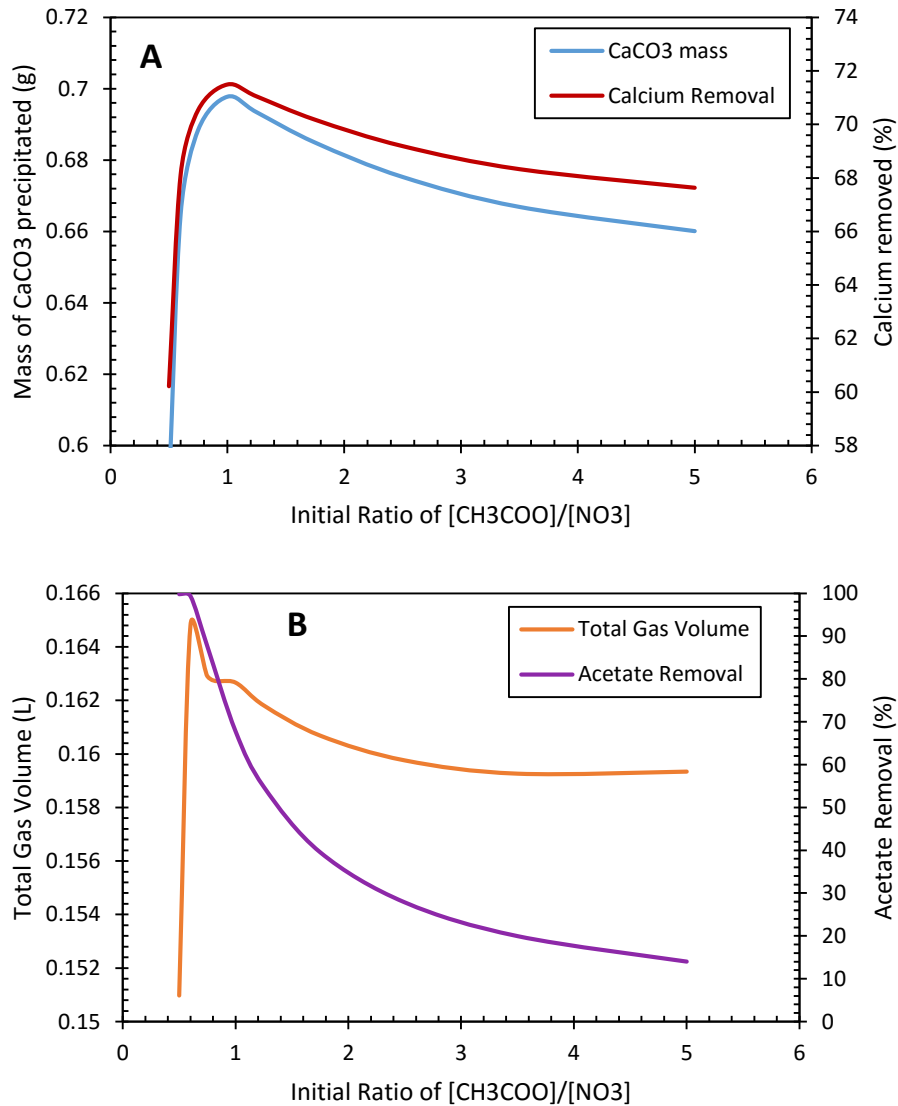
Also shown in Figure 57A is the relationship of the percentage removal of calcium from the pore fluid to the initial ratio of calcium to nitrate. As shown in the figure, calcium removal decreases rapidly when the calcium to nitrate ratio increases from 0.75 to 3 and then slows down as the initial ratio exceeds 3. Calcium removal is important to consider

because of the potential environmental impact and the associated impact on the total cost of implementing soil improvement via denitrification. Lower removal of calcium indicates there will be more residual calcium in the groundwater following treatment that may need to be removed by other means, raising the total cost of the process. Residual calcium also represents money wasted on calcium salts that did not react to form calcium carbonate, and hence did not help to treat the soil mass. Based on the results of Figure 57, it appears that the optimum ratio of calcium to nitrate to use for treatment is 1, as this ratio results in high amounts of carbonate precipitate with relatively high amounts of calcium removal.

As shown in Figure 57B, the total gas volume increases continuously from an initial calcium to nitrate ratio of 0.75 to 5, with greater sensitivity below an initial ratio of 1. Also shown in Figure 57B, the final pH of the groundwater decreases continuously with increasing calcium to nitrate ratio. However, the final pH remains relatively neutral regardless of the ratio of calcium to nitrate. This data also indicate that an initial calcium to nitrate ratio of 1 would lead to significant gas production, which is good for desaturation, as well as a relatively neutral final pH, which decreases the environmental impact of the process.

### **Varying Acetate Concentration**

To analyze the sensitivity of MICP via denitrification to initial acetate concentration, the initial concentrations of nitrate, calcium, sulfate, glycine, and glucose were maintained at 0.1 M, 0.1 M, 0.002 M, 0.0075 M, and 0.0025 M respectively, while varying the initial acetate concentration from 0.05 to 0.5 M. The results of the analysis are presented in Figure 58.



**Fig. 58.** Results of sensitivity analysis. Total calcium carbonate mass and calcium removal from pore water (A) and total gas generated and acetate removal (B) versus initial ratio of acetate concentration to nitrate concentration.

As shown in Figure 58A, the total mass of carbonate precipitated rises very quickly from an initial acetate to nitrate ratio of 0.5 to 1, but then declines gradually at ratios greater than 1. The amount of calcium removal from the pore fluid follows the same pattern. As stated previously, it is important for soil improvement to maximize both the amount of

carbonate precipitated (to optimize soil improvement) and calcium removal (in order to avoid environmental contamination). So, it appears that the optimum ratio of acetate to nitrate is 1.0 for both soil improvement and environmental protection.

As shown in Figure 58B, the total gas volume generated via denitrification increases rapidly from an initial ratio of 0.5 to 0.6, but then decreases gradually above a ratio of 0.6. For soil improvement via desaturation, this would indicate that the optimum initial ratio of acetate to nitrate would be 0.6, but a ratio greater than or equal to 0.6 would still yield decent results. Figure 58B also shows the percentage of acetate removal from the pore fluid with increasing acetate to nitrate ratio. As shown in the figure, acetate removal is at 100% from an initial acetate to nitrate ratio of 0.5 to 0.6, but quickly decreases above a ratio of 0.6. In a field setting, it is important to have high removal of acetate from the groundwater in order to avoid environmental contamination and potential stimulation of the growth of other, less useful bacteria. However, it is also important that acetate removal be less than 100%, as a removal rate of 100% indicates that nitrate may not be fully removed from the groundwater. As a potentially toxic chemical, nitrate is very undesirable in the groundwater. So, while a high acetate removal rate is necessary, it is wise to avoid 100% removal of acetate. With this in mind, a ratio of acetate to nitrate of 1 shows promise as it results in a high volume of gas generation and a high amount of acetate removal (>70%). So, based on this sensitivity analysis, it would appear that an optimum ratio of acetate to nitrate to calcium for soil improvement would be 1:1:1.

### **Varying Carbon Source**

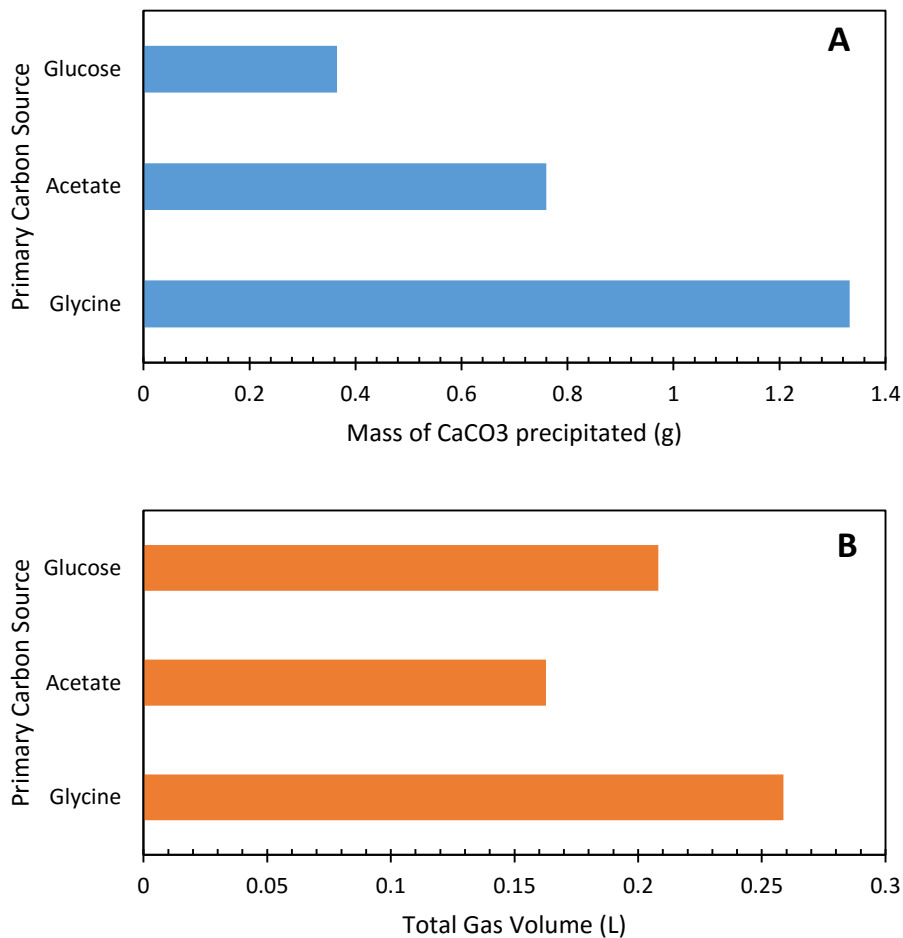
For analysis of the sensitivity of MICP via denitrification to the carbon source, the predominant carbon (and electron) source was varied between acetate, glucose, and

glycine. The concentration of calcium, nitrate, and sulfate were maintained at 0.175 M, 0.1 M, and 0.002 M respectively for each of the simulations, while the concentrations of the carbon sources were maintained at a level sufficient to ensure full nitrate reduction but leaving a minimal amount of residual carbon source in solution following denitrification (0.35 M glycine, 0.08 M acetate, and 0.06 M glucose). For scenarios with glucose and acetate as the predominant carbon source, the glycine concentration was maintained at 0.0075 M to serve as a source of reduced nitrogen for cell growth. The results of the analysis can be seen in Figure 59.

As shown in Figure 59A, the amount of carbonate precipitation is highest when glycine is used as the predominant carbon source, and lowest when glucose is used as the predominant carbon source. Glycine results in the most carbonate precipitation for a variety of reasons. First, it results in the most CO<sub>2</sub> generation per electron (Eq. 5). This means that there is more aqueous carbon capable of precipitating as calcium carbonate. Also, glycine oxidation results in the production of large amounts of ammonia, a weak base. Ammonia speciation to ammonium (Eq. 20) results in significant removal of protons, further favoring carbonate precipitation. Acetate acts as a decent carbon source for carbonate precipitation because, while it does not generate as much CO<sub>2</sub> per electron (Eq. 3) as glycine, it does result in the consumption of a significant amount of protons, driving up the pH and causing precipitation of carbonate. This is most likely due to the fact that acetate is a charged molecule. More proton consumption is necessary to maintain charge balance. Finally, the least amount of carbonate precipitation is observed when glucose is used as the predominant carbon source because glucose is neither charged nor does it result in the production of a weak base capable of driving up the pH. So, the best carbon source



for carbonate precipitation would be a charged molecule that, when consumed, produces ammonia or some other weak base. An excellent example of such a carbon source would be glutamate. However, it is important to consider the environmental compatibility of the carbon source, and using glutamate would produce ammonium. Ammonium is widely considered an environmental contaminant that may need to be removed from the soil. So, while ammonium production would benefit carbonate precipitation, it could also result in environmental contamination.



**Fig. 59.** Results of sensitivity analysis. Total carbonate precipitation (A) and total gas volume generated (B) with varying carbon source.

Total gas production for each carbon source is shown in Figure 59B. As shown in this figure, the most gas is produced when glycine is used as the predominant carbon source, followed by glucose, and finally acetate. Glucose results in the higher gas production than acetate because it results in a lower amount of proton consumption per nitrate consumed (Eq. 4, 7, 8). This leads to a lower pH, a corresponding higher concentration of dissolved CO<sub>2</sub>, and hence a higher amount of gaseous CO<sub>2</sub> (Eq. 13). Glycine also results in a large total gas volume because it produces the most CO<sub>2</sub> per electron (Eq. 5). This results in a higher concentration of dissolved CO<sub>2</sub> and hence a greater volume of gaseous CO<sub>2</sub>.

## **CONCLUSIONS**

A stoichiometric model was developed to predict the amount of CaCO<sub>3</sub> precipitation and gas production for MICP via denitrification. This model represents an important first step in the analysis of large scale biogeotechnical ground improvement projects. The model was formulated for batch reactors (no-flow condition). However, the model can easily be modified to account for continuous flow, making it applicable to field conditions. Through sensitivity analysis, it was discovered that the optimum ratio of calcium to nitrate for gas production, carbonate precipitation, and environmental and cost considerations is 1:1, while the optimum carbon source was identified as glycine. Overall, the stoichiometric model presented herein shows promise for understanding and predicting the complex biological and chemical interactions involved with MICP via denitrification.

## CHAPTER 8

### CONCLUSIONS AND RECOMMENDATIONS FOR FUTURE WORK

#### OVERVIEW

The work described in this dissertation details the use of microbial denitrification for liquefaction mitigation as a two stage process, with desaturation via biogas production providing short term mitigation and microbially induced carbonate precipitation (MICP) providing long term mitigation. Chapter 2 of this work described the relevant work conducted by others in the use of microbial techniques for soil improvement via desaturation and MICP. Chapter 3 addressed the baseline properties of the soils used in this work and demonstrated the potential for abiotic desaturation to mitigate liquefaction resistance. The properties of the two different soils used throughout this work, Ottawa 20-30 silica sand and a beach sand from Bolsa Chica state beach in Huntington Beach, CA, were presented in Chapter 3. Chapter 4 described testing of semi-stagnant biotic soil columns augmented with denitrifying microorganisms. Semi-stagnant testing demonstrated the ability of denitrifying microorganisms to desaturate the soil and induce carbonate precipitation. P-wave analysis and direct measurements of dialysis bags above the columns were used to assess the ability of denitrifying microbes to desaturate the soil. Ion chromatography (IC) analysis and acid digestion techniques were used to quantify carbonate precipitation in these columns. Mechanical testing (S-wave measurements, undrained and drained triaxial testing, cyclic direct simple shear testing) of the soil from the semi-stagnant soil columns subsequent to treatment was used to demonstrate the ability of MICP to improve the stiffness, strength, and dilatant behavior of the test soils via particle roughening and interparticle cementation.

In Chapter 5, indigenous denitrifying micro-organisms were stimulated in soil columns subjected to continuous flow to demonstrate the ability of naturally occurring denitrifying organisms to induce desaturation and MICP. Desaturation was observed qualitatively in the columns while carbonate precipitation was measured through IC analysis of pore fluid recovered while the column tests were in progress and acid digestion subsequent to column testing. P-wave and S-wave velocity measurements were used to monitor desaturation and improvement in soil stiffness while these tests were in progress. Chapter 6 addressed the role of the microbial community in desaturation and MICP via denitrification in both the semi-stagnant columns and the columns subjected to continuous flow. In Chapter 7, the development of a stoichiometric model for the prediction of gas production and carbonate precipitation from denitrification was described.

## **CONCLUSIONS**

Abiotic testing of soils provided a baseline from which to assess the ability of denitrification to improve the liquefaction resistance of soils via desaturation and MICP. Specifically, cyclic direct simple shear testing of Ottawa 20-30 sand at different degrees of saturation showed that very little desaturation is necessary to induce significant improvements in the cyclic resistance of the soil. Only a 3% reduction in the degree of saturation resulted in an improvement of upwards of 40% in cyclic resistance. This shows that if gas production from denitrifying microbes is able to desaturate the soil to a 97% degree of saturation, liquefaction resistance can be significantly improved. Abiotic testing also showed a strong correlation between P-wave velocity and degree of saturation in Ottawa 20-30 sand samples between 95% and 100% saturation. This result indicates that P-wave velocity may be used to monitor the reduction of the degree of saturation, and

hence the increase in cyclic resistance of the soil due to microbial desaturation at a degree of saturation between 95% and 100%.

P-wave analysis and dialysis bag measurements of semi-stagnant soil columns augmented with denitrifying microbes showed the ability of denitrifying organisms to quickly desaturate both Ottawa 20-30 sand and natural Bolsa Chica sand to degrees of saturation of 95% or below within one to three days of treatment. This result indicates that desaturation via denitrification occurs quickly and to an extent such that significant liquefaction resistance is achieved. Carbonate precipitation, as verified via IC analysis, acid digestion, and SEM analysis, was observed in all of the semi-stagnant columns. While the observed carbonate precipitation was slow compared to the rate of carbonate precipitation reported in the literature for precipitation via hydrolysis of urea (ureolysis), subsequent testing in continuous flow columns suggested that this may to some extent be an artifact of the treatment schedule (draining and refilling every two weeks) rather than the speed of denitrification.

Measurements of soil column dimensions before and after treatment revealed decreases in relative density of almost all of the semi-stagnant soil columns treated via denitrification. This effect is most likely due to the buildup of gas pressure in the soil voids under the low overburden pressure in the benchtop columns. This effect requires further study, as loosening of the soil structure has the potential to decrease the strength, stiffness, and dilatant behavior of soils treated via denitrification at low confining stresses. However, it is anticipated that field overburden pressures should be sufficient to suppress this effect in all but the top foot or two of soil.

Measurements of S-wave velocity ( $V_s$ ) in the semi-stagnant columns before, during, and after testing revealed increases in  $V_s$  with increasing carbonate content. It was shown that  $V_s$  improvements in specimens treated via denitrification were greater than in those in specimens treated via ureolysis. This effect is attributed to two different mechanisms. Denitrification, as a slower precipitation process, is likely to result in larger carbonate crystals than ureolysis (a hypothesis supported by visual observation). These larger crystals are hypothesized to provide better bridging between soil particles and hence larger improvements in  $V_s$ . Also, the interaction between gas production and carbonate precipitation in denitrification was shown through SEM imagery to concentrate carbonate precipitation at particle contacts, increasing interparticle bridging and hence  $V_s$  improvement.

Undrained and drained triaxial testing of the soil from the semi-stagnant soil columns following treatment showed improvements in stiffness, strength, and dilatant behavior at small carbonate content (e.g. less than 1%), with the degree of improvement increasing with increasing carbonate content regardless of initial relative density or soil type. Similarly, cyclic direct simple shear testing revealed significant improvements in the cyclic resistance of the soil with relatively small amounts of carbonate precipitation (i.e., carbonate content as low as 0.5% by weight). These results show that treatment of soils via MICP can significantly improve the mechanical properties and liquefaction resistant of a soil, even at very low carbonate contents.

Improvement in the mechanical behavior of the treated soil was observed in reconstituted, disaggregated (i.e., uncemented) samples of treated Ottawa 20-30 soil with low carbonate contents. The tests (both undrained triaxial and cyclic direct simple shear

testing) on reconstituted treated soil revealed improvements in strength, stiffness, dilatant behavior, and cyclic resistance in the reconstituted specimens when compared to untreated soil but also showed decreasing improvement with multiple reconstitutions. SEM imagery of the tested soil suggested that particle roughening via carbonate precipitation was the mechanism for the improvement of the reconstituted samples. It is hypothesized that when the soil is subjected to multiple shearing events, this roughening effect is reduced due to abrasion and smoothing of the precipitated carbonate crystals. Thus, the primary improvement mechanism in soil lightly treated via MICP may be particle roughening rather than interparticle cementation. This particle roughing via MICP still results in measureable improvement in the mechanical properties and liquefaction resistance of treated soils.

Testing of soil columns subjected to continuous flow revealed that biostimulation of native microbes for treatment via denitrification is not only possible but easy to achieve in the laboratory. Stimulation of un-inoculated sand samples resulted in observed gas generation within 5 days and improved  $V_s$  within 10 days of treatment. Treatment in continuous flow columns also resulted in considerably more carbonate precipitation than in semi-stagnant columns treated over the same time period. In fact, cementation of soil was observed in continuous flow experiments within 4 – 6 weeks of the beginning of treatment.

Improvement via desaturation and MICP was observed to occur quickly in columns subjected to continuous flow. However, the resulting carbonate precipitation was found to concentrate near the inlet of the soil columns. Also, higher flow rates were found to result in nitrite accumulation in the columns and subsequent inhibition of microbial growth. So, while improvement under continuous flow conditions may occur more quickly than in

semi-stagnant conditions, optimum parameters for treatment, including flow rate and concentrations of input chemicals, should be investigated before field tests are conducted.

Comparison of acrylic columns inoculated with a pure culture of *Pseudomonas denitrificans*, and mixed culture stimulated from natural sand and water from Bolsa Chica State Beach in Huntington Beach, CA, and an uninoculated biostimulated soil column revealed that the microbial community stimulated in the uninoculated column was able to reduce nitrate and induce carbonate precipitation at a faster rate than either of the inoculated columns. This suggests that biostimulation may be the best method to implement soil improvement via denitrification in the field.

Analysis of the microbial communities in the continuously flowing column and the semi-stagnant columns showed that the microbial community stimulated in the continuously flowing column was more diverse at all points in space in time than the communities in the semi-stagnant columns. While this could be an artifact of the treatment type (continuous flow versus semi-stagnant), it would also indicate that the biostimulated community in the continuous flow column was more diverse than that in the inoculated semi-stagnant columns. This could be further evidence that biostimulation results in a more diverse and adaptive community than bioaugmentation.

The taxonomic breakdown of the microbial communities in the semi-stagnant and continuous flow columns indicated that the predominant genera in both columns responsible for denitrification are *Pseudomonas* and *Bacillus*, with both genera being significantly stimulated during treatment. The relative abundance of DNA from each genera was also found to be linked to the environmental conditions in the columns, with *Bacillus* species found in greater abundance in areas with lower pH, higher ionic strength,



and higher concentrations of nitrate and nitrite. *Anoxybacillus* species were also found in great abundance in the semi-stagnant columns, but this is thought to be an artifact of the feast-famine nutrient conditions in these columns, which tend to favor spore forming extremophiles, like *Anoxybacillus* species. *Brevundimonas* species were also found to be present in the top of the continuous flow column, and seemed to be replacing *Pseudomonas* and *Bacillus* species in this location with time. This result indicates that *Brevundimonas* species may also play an integral part in biostimulated denitrifying microbial communities.

Stoichiometric modeling of soil improvement via denitrification showed that the coupling of stoichiometry, microbial growth kinetics, and the thermodynamics of carbonate precipitation can be used to model gas production and carbonate precipitation via denitrification in batch reactors reasonably accurately. A sensitivity analysis using the model suggested that the optimum carbon source for carbonate precipitation and gas production via denitrification should be rich in nitrogen (i.e., a protein source). It also suggested that the optimum ratio of calcium to nitrate would be 1:1 to optimize carbonate precipitation and gas production while minimizing cost and environmental impact.

Overall, the results of this study demonstrate the feasibility of denitrification as a two-stage process for liquefaction mitigation. It was found that desaturation via denitrification occurs very quickly (1-3 days) and to an extent (90-95% saturation) that will significantly improve the cyclic resistance of the soil (upwards of 40% improvement). So, desaturation via denitrification should quickly provide significant liquefaction mitigation after inception and for the duration of treatment. Similarly, it was found that both the static and cyclic mechanical properties of the soil can be significantly improved with MICP via denitrification, with very little carbonate precipitation (less than 1% by weight) and no

observed interparticle cementation. From continuous flow column tests, it was demonstrated that this amount of precipitation can be achieved in a matter of weeks following the inception of treatment. As carbonate minerals (particularly calcite) are fairly stable in the environment, MICP via denitrification represents a viable long-term liquefaction mitigation technique. Finally, the results of this study show that denitrifying microbial communities capable of inducing significant desaturation and MICP can be stimulated from native soils within a matter of days. This indicates that liquefaction mitigation via denitrification can potentially be applied as a biostimulation technique if it is applied in the field. Overall, these results indicate the applicability of denitrification as a two-stage process for liquefaction mitigation.

#### **RECOMMENDATIONS FOR FURTHER STUDY**

The work presented in this dissertation has confirmed the applicability of denitrification as a two-stage process for the mitigation of earthquake-induced soil liquefaction. However, there are still quite a few hurdles to overcome before this technique can be applied in the field. First, it is important to conduct cyclic testing on soil treated to different degrees of saturation with biogas to confirm that desaturation via biogas production actually induces the same increases in cyclic resistance observed in desaturated abiotic columns. Undrained triaxial testing of biologically treated sand should also be undertaken to determine the impact of biogas desaturation on the undrained properties of the soil subjected to monotonic loading.

More testing is also required to determine the optimum conditions for treatment via denitrification under continuous flow conditions. While the testing presented herein showed that both desaturation and cementation can be achieved via denitrification under

continuous flow, it also showed that treatment in these conditions is far from uniform and can be subject to nitrite accumulation and inhibition of biomass growth. It is important to understand the interactions among the various factors that influence denitrification, including flow rate, chemical concentrations, and distribution and growth of biomass, in order to predict how treatment will occur in the field. On the same note, it is important to extend the stoichiometric model developed herein to conditions of continuous flow so that this model may be used to optimize treatment regimens. Physical testing of soil columns can take weeks to months, while computer simulations may only take minutes to hours to run. Therefore, it is extremely important to continue to expand the stoichiometric model so it can be applied to a broader range of conditions (particularly to conditions of continuous groundwater flow).

It is also important to investigate denitrification under higher overburden stresses than those used in the columns reported herein. Of particular concern is the potential that higher steady state pore pressures could result in compression of gas bubbles and lower reductions in the degree of saturation reported herein. For this testing, specialized equipment will need to be built to provide a continuous supply of nutrients to the soil column while the system is maintained at constant pressure (both confining pressure and pore pressure), e.g., in a triaxial testing cell. This equipment should allow for continuous monitoring (via P-wave and S-wave velocity measurements as well as sampling for IC analysis) of the sample under pressurized conditions. It will also be interesting to study how the higher pressures affect the microbial community structure as well as the carbonate crystal morphology.

It is also recommended to study the applicability of denitrification to a broader range of potentially liquefiable soils. While this work demonstrated the ability to treat two uniform,

clean sands (Ottawa 20-30 sand and Bolsa Chica beach sand), the applicability of this process to finer grained liquefiable materials, e.g., non-plastic silts, should be explored. Finer grained materials display significant matric suction even at fairly high degrees of saturation. So, it would be very interesting to see if these suction values develop as the soil desaturates through treatment via denitrification and how this affects the liquefaction resistance of the material. It would also be interesting to see if uniform desaturation could be achieved in these samples, as microbes may not fit through the smaller pore throats.

Finally, it would be very interesting to study the ability to stimulate, in-situ, microbial communities capable of performing both ureolysis and denitrification simultaneously. As these processes are not mutually exclusive, it might be beneficial to pursue inducing both processes at once, as ureolysis and denitrification may complement each other well. Ureolysis causes the pH to rise considerably, but it does not produce very much carbonate. Denitrification, by contrast, produces a lot of carbonate, but does not induce as large a change in pH. By combining the denitrification and ureolysis processes, a mixed microbial community may create an extremely favorable environment (high pH, high carbonate) for carbonate precipitation. Under the combined processes, this microbial community will still produce gas and may consume some of the potentially toxic ammonium produced via ureolysis as a nitrogen source. This may result in a more efficient MICP process, with the added benefit of desaturation and reduced environmental contamination.

## REFERENCES

- Almeida, J.S., Julio, S.M., Reis, M.A.M., and Carrondo, M.J.T. (1994) "Nitrite Inhibition of Denitrification by *Pseudomonas fluorescens*." *Biotechnology and Bioengineering*, 46 (3): 194-201.
- Anderson, Greg. (2009). "Thermodynamics of Natural Systems, 2<sup>nd</sup> Edition." Cambridge University Press, Cambridge, England.
- Andrus, Ronald D., and Chung, Riley M. (1995). "Ground Improvement Techniques for Liquefaction Remediation near Existing Lifelines." Building and Fire Research Laboratory, National Institute of Standards and Technology, Gaithersburg, MD.
- Andrus, Ronald D., and Stokoe, Kenneth H. II. (1996). "Liquefaction Resistance Based on Shear Wave Velocity." Proceedings, Evaluation of Liquefaction Resistance of Soils, National Center for Earthquake Engineering Research (NCEER) Workshop, Salt Lake City, UT.
- Arab, A., Shahrou, I., Lancelot, L. (2011). "A Laboratory Study of Liquefaction of Partially Saturated Sand." *Journal of Iberian Geology* 37(1): 29-36.
- ASTM D6913-04. (2009) "Standard Test Methods for Particle-Size Distribution (Gradation) of Soils Using Sieve Analysis." *American Society of Testing and Materials*, West Conshohocken, PA.
- ASTM D6836-02. (2008) "Standard Test Methods for Determination of the Soil Water Characteristic Curve for Desorption Using Hanging Column, Pressure Extractor, Chilled Mirror Hygrometer, or Centrifuge." *American Society of Testing and Materials*, West Conshohocken, PA.
- Bae, Wookeun, and Rittmann, Bruce E. (1996) "A Structured Model of Dual-Limitation Kinetics." *Biotechnology and Bioengineering*, 49: 683-689.
- Bengtson, Stefan, Belivanova, Veneta, Rasmussen, Birger, and Whitehouse, Martin. (2009). "The Controversial 'Cambrian' Fossils of the Vindhyan are Real but More than a Billion Years Older." *PNAS*, 106(19): 7729-7734.
- Bundeleva, Irina A., Shirokova, Liudmila S., Pokrovsky, Oleg S., Benezeth, Pascale, Menez, Benedicte, Gerard, Emmanuelle, and Balor, Stephanie. (2014). "Experimental Modeling of Calcium Carbonate Precipitation by Cyanobacterium *Gloeocapsa* sp." *Chemical Geology* 374-375: 44-60.
- Burbank, Malcolm, B., Weaver, Thomas J., Green, Tonia L., Williams, Barbara C., and Crawford, Ronald L. (2011). "Precipitation of Calcite by Indigenous Microorganisms to Strengthen Liquefiable Soil." *Geomicrobiology Journal* 28: 301-312.

- Burbank, Malcolm, Weaver, Thomas, Lewis, Ryan, Williams, Thomas, Williams, Barbara, and Crawford, Ronald. (2013) "Geotechnical Tests of Sand Following Bioinduced Calcite Precipitation Catalyzed by Indigenous Bacteria." *J. Geotech. Geoenviron. Eng.* 139: 928-936.
- Caporaso, J. Gregory, Kuczynski, Justin, Stombaugh, Jesse, Bittinger, Kyle, Bushman, Frederic D., Costello, Elizabeth K., Fierer, Noah, Pena, Antonio Gonzalez, Goodrich, Julia K., Gordon, Jeffrey I., Huttley, Gavin A., Kelley, Scott T., Knights, Dan, Koenig, Jeremy E., Ley, Ruth E., Lozupone, Catherine A., McDonald, Daniel, Muegge, Brian D., Pirrung, Meg, Reeder, Jens, Sevinsky, Joel R., Turnbaugh, Peter J., Walters, William A., Widmann, Jeremy, Yatsunenko, Tanya, Zaneveld, Jesse, and Knight, Rob. (2010). "QIIME Allows Analysis of High-Throughput Community Sequencing Data." *Nature Methods*, 7(5): 335-336.
- Carlson, Curtis A., and Ingraham, John L. (1983). "Comparison of Denitrification by *Pseudomonas stutzeri*, *Pseudomonas aeruginosa*, and *Paracoccus denitrificans*." *Applied and Environmental Microbiology*, 45(4): 1247-1253.
- Cheng, L., Shahin, A., Cord-Ruwisch, R., Addis, M., Hartanto, M., and Elms, C. (2014). "Soil Stabilisation by Microbial-Induced Calcite Precipitation (MICP): Investigation into Some Physical and Environmental Aspects." Proc. 7ICEG, Melbourne, Australia (on CD ROM).
- Cho, Gye-Chun, Dodds, Jake, and Santamarina, J. Carlos. (2006). "Particle Shape Effects on Packing Density, Stiffness, and Strength: Natural and Crushed Sands." *Journal of Geotech. and Geoenviron. Eng.* 132(5): 591-602.
- Cubrinovski, M., Henderson, D., Bradley, B. (2012) "Liquefaction impacts in residential areas in the 2010–2011 Christchurch Earthquakes." Proceedings of the International Symposium on Engineering Lessons Learned from the 2011 Great East Japan Earthquake (2012), pp. 811–824
- Cubrinovski, Misko, Bradley, Brendon, Wotherspoon, Liam, Green, Russel, Bray, Jonathon, Wood, Clint, Pender, Michael, Allen, John, Bradshaw, Aaron, Rix, Glenn, Taylor, Merrick, Robinson, Kelly, Henderson, Duncan, Giorgini, Simona, Ma, Kun, Winkley, Anna, Zupan, Josh, O'Rourke, Thomas, DePascale, Gred, and Wells, Donald. (2011). "Geotechnical Aspects of the 22 February 2011 Christchurch Earthquake." *Bulletin of the New Zealand Society for Earthquake Engineering* 44(4): 205-226.
- Davies, C.W. (1962). *Ion Association*. London: Butterworths. pp. 37–53.
- DeJong, Jason T., Mortenson, Brina M., Martinez, Brian C., and Nelson, Douglas C. (2010) "Bio-mediated Soil Improvement." *Ecological Engineering* 36: 197-210.

- DeJong, J.T., Soga, K., Banwart, S.A., Whalley, R.W., Ginn, T.R., Nelson, D.C., Mortensen, B.M., Martinez, B.C., and Barkouki, T. (2011) "Soil Engineering *in vivo*: Harnessing Natural Biogeochemical Systems for Sustainable, Multi-Functional Engineering Solutions." *J. R. Soc. Interface* 8: 1-15.
- DeJong, J.T., Martinez, B.C., Ginn, T.R., Hunt, C., Major, D., and Tanyu, B. (2014). "Development of a Scaled Repeated Five-Spot Treatment Model for Examining Microbial Induced Calcite Precipitation Feasibility in Field Applications." *Geotechnical Testing Journal*, 37(3), DOI: 10.1520/GTJ20130089.
- Denariuz, Gerard, Payne, William J., and Le Gall, Jean. (1989). "A Halophilic Denitrifier, *Bacillus halodenitrificans* sp. nov." *International Journal of systematic Bacteriology*, 39(2): 145-151.
- Dick, Jeffrey M. (2008) "Calculation of the relative metastabilities of proteins using the CHNOSZ software package." *Geochemical Transactions*, 9 (10): 1-17.
- Dulger, Sabriye, Demirbag, Sihni, and Belduz, Ali Osman. (2004). "*Anoxybacillus ayderensis* sp. nov and *Anoxybacillus kestanbolensis* sp. nov." *International Journal of Systematic and Evolutionary Microbiology*, 54: 1499-1503.
- Ehrlich, Henry Lutz and Newman, Dianne K. (2009) "Geomicrobiology, Fifth Edition." CRC Press, Taylor and Francis Group, LLC, Boca Raton, FL.
- Eseller-Bayat, Ece, Yegian, Mishac, K., Alshawabkeh, Akram, and Gokyer, Seda. (2013). "Liquefaction Response of Partially Saturated Sands. I: Experimental Results." *Journal of Geotech. and Geoenviron. Eng.* 139(6): 863-871.
- Faith, Daniel P. (1992). "Conservation Evaluation and Phylogenetic Diversity." *Biological Conservation*, 61: 1-10.
- Farrell, Tom M., Wallace, Kyle, and Ho, John. (2010). "Liquefaction Mitigation of Three Projects in California." Proceedings, 5<sup>th</sup> International Conference on Recent Advances in Geotechnical Earthquake Engineering and Soil Dynamics, San Diego, CA.
- Fidaleo, M. and Lavecchia, R. (2003) "Kinetic Study of Enzymatic Urea Hydrolysis in the pH Range 4-9." *Chem. Biochem. Eng. Q.* 17 (4): 311-318.
- Fredlund, D.G. and Rahardjo, H. (1993). "Soil Mechanics for Unsaturated Soils." John Wiley and Sons, Inc. Hoboken, NJ.
- Gallagher, Patricia M., Conlee, Carolyn T., and Rollins, Kyle M. (2007). "Full-Scale Field Testing of Colloidal Silica Grouting for Mitigation of Liquefaction Risk." *Journal of Geotech. and Geoenviron. Eng.* 133(2): 186 -196.

- Goh, Kian Mau, Gan, Han Ming, Chan, Kok-Gan, Chan, Giek Far, Shahar, Saleha, Chong, Chun Shiong, Kahar, Ummirul Mukminin, and Chai, Kian Piaw. (2014). "Analysis of *Anoxybacillus* Genomes from the Aspects of Lifestyle Adaptations, Prophage Diversity, and Carbohydrate Metabolism." *PLOS ONE*, 9(3): e90549.
- Gomez, M.G., DeJong, J.T., Martinez B.C., Hunt, C.E, deVlaming, L.A, Major, D.W., and Dworatzek, S.M. (2013). "Bio-mediated Soil Improvement Field Study to Stabilize Mine Sands." Proceedings, Geo-Montreal, Montreal, Canada.
- Haile, Beyene Girma. (2011) "An Experimental Study of the Effect of Dissolved Acetate ion on the Calcite Precipitation Kinetics and its Implications for Subsurface CO<sub>2</sub> Storage." Master's Thesis, University of Oslo.
- Hamdan, Nasser, Kavazanjian Edward Jr., Rittmann, Bruce E., and Karatas, Ismail. (2011). "Carbonate Mineral Precipitation for Soil Improvement through Microbial Denitrification." Proceedings, Geo-Frontiers, Dallas, TX.
- Hamdan, Nasser. (2013). "Carbonate Mineral Precipitation for Soil Improvement through Microbial Denitrification." Master's Thesis, Arizona State University.
- Hamdan, Nasser M. (2015) "Applications of Enzyme Induced Carbonate Precipitation (EICP) for Soil Improvement." Dissertation, Arizona State University.
- Hamdan, N., and Kavazanjian, E. (2016). "Enzyme Induced Carbonate Mineral Precipitation for Fugitive Dust Control." *Geotechnique* DOI: 10.1680/geot/15-P-168.
- Hatanaka, Munenori, and Masuda, Takemi. (2008). "Experimental Study on the Relationship between Degree of Saturation and P-wave Velocity in Sandy Soils." Proceedings, 2<sup>nd</sup> International Conference GEDMAR, Nanjing, China.
- He, J., Chu, J., and Ivanov, V. (2013) "Mitigation of Liquefaction of Saturated Sand Using Biogas." *Geotechnique*, 63 (4): 267-275.
- He, Jia and Chu, Jian. (2014). "Undrained Responses of Microbially Desaturated Sand under Monotonic Loading." *Journal of Geotech. and Geoenviron. Eng.* 140(5): 04014003.
- Kamennaya, Nina A., Ajo-Franklin, Caroline M., Northen, Trent, and Jansson, Christer. (2012). "Cyanobacteria as Biocatalysts for Carbonate Mineralization." *Minerals* 2: 338-364.
- Karatas, Ismail, Kavazanjian, Edward Jr., Rittmann, Bruce E. (2008) "Microbially Induced Precipitation of Calcite using *Pseudomonas denitrificans*." Proceedings 1<sup>st</sup> International Conference on BioGeoCivil Engineering, Delft, the Netherlands.



- Karatas, Ismail. (2008). "Microbiological Improvement of the Physical Properties of Soils." Dissertation, Arizona State University.
- Kavazanjian, Edward, and Hamdan, Nasser. (2015) "Enzyme Induced Carbonate Precipitation (EICP) Columns for Ground Improvement." Proceedings, IFCEE, San Antonio, TX.
- Kavazanjian, Edward Jr., O'Donnell, Sean T., and Hamdan, Nasser. (2015) "Biogeotechnical Mitigation of Earthquake-Induced Soil Liquefaction by Denitrification: A Two Stage Process." Proceedings 6ICEGE, Christchurch, NZ.
- Kavitha, S., Sulvakumar, R., Sathishkumar, M., Swaminathan, K., Lakshmanaperumalsamy, P., Singh, A., and Jain, S.K. (2009). "Nitrate Removal Using *Brevundimonas diminutia* MTCC 8486 from Ground Water." *Water Science and Technology*, 60(2): 517-524.
- Kazmierczak, Jozef, Fenchel, Tom, Kuhl, Michael, Kempe, Stephan, Kremer, Barbara, Lacka, Bozena, and Malkowski, Krzysztof. (2015). "CaCO<sub>3</sub> Precipitation in Multilayered Cyanobacterial Mats: Clues to Explain the Alternation of Micrite and Sparite Layers in Calcareous Stromatolites." *Life* 5: 744-769.
- Kitano, Yasushi, Kanamori Nobuko, and Tokyuama, Akira. (1969) "Effects of Organic Matter on Solubilities and Crystal Form of Carbonates." *American Zoologist*, 9 (3): 681-688.
- Knorr, Brian. (2014). "Enzyme-Induced Carbonate Precipitation for the Mitigation of Fugitive Dust." Master's Thesis, Arizona State University.
- Kramer, Steven L. (1996). "Geotechnical Earthquake Engineering." Prentice Hall, Inc., Upper Saddle River, NJ.
- Lade, Poul V., and Pradel, Daniel. (1990). "Instability and Plastic Flow of Soils. I: Experimental Observations." *J. Eng. Mech.* 116: 2532-2550.
- Li, Yishan. (2014). "Mitigation of Sand Liquefaction Using *in situ* Production of Biogas with Biosealing." Master's Thesis, Iowa State University.
- Lin, H., Suleiman, M.T., Jabbour H.M., Brown, D.G. and Kavazanjian E. (2016) "Enhancing the Axial Compression Response of Pervious Concrete Ground Improvement Piles Using Bio-Grouting." *Journal of Geotech. and Geoenviron. Eng.* (In Press).

- Martin, Derek, Dodds, Kevin, Butler, Ian B., and Ngwenya, Bryne T. (2013). "Carbonate Precipitation under Pressure for Bioengineering in the Anaerobic Subsurface via Denitrification." *Environmental Science and Technology* 47: 8692-8699.
- Meyer, F.D., Bang, S., Min, S., Stetler, L.D., and Bang, S.S. (2011). "Microbiologically-Induced Soil Stabilization: Application of *Sporosarcina pasteurii* for Fugitive Dust Control." Proceedings, Geo-Frontiers, Dallas, TX.
- Montoya, B.M., and DeJong, J.T. (2015) "Stress-Strain Behavior of Sands Cemented by Microbially Induced Calcite Precipitation." *J. Geotech. Geoenviron. Eng.* 141(6): 04015019.
- Montoya, B.M., DeJong, J.T., and Boulanger, R.W. (2013) "Dynamic Response of Liquefiable Sand Improved by Microbial-Induced Calcite Precipitation." *Geotechnique* 63(4): 302-312.
- Nakai, S., Sekiguchi, T., and Mano, H. (2015). "A Study on Dewatering Effect as a Liquefaction Countermeasure for Existing Residential Areas by Centrifuge Shaking Table Tests." Proceedings, 6ICEGE, Christchurch, New Zealand.
- Neumeier, Urs. (1999). "Experimental Modelling of Beachrock Cementation Under Microbial Influence." *Sedimentary Geology* 126: 35-46.
- O'Donnell, Sean Thomas and Kavazanjian, Edward Jr. (2015) "Stiffness and Dilatancy Improvements in Uncemented Sands Treated through MICP." *Journal of Geotechnical and Geoenvironmental Engineering*, 141 (11): 02815004.
- Ojuri, Oluwapelumi O., and Fijabi, David O. (2012). "Standard Sand for Geotechnical Engineering and Geoenvironmental Research in Nigeria: Igbokoda Sand." *Advances in Environmental Research*, 1(4): 305-321.
- Okamura, Mitsu and Soga, Yasumasa. (2006). "Effects of Pore Fluid Compressibility on Liquefaction Resistance of Partially Saturated Sand." *Soils and Foundations* (Japanese Geotechnical Society) 46(5): 695-700.
- Okamura, Mitsu, and Teraoka, Taiji. (2006). "Shaking Table Tests to Investigate Soil Desaturation as a Liquefaction Countermeasure." Proceedings, Seismic Performance and Simulation of Pile Foundations in Liquefied and Laterally Spreading Ground, Davis, CA.
- Orense, R.P. (2008). "Liquefaction Remediation by Compaction Grouting." Proceedings, NZSEE Conference, Wairakei, New Zealand.
- Orense, R.P. (2015). "Recent Trends in Ground Improvement Methods as Countermeasure against Liquefaction." Proceedings, 6ICEGE, Christchurch, New Zealand.

- Ozener, P., Dulger M. and Berilgen M. (2015). “Numerical Study of Effectiveness of Jet-Grout Columns in Liquefaction Mitigation.” Proceedings, 6ICEGE, Christchurch, New Zealand.
- Poli, Annarita, Esposito, Enrico, Lama, Licia, Orlando, Pierangelo, Nicolaus, Giancarlo, de Appolonia, Francesca, Gambacorta, Agata, and Nicolaus, Barbara. (2006). “*Anoxybacillus anylolyticus* sp. nov., A Thermophilic Amylase Producing Bacterium Isolated from Mount Rittmann (Antarctica).” *Systematic and Applied Microbiology*, 29: 300-307.
- Rajakumar, Sundaram, Ayyasamy Pudukadu Munusamy, Shanthi, Kuppusamy, Thavamani Palanisami, Velmurugan, Palanivel, Song, Young Chae, and Lakshmanaperumalsamy, Perumalsamy. (2008). “Nitrate Removal Efficiency of Bacterial Consortium (*Psuedomonas* sp. KW1 and *Bacillus* sp. YW4) in synthetic nitrate-rich water.” *Journal of Hazardous materials*,
- Rebata-Landa, Veronica, and Santamarina, J. Carlos. (2012). “Mechanical Effects of Biogenic Nitrogen Gas Bubbles in Soils.” *Journal of Geotech. and Geoenviron. Eng.* 138(2): 128-137.
- Rittmann, Bruce E. and McCarty Perry L. (2001) “Environmental Biotechnology: Principles and Applications.” McGraw Hill, New York, NY.
- Robertson, P.K. and Wride C.E. (Fear). (1998) “Evaluating Cyclic Liquefaction Potential using the Cone Penetration Test.” *Can. Geotech. J.* 35, pp 442-459.
- Rogers, N., van Ballegooy, S., Williams, K., and Johnson, L. (2015) “Considering Post Disaster Damage to Residential Building Construction – Is Our Modern Building Construction Resilient?” *Proceedings of 6ICEGE*, Christchurch, New Zealand.
- Rugg, D.A., Yoon, J., Hwang, H., and El Mohtar, C.S. (2011). “Undrained Shearing Properties of Sand Permeated with a Bentonite Suspension for Static Liquefaction Mitigation.” Proceedings, Geo-Frontiers, Dallas, TX
- Saleh-Lakha, Saleema, Shannon, Kelly E., Handerson, Sherri L., Goyer, Claudia, Trevors, Jack T., Zebarth, Bernie J., and Burton, David L. (2009). “Effect of pH and Temperature on Denitrification Gene Expression and Activity in *Pseudomonas mandelii*.” *Applied and Environmental Microbiology*, 75(12): 3903-3911.
- Salifu, Emmanuel, MacLachlan, Erica, Iyer, Kannan R., Knapp, Charles W., and Tarantino Alessandro. (2016). “Application of Microbially Induced Calcite Precipitation in Erosion Mitigation and Stabilisation of Sandy Soil Foreshore Slopes: A Preliminary Investigation.” *Environmental Geology* 201: 96-105.

- Santamarina, C., and Cascante, G. (1998). "Effect of Surface Roughness on Wave Propagation Parameters." *Geotechnique*, 48(1): 129-136.
- Santamarina, J. Carlos, and Cho, Gye Chun. (2001). "Determination of Critical State Parameters in Sandy Soils – Simple Procedure." *Geotechnical Testing Journal*, 24(2): 185-192.
- Sharma, Ram Prasad. (2010). "Soil Improvement Techniques for Mitigation of Seismic Hazards – An Overview." Proceedings, 5<sup>th</sup> International Conference on Recent Advances in Geotechnical Earthquake Engineering and Soil Dynamics, San Diego, CA.
- Sijbesma, Wilbert F.H., Almeida, Jonas S., Reis, Maria A.M., and Santos, Helena. (1996) "Uncoupling Effect of Nitrite During Denitrification by *Pseudomonas fluorescens*: An In Vivo <sup>31</sup>P-NMR Study." *Biotechnology and Bioengineering*, 52 (1): 176-182.
- Takii, Susumu, Hanada, Satoshi, Tamaki, Hideyuki, Ueno, Yutaka, Sekiguchi, Yuji, Ibe, Akihiro, and Matsuura, Katsumi. (2007). "*Dethiosulfatibacter aminovorans* gen. nov., sp. nov., A Novel Thiosulfate-Reducing Bacterium Isolated from Coastal Marine Seiment via Sulfate-Reducing Enrichment with Casamino Acids." *International Journal of Systematic and Evolutionary Microbiology*, 57: 2320-2326.
- Tsubouchi, Taishi, Koyama, Sumihiro, Mori, Kozue, Shimane, Yasuhiro, Usui, Keiko, Tokuda, Maki, Tame, Akihiro, Uematsu, Katsuyuki, Maruyama, Tadashi, and Hatada, Yuji. (2014). "*Brevundimonas denitrificans* sp. nov., a Denitrifying Bacterium Isolated from Deep Subseafloor Sediment." *International Journal of Systematic and Evolutionary Microbiology*, 64: 3709-3716.
- Tsukamoto, Yoshimichi, Ishihara, Kenji, Nakazawa, Hiroshi, Kamada Kunio and Huang, Yongnan. (2002). "Resistance of Partly Saturated Sand to Liquefaction with Reference to Longitudinal and Shear Wave Velocities." *Soils and Foundations* 42(6): 93-104.
- U.S. Silica Co. (2016) "Testing Silica: The Original Ottawa Silica." <<http://www.ussilica.com/products/testing-silica>>.
- Valle-Molina, Celestino and Stokoe, Kenneth II. (2012). "Seismic Measurements in Sand Specimens with Varying Degrees of Saturation using Piezoelectric Transducers." *Can. Geotech. J.* 49: 671-685.
- van der Star, W.R.L., van Wijngaarden-van Rossum, W.K., van Paassen, L.A., van Baalen, L.R., and van Zwieten G. (2011). "Stabilization of Gravel Deposits Using Microorganisms." Proceedings, 15<sup>th</sup> European Conference on Soil Mechanics and Geotechnical Engineering, Athens, Greece.
- van Paassen, Leon A., Ghose Ranajit, van der Linden Thomas J.M., van der Star, Wouter

- R.L., and van Loosdrecht, Mark C.M. (2010) “Quantifying Biomediated Ground Improvement by Ureolysis: Large-Scale Biogrout Experiment.” *Journal of Geotechnical and Geoenvironmental Engineering*, 136 (12): 1721-1728.
- van Paassen, Leon A., Daza, Claudia M., Stall, Marc, Sorokin Dimitri Y., van der Zon Willem, and van Loosdrecht, Mark C.M. (2010) “Potential Soil Reinforcement by Biological Denitrification.” *Ecological Engineering* 36: 168-175.
- Verbaendert, Ines, Boon, Nico, De Vos, Paul, and Heylen, Kim. (2011). “Denitrification is a Common Feature among Members of the Genus *Bacillus*.” *Systematic and Applied Microbiology*, 34: 385-391.
- Wang, Y.H. and Fredlund D.G. (2003). “Towards a Better Understanding of the Role of the Contractile Skin.” Proceedings, 2<sup>nd</sup> Asian Conference on Unsaturated Soils, Osaka, Japan.
- Warren, John R. (2007). “The *Enterobacteriaceae* Basic Properties.” Presentation at Northwestern University, Feinberg School of Medicine, Evanston, IL.
- Warthmann, Rolf, van Lith, Yvonne, Vasconcelos, Crisogono, McKenzie, Judith A., and Karpoff, Anne Marie. (2000). “Bacterially induced dolomite precipitation in anoxic culture experiments.” *Geology* 28(12): 1091-1094.
- Whiffin, Victoria S., van Paassen, Leon A., and Harkes, Marien P. (2007) “Microbial Carbonate Precipitation as a Soil Improvement Technique.” *Geomicrobiology Journal* 24: 417-423.
- Yang, Jun, Savidis, Stavros, and Roemer Matthias. (2004). “Evaluating Liquefaction Strength of Partially Saturated Sand.” *Journal of Geotech. and Geoenviron. Eng.* 130(9): 975-979.
- Yegian, M.K., Eseller-Bayat, E., Alshawabkeh, A., and Ali, S. (2007). “Induced-Partial Saturation for Liquefaction Mitigation: Experimental Investigation.” *Journal of Geotech. and Geoenviron. Eng.* 133(4): 372-380.
- Zhang, Chun-Mei, Huang, Xiao-Wei, Pan, Wen-Zheng, Zhang, Jing, Wei, Kang-Bi, Klenk, Hans-Peter, Tang, Shu-Kun, Li, Wen-Jun, and Zhang, Ke-qin. (2011). “*Anoxybacillus tengchongensis* sp. nov. and *Anoxybacillus eryuanensis* sp. nov., Facultatively Anaerobic, Alkalitolerant Bacteria from Hot Springs.” *International Journal of Systematic and Evolutionary Microbiology*, 61: 118-122.

Zhao, Qian, Li, Lin, Li, Chi, Li, Mingdong, Amini, Farshad, and Zhang, Huanzhen. (2014).  
“Factors Affecting Improvement of Engineering Properties of MICP-Treated Soil  
Catalyzed by Bacteria and Urease.” *J. Mater. Civ. Eng.* 26, 04014094.